SIMULATION OF A NON-PREMIXED SWIRL BURNER

A THESIS SUBMITTED TO
THE GRADUATE SCHOOL OF NATURAL AND APPLIED SCIENCES
OF
MIDDLE EAST TECHNICAL UNIVERSITY

BY

MEHMET BURAK SOLMAZ

IN PARTIAL FULFILLMENT OF THE REQUIREMENTS
FOR
THE DEGREE OF MASTER OF SCIENCE
IN
AEROSPACE ENGINEERING

SEPTEMBER 2014

Approval of the thesis:

SIMULATION OF A NON-PREMIXED SWIRL BURNER

submitted by **MEHMET BURAK SOLMAZ**in partial fulfillment of the requirements for the degree of **Master of Science in Aerospace Engineering Department, Middle East Technical University** by,

Prof. Dr. Canan Özgen _____
Dean, Graduate School of **Natural and Applied Sciences**

Prof. Dr. Ozan Tekinalp _____
Head of Department, **Aerospace Engineering**

Assoc. Prof. Dr. Oğuz Uzol _____
Supervisor, **Aerospace Engineering Dept., METU**

Asst. Prof. Dr. Sıtkı Uslu _____
Co-Supervisor, **Mechanical Engineering Dept., TOBB ETU**

Examining Committee Members:

Prof. Dr. Sinan Akmandor _____
Aerospace Engineering Dept., METU

Assoc. Prof. Dr. Oğuz Uzol _____
Aerospace Engineering Dept., METU

Asst. Prof. Dr. Sıtkı Uslu _____
Mechanical Engineering Dept., TOBB ETU

Assoc. Prof. Dr. Sinan Eyi _____
Aerospace Engineering Dept., METU

Asst. Prof. Dr. Ahmet Yozgatlıgil _____
Mechanical Engineering Dept., METU

Date: 05.09.2014

I hereby declare that all information in this document has been obtained and presented in accordance with academic rules and ethical conduct. I also declare that, as required by these rules and conduct, I have fully cited and referenced all material and results that are not original to this work.

Name, Last name :MehmetBurak SOLMAZ

Signature :

ABSTRACT

SIMULATION OF A NON-PREMIXED SWIRL BURNER

Solmaz, Mehmet Burak
M.S. Department of Aerospace Engineering
Supervisor: Assoc. Prof. Dr. Oğuz UZOL
Co-Supervisor: Asst. Prof. Dr. Sıtkı USLU

September 2014, 127 pages

Flame stabilizing in a gas turbine combustion chamber is one of the designing issues. Non-premixed swirling flames are commonly applied to aerial vehicles' combustors due to their advantages in flame stabilizing and flame length shortening. However, swirling flows are very complex and hard to simulate even without reaction. Previous studies have showed that Large Eddy Simulation (LES) is able to predict swirling flow with a good degree of accuracy. On the other, it is quite expensive and is still far away for being a routine approach as a design tool in industry. Unsteady Reynolds Averaged Navier Stokes (URANS) approach alters LES for being cheaper and reasonably accurate. This study aims to simulate a non-premixed highly swirling flame. TECFLAM S09 methane-air flame case with 0.9 swirling number and 150kW thermal power is selected which is a good candidate for investigating such flows. Realizable k-epsilon turbulence model is used with various combustion models. Mesh study is performed up to 38 million hexahedral elements. Results of URANS solutions are compared with LES. It is seen that flow field calculation is highly dependent on combustion phenomenon. But, LES predicts far better accurate solutions than URANS. On the other hand, LES is at least 10 times more expensive than URANS and turbulence models other than Realizable k-epsilon should be investigated to totally eliminate URANS for a highly swirling reactive flow.

Keywords:CFD, Non-premixed combustion, swirl flow, TECFLAM, methane-air flame, Unsteady RANS, LES,realizable k-epsilon, dynamic Smagorinsky-Lilly subgrid scale model, finite rate chemistry, infinitely fast chemistry, QUICK, Second Order Upwind, DO Radiation Model.

ÖZ

ÖN KARIŞIMSIZ SWİRL BRÜLÖR SİMULASYONU

Solmaz, Mehmet Burak
YüksekLisans, HavacılıkveUzayMühendisliğiBölümü
Tez Yöneticisi: Doç. Dr. Oğuz UZOL
Ortak Tez Yöneticisi:Yrd.Doç. Dr. Sıtkı USLU

Eylül 2014, 127sayfa

Gaz türbini yanma odalarında alev stabilizasyonu önemli bir tasarım parametresidir. Havacılık uygulamalarında kısa measafede etkin yanmaya olanak sağlayan apartlara yer verilir. Bu apartlardan bir tanesi rotasyonal akış üreteci olan swirl karıştırıcılardır. Fakat rotasyonal akışlar oldukça kompleks yapılardır ve reaksiyon olmadığı durumlarda bile simülasyonlarını yapmak oldukça zordur. Yapılan çalışmalar rotasyonel akışların "LES" tekniği ile başarılı sayılacak nitelikte simüle edilebildiğini göstermiştir. Ancak bu yöntem, ihtiyaç duyduğu bilgisayar gücü nedeni ile henüz sanayi için standart yöntem olamayacak kadar pahalı bir metoddur. "URANS" metodu ise kabul edilebilir doğruluk oranı ve ucuz oluşu sebebi ile "LES" için iyi bir alternatif olarak düşünülmektedir. Bu çalışmanın amacı ise, yüksek swirllü ön karışımsız bir akışın simüle edilmesidir. Simülasyon problemi olarak metan-hava alevi yakan "TECFLAM S09" koşulu ele alınmıştır. Bu koşulun swirl sayısı 0.9, termal gücü ise 150kW'dır. Farklı yanma modelleri de kullanılarak Realizable k-epsilon turbulance modeli ise simülasyonlar yapılmıştır. 38 Milyon altı yüzlü (hexahedral) eleman sayısına varıncaya kadar ağ yapısı çalışması gerçekleştirilmiştir. Aynı zamanda LES simülasyonları gerçekleştirilmiş ve URANS sonuçları ile karşılaştırılmıştır. Yapılan çalışmalar göstermiştir ki akış alanı hesaplamaları reaksiyonlara oldukça bağlıdır. Fakat yine de LES, URANS'a kıyasla

çok daha başarılı sonuçlar üretebilmiştir. Bunun yanında, LES için en az 10 kat daha fazla hesaplama zamanı gerekmiştir ki bu da URANS metodunun tamamen elenmeden önce farklı turbulans modelleri uygulanarak yeniden denenmesi gerekliliğini doğurmaktadır.

Anahtarkelimeler:HAD, Önkarışımsızyanma, Swirl akış, TECFLAM, metan-havaalevi,Zamanabağlı RANS, realizable k-epsilon, sonlu hızlı kimya

To My Parents, My Wifeand My Child

“Olmayacihandadevletbirnefessıhhatgibi.”

Her nefestesıhhatekavuşmamızdileğiile…

Sabrınızvedesteğiniziçinminnettarım.

ACKNOWLEDGEMENTS

There are many people that I want to show my appreciations who really deserve a grateful thanks but not named here. Instead I just give my special thanks here and hope others to understand me.

First of all, I would like thank a man who is very tolerant toward me, my dear and only father. There are lots of things to tell about him butnone of them would truly describe him. Thank you for everything…

I really am very grateful to my advisor Dr. Sitki USLU, for his guidance and friendship throughout my MSc. thesis. This work would never exist without his patience. And Dr. Oğuz UZOL, my supervisor, was very helpful for all the issues that I encounteredthroughout my study in METU.

I also want to give my thanks to Bora YAZICI for his instructive talks and to Prof. Sinan AKMANDOR for his simple and valuable advice at the first defense of my thesis.

This study is started for the will of TUBITAK SAGE and carried out with the sources of TUBITAK SAGE. I want to thank all my managers who support this work. And I want to give my thanks to METU RUZGEM office for providing their computing sources and their help to use them.

Last but not the least; I want to thank my mother who was volunteer to give her youth to see these days and my wife who has selected to get old to see others.

TABLE OF CONTENTS

LIST OF TABLES

TABLES

LIST OF FIGURES

FIGURES

LIST OF ABBREVIATIONS

2D	:	Two-dimensional
3D	:	Three-dimensional
CAD	:	Computer aided design
CDS	:	Central Differencing Scheme
CFD	:	Computational Fluid Dynamics
CFL	:	Courant FredericsLewy (Cell Courant) Number
CRZ	:	Central Recirculation Zone
CV	:	Control Volume
DES	:	Detached Eddy Simulation
DNS	:	Direct Numerical Simulation
EDM	:	Eddy Dissipation Model
FR/EDM	:	Finite Rate / Eddy Dissipation Model
FSM	:	Fractional Step Method
HPC	:	High Performance Computing
LDV	:	Laser Doppler Velocimetry
LES	:	Large Eddy Simulation
LFA	:	Laminar Flamelet Assumption
M	:	Million
PDF	:	Probability Density Function
PDPA	:	Phase Doppler Particle Analyzer
PISO	:	Pressure-Implicit with Splitting of Operators
PIV	:	Particle Image Velocimetry
PLIF	:	Planer Laser Induced Fluorescence

PVC : Precessing Vortex Core

QUICK : Quadratic Upwind Interpolation for Convective Kinematics

RANS : Reynolds Averaged Navier Stokes

RFZ : Reverse Flow Zone

RNG : Renormalization Group

RSM : Reynolds Stress Model

SIMPLEC : SIMPLE-Consistent

TNF : International Workshop on Measurement and Computation of Turbulent Non-premixed Flames

URANS : Unsteady Reynolds Averaged Navier Stokes

vs : Versus

LIST OF SYMBOLS

Basic Latin letters:

A	:	Area
A_r	:	Arrhenius pre-exponential factor
D	:	Diameter
Da	:	Damköhler number
Da_t	:	Turbulent Damköhler number
$\overline{D}_k$	:	Mean species molecular diffusion coefficient
E_r	:	Arrhenius activation energy
F	:	Fuel
f	:	Precession frequency
g	:	Gravitational force (9.81 m/s^2)
h_s	:	Enthalpy
k	:	Turbulent kinetic energy
O	:	Oxidizer
p	:	Pressure
P	:	Products
P_k	:	Source term
r	:	Radius
R	:	Radius of swirler
$R_{swirler}$	:	Outer radius of swirler
Re	:	Reynolds Number
S	:	Swirl number
S_g	:	Geometric swirl number

S_L	:	Laminar flame speed
St	:	Strouhal number
Sc_{kt}	:	Turbulent Schmidt number
S_{ij}	:	Strain tensor
T	:	Temperature value
t	:	Time variable
U	:	Velocity magnitude
U_θ	:	Tangential velocity
U_a	:	Axial velocity
U_r	:	Radial velocity
u'	:	Turbulence intensity
$V_{k,i}$	:	The diffusion velocity of the species
Y_k	:	Species mass fraction
Z	:	Mixture fraction
$x\,,y\,,z$	:	Cartesian coordinates
$i\,,j\,,k$	:	Tensor coordinates

Greek letters:

$\Delta\tau$	:	Time step size
δ_F	:	Laminar flame thickness
δ_{ij}	:	Kronecker delta
π	:	Pi number
ε	:	Eddy dissipation rate
η_k	:	Kolmogorov scale
ϕ	:	Any scalar
$\bar{\phi}\,,\ \phi'$	:	Mean and fluctuation of any scalar

$\tilde{\phi}$, ϕ''	:	Favre mean and Favre fluctuating part of any scalar
μ	:	Viscosity
ν	:	Laminar viscosity
ρg_i	:	Body force
τ_{ij}	:	Stress tensor
τ	:	Time scale
$\tau_{eddy\ time}$	:	Eddy turnover time
τ_0	:	Integral time scale
τ_t	:	Turbulent time scale
τ_{ch}	:	Chemical time scale
$\dot{\omega}_k$	:	Reaction rate
β_r	:	Arrhenius temperature exponent
∅	:	Equivalence rat

CHAPTER 1

INTRODUCTION

1.1 General information

Swirl flows are very common both in engineering applications and in climatic behaving. While tornadoes are example for natural swirling flows some reacting flows such as internal combustion engines or gas turbine combustors are swirling flows for engineering applications. Because its various advantages like a better stabilization or reduction of the flame length, swirling flow one of the key design parameter of gas turbine engine combustors which is the main interest of investigating of this topic.

Creating a swirl motion in a combustion chamber helps reactants for better mixing thus effectively burning. With recirculation effect, hot products heat up the fresh gasses and unburnt reactants get some extra time for burning. This motion helps to reduce the flame length which makes an opportunity to decrease the length of combustion chamber. Although the length of combustion chamber is not crucial for some ground applications like a furnace burner, it is really an important design parameter for a gas turbine application because of the rode length. The length of combustion chamber also affects the total length of the engine which ends up with performance of the engine for drag issues on aerial applications [1].

Another effect of a swirl motion is its controlling power on flame stabilization. On aerial applications, continuesthrust is so crucial since the aerial vehicle can crash in to ground. By holding hot products near to the fresh gasses, recirculation motion makes the flame held[1].

There is a schematic of a liquid fueled gas turbine engine combustor in Figure 1. In this figure, the effect of swirl motion helps to the atomized fuel droplets to be mixed

while the recirculation effect decreases the length of flame for efficiency of combustion and combustor volume [2].

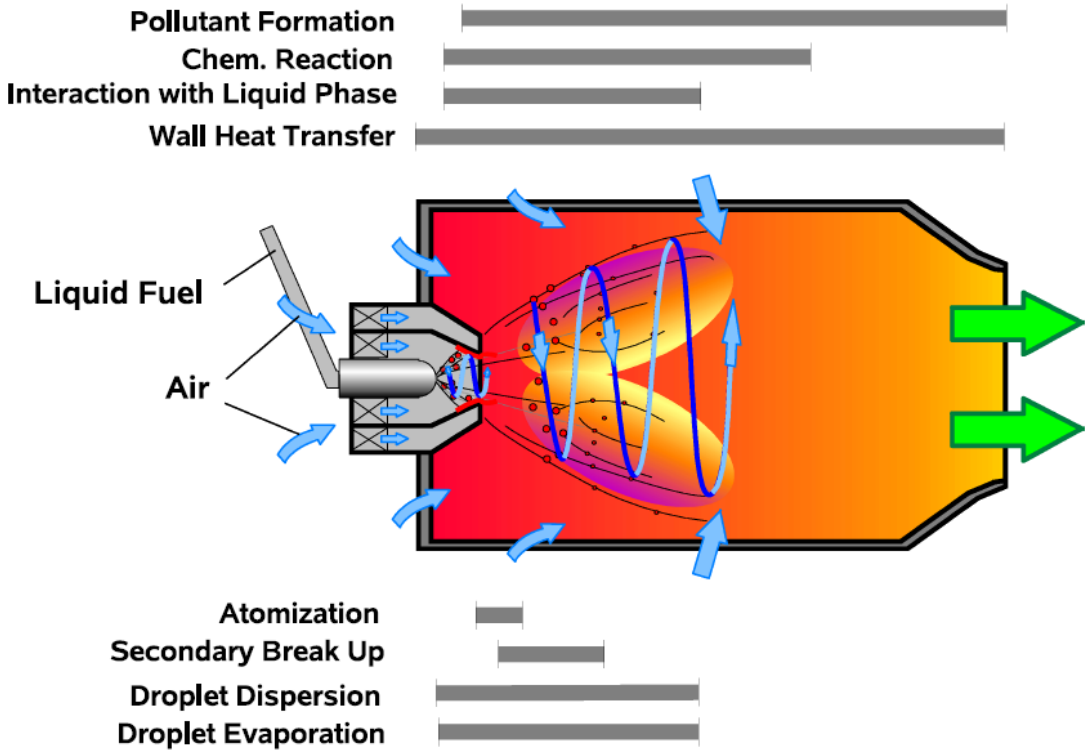

Figure 1.Swirl and recirculation motion in an aerial engine combustor [2]

However the swirl motion is very helpful effect for interested combustion applications, because of its complex aerodynamic structure it is hard to be modeled even without chemistry. Although some geometrical dimensionless parameters like swirl number gives an idea about swirl motion, its behaving shall be observed when it is coupled with chemistry and turbulence effects.

Experiments are one of the highest budget items in a design projects. Testing of every combustion chamber for its efficiency is not applicable or very hard and expensive to do. In order to decrease the number of experiments, thus to decrease the budget, engineers are driven to simulations. For a trustable and meaningful simulation, a right configuration for flow simulation should be searched by the help of experimental values. Further the simulations are verified, the reliability of the simulation results will increase.

1.2 Scope of the thesis

A Small, light weighted and cheap combustor is always desired due to low drag index for flying systems. Swirling flows allow a better mixing in small distances while keeping the reactants longer in combustion area by increasing combustion efficiency and decreasing emissions. Mixing of hot gasses with fresh combustible mixture is also possible with swirling flow which increases the combustion efficiency further. However aerodynamics of a swirling flow is very complex. In combustion processes, a strong coupling with aerodynamic effect and reaction effect occurs in flow. Although swirling flows are studied very much due to its wide application area in combustion systems, existing of high level of turbulence(which is still has no mathematical definition), mixing and combustion phenomenon (which is highly depended on flow state and its turbulence) make predictions difficult to do. Therefore, further understanding is needed for a better design guide. The thesis aims at investigating the coupling between swirl flow and reactive flow and capability of Unsteady Reynolds Averaged Navier Stokes calculation for these kinds of problems. Because of its similarity to gas turbine engines, non-premixed TECFLAM test case is studied. Wide experimental library helped to study the case deeply. The findings of the study will help to simulate a combustion chamber with swirl injector. Since this work is done for industrial applications, quicker simulation methods like Reynolds Averaged Analogy or time dependent solution of it, is studied while Large Eddy Simulation is known for its promising results [3].

Studies carried out in this thesis are outlined below:

In the following section of this chapter, the other studies and their findings are investigated.

In Chapter 2, theory lies on background of this work is summarized. Starting points of the study is outlined.

A definition of the problem and case studies are given in Chapter 3. Meshing of geometry, boundary conditions, turbulence models, chemistry models and solution methods are outlined in Chapter 4.

Chapter 5 includes the results of the simulations. Since the work is done step by step, Chapter 5 has subheadings for every part of the work.

Finally, discussions and conclusions about the findings in this thesis are indicated and future works which can be performed are mentioned in Chapter 6.

1.3 Literature Survey

Combustion is one of the fundamental physical processes in everyday life. 80% of the energy comes from combustion of liquids, solids and gases. Thus, improving the efficiency of combustion will certainly decrease energy budgets and pollutions. In order to solve the combustion problem, problems are classified [4]. Modeling and solving of non-premixed turbulence combustion is the main objective of this thesis.

Turbulence and chemistry models, boundary conditions, solution methodology must be clarified to solve a combustion problem properly. Various studies are available for the approach to the problem.

Flame stabilization is one of the key problems in combustors [1,5- 7]. Temperature, flow speed and mixture ratio of reactants affect the burning and ignition mechanism. Once the flame is ignited, flow speed and mixture ratio of the incoming reactants control the burning rate. Several stabilization mechanisms are used to hold the flame. The proper stabilization mechanism depends on inlet speed of reactants. If the flow speed is lower than laminar flame speed, flame is stabilized by a triple flame or a rim flame. If the flow speed is much higher than laminar flame speed a method should be applied to stabilize the flame. One of the most common methods is to employ a pilot flame which is a premixed flame and burns in every inlet flow condition. One other solution is to locate a bluff body or dump geometry which causes a recirculation zone.This bluff body geometry causes a wake at the back of the geometry which slows the flow and recirculates it. This effect gives reactants some time for combustion. A hot recirculating zone heats up the reactants to ignite incoming flow.The flame may be attached to the geometry. Further the flow become faster, flame can detach from the bluff body and lift off or even blow off. Flame holders are good candidates for holding the light in a desired position. Another method is creating a swirling flow which provides a low speed region on the combustion chamber axis. Swirl stabilized flames are used in large powers and inlet flow speeds.

To prevent the flame from extinguish, a recirculation should be exist in combustion zone. Flame holders one of the basic design and geometric way of creating a recirculation zone. However, it is not suitable for wide Reynolds number range. Reynolds number defined as [8]:

$$\mathrm{Re} = \frac{\rho U D}{\mu} \tag{1.1}$$

where ρ is density of the fluid, U is velocity of the fluid, D is characteristic length or diameter, μ is viscosity of the fluid.

Another option to retain a recirculation zone is creating a swirl flow. An azimuthal velocity causes a low pressure region in the middle. Therefore hot species heat up the fresh gases and hold the fire in middle region. The degree of the swirl flow is characterized with swirl number. It is introduced by Beer and Chigier [9] and simplifications are done by so many academicians. The simplified form is defined as:

$$S = \frac{\int \rho U_\theta U_r r dA}{R \int \rho U_r^2 dA} \tag{1.2}$$

where R is radius of the nozzle, U_θ is tangential component of velocity and U_r axial component of velocity. Thus, the definition is actually the dimensionless ratio of the momentum fluxes. Which is defined as :

$$S = \frac{\text{axial flux of the swirl momentum}}{\text{axial flux of axial momentum times equal nozzle diameter}}$$

Swirl number with Reynolds number and Strouhal number define the properties of flow in dimensionless form. Strouhal number is defined as [4]:

$$\mathrm{St} = \frac{fD}{U} \tag{1.3}$$

where f is precession frequency.

Turbulent Damköhler number is another important parameter for non-premixed turbulent combustion flows. To describe turbulence – chemistry interaction ratio of a characteristic flow time to a characteristic chemical time, Damköhler number (Da) is defined. Due to lack of information about any reference length scales or time scales,

a chemical time scale can be compared with a characteristic turbulence time. Therefore turbulent Da is defined as [10]:

$$\mathrm{Da_t} \equiv \frac{\text{Turbulence time scale}}{\text{Chemical time scale}} = \frac{\tau_t}{\tau_{ch}} \tag{1.4}$$

Or

$$\mathrm{Da_{t,0}} = \frac{\tau_0}{\tau_{ch}} = \frac{(l_0/u')}{\delta_F/S_L} \tag{1.5}$$

whereu' is turbulence intensity, l_0 is integral length scale, τ_0 is integral time scale, S_L is laminar flame speed and δ_F is laminar flame thickness.

By choosing different reference length scales, Different Da number definitions may be made [8,10,11].The Da with Turbulent Re defines the flame regimes which can be seen in Figure 2. The Turbulent Reynolds Number is defined as [10]:

$$\mathrm{Re_t} \equiv \frac{u'l_0}{\nu} \cong \frac{k^{1/2}}{\nu}\left(\frac{k^{3/2}}{\varepsilon}\right) = \frac{k^2}{\nu\varepsilon} \tag{1.6}$$

whereν is laminar viscosity, k is turbulent kinetic energy and ε is dissipation rate.

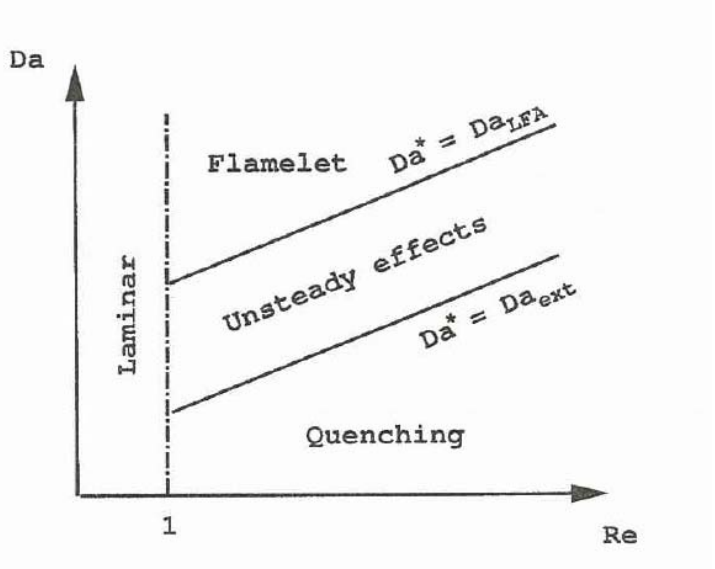

Figure 2.Schematic of non-premixed turbulent combustion regimes as a function of Damköhler Number and Turbulent Reynolds Number. (“LFA” for Laminar Flamelet Assumption and “ext” for extinction) [8,11]

Combustion process includes high intensity. To stabilize the flame, swirling flows are used in combustion applications for years. As a result of toroidal recirculation zone, the flame instability is improved. This effect also reduces the combustion length by producing high shear forces in mixing layer. However it is widely used, because of its complexity, swirling flows are poorly understood [1,8,11].Swirling flow can be created by adding momentum to both in axial way and tangential way. Two types of swirl combustor may be found in literature [12].

The swirl burner: Swirling flow exhaust into combustion chamber. Reaction occurs generally just outside the burner exit. Sketch of a swirl burner can be seen inFigure 3.

The cyclone combustion chamber: A tangential air is injected into a cylindrical combustion chamber. Exhaust is at the end of the chamber in the center.

Cyclone combustion chamber is generally used for hard burningreactants such as brown coal or damp vegetable refuse. Since the aerial applications need fast and efficient burning, this combustion chambers are not further investigated in the thesis.

Swirl burners create centrifugal force thanks to tangential inlet at injector enter. Generally no data can be taken from inside the burner or injector. Also, the difficulty to take pressure data at the exit of the burner generates errors in calculating swirl number. However, geometrical calculation is another way. This geometric swirl number is defined by Claypole and Syred [15] as:

$$S_g = \frac{R_0 \pi r_e}{A_t} \frac{(\text{Tangential Flow Rate})^2}{(\text{Total Flow Rate})^2} \tag{1.7}$$

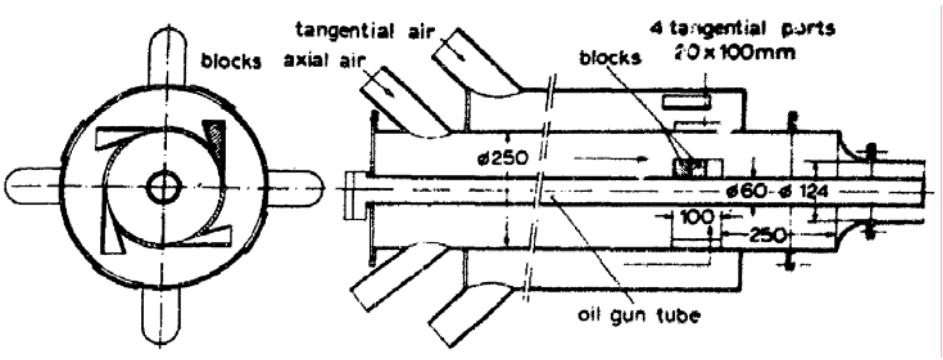

Figure 3. Sketch of a swirl burner [13]

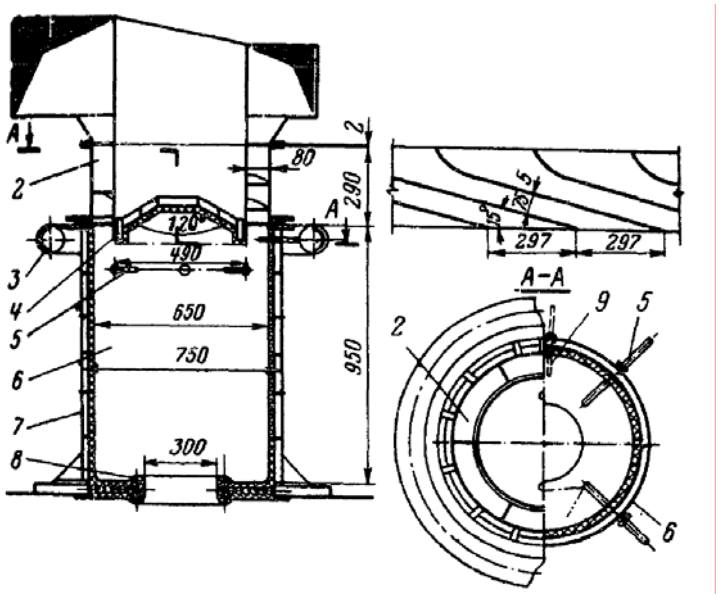

Figure 4.Sketch of a Russian Enin Cyclone Chamber.1.Secondary air box, 2.vortex ring, 3. Gas collector, 4.Furnace roof, 5.Oil atomizers, 6.Cyclone chamber, 7. Water cooled casing, 8. Outlet throat, 9.Electrical ignition. [14]

The tangential velocity also creates a low pressure region in the center of the flow. This pressure distribution in radial direction generates a recirculation zone. The velocity distribution and pressure distribution are damped in axial direction. The formation of recirculation can be seen in Figure 5. This recirculation is named as Central Recirculation Zone (CRZ) [1,3,9,12,16-18]. Spatial distribution of streamlines in a swirl burner exit is shown in Figure 6. The CRZ can be seen clearly. After a vortex generated by axial and tangential velocities in high swirl number flows, vortex breakdown mechanism is also generated due to the dynamical effects[19]. Instabilities due to shear layers make vortex breakdown mechanism highly unstable and sometimes unsteady. Center location of vortex core may change in time and turn around the axis line. This effect is called Precessing Vortex Core (PVC) [16]. With PVC effect, vortex breakdown becomes highly time-dependent and asymmetric.Results of Large Eddy Simulation of Turbomeca DLN Injector can be seen in Figure 7. Displacement in vortex core causes another displacement in reverse flow zone (RFZ). The PVC is feed by this RFZ also [20].

Studies showed that combustion has an effect on recirculation strength. Hillemanz et al. did an experiment for a strong swirling natural gas flame. Data taken with two color LDV and mean values are investigated. Results showed that intensity of the recirculation is reduced compared to reactive case. Combustion causes a decrease in effective swirl number. The reverse flow density does not change. But radial extension is observed. A reduction in turbulent exchange is also observed in reactive case. Streamlines can be seen in Figure 8 [21].

TECFLAM studies are started by cooperation of university and research groups in order to investigate reacting swirling flows. Measurements are made for different configurations of flame. Each group has its own research area. Data library is created for tuning the simulations and understand the swirling combustion better [23-29]. In the meantime, simulations are performed with different approaches. Premixed and non-premixed flames are studied [3,7,28,30-38]. One of the first studies about non-premixed TECFLAM burner is made by Landenfeld et al. as a part of TECFLAM project [28]. The configuration of the TECFLAM in this study is listed as; 150kW total thermal power, 180m3/h air stream and 15m3/h fuel (methane) stream where swirl number is 0.95. In this work, 2D analysis has been performed by using SIMPLE algorithm. Beta-PDF chemistry model with k-epsilon turbulence model are chosen because of their simplicity. 50x60 grid points defined with symmetry axis. Swirler has not been meshed. Instead, an inlet definition is made by a correction with experimental data. Results are a bit far away from experimental values. Since the measurement data itself given in the inlet, flow distribution near to burner is very close to measurements. Temperature distribution is also over estimated in most of the chamber regions. Since the study is done by 2D steady state approach, there is also no information about so called Processing Vortex Core.

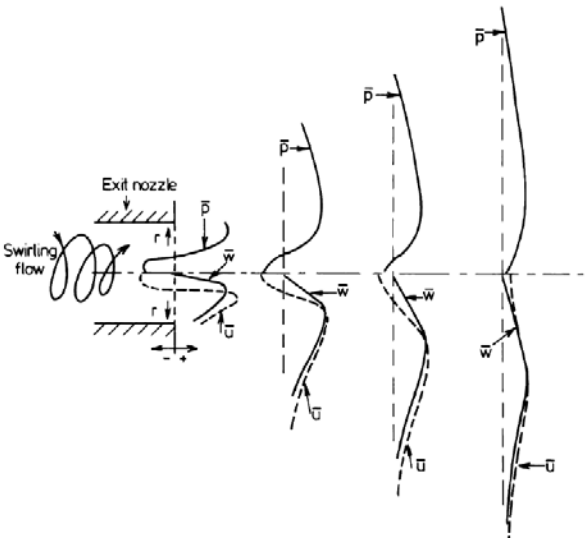

Figure 5. A Schematic view of central recirculation zone in swirling flow [17]

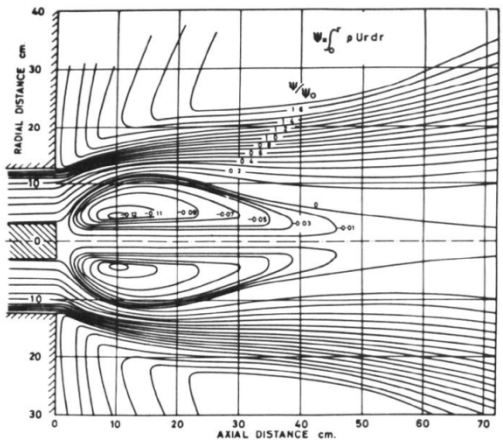

Figure 6. Spatial distribution of streamlines formed by swirling jets [13]

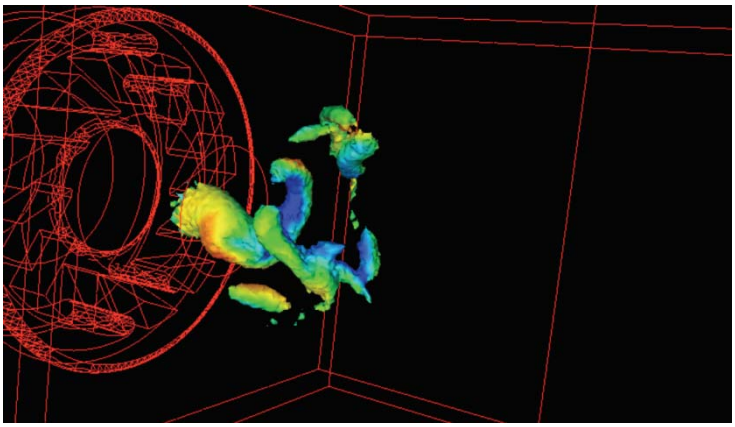

Figure 7. Cold flow dominated by a large PVC. Pressure isosurface colored by velocity [22]

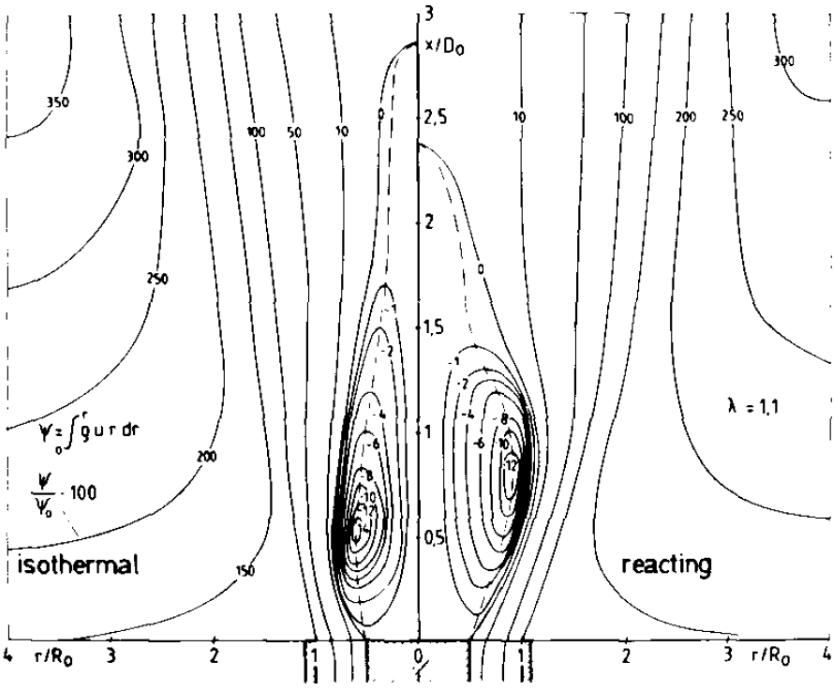

Figure 8. Streamline pattern in isothermal and reacting case [21]

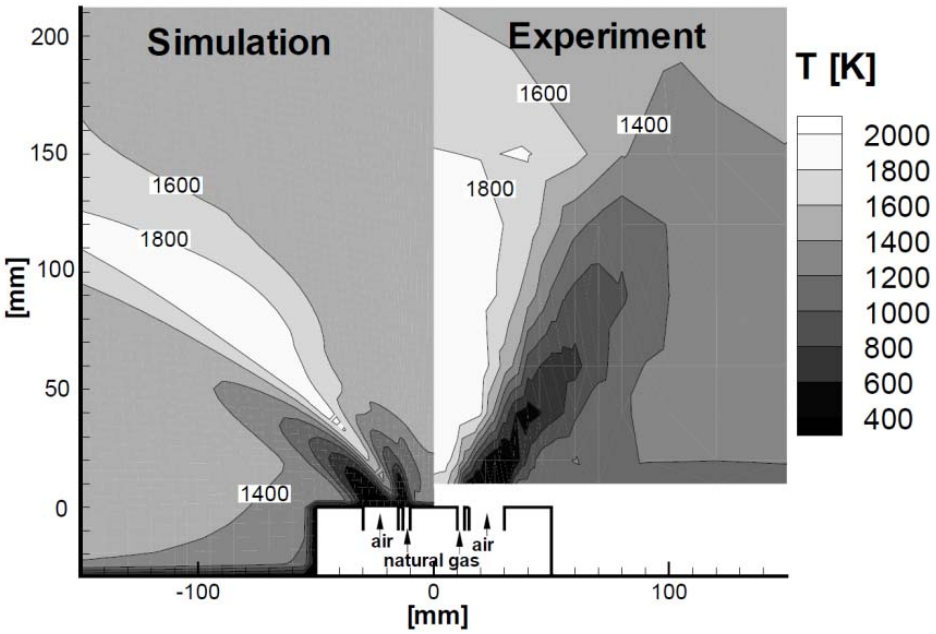

Figure 9. Favre-averaged mean temperatures. Right side: experiment, Left side: simulation [24]

Another study is done by Meier et. al [24] again as a part of TECFLAM project. The details of the TECFLAM configuration are: 150kW thermal power of system with 0.9 swirl number, 180m3/h air stream and 15m3/h fuel (methane) stream where flame Reynolds number is 42900. Commerciallyavailable Fluent 5 code is used with 180x80 grid points and axis-symmetric definition. Second order upwind discretization scheme is chosen. It is stated that, the solution is both mesh independent and turbulence model independent. Results of Reynolds Stress turbulence model are given. Presumed β-PDF chemistry model with equilibrium definition is used. Another note gives the information about finite rate chemistry solutions. It is stated that, results are very much similar compared to β-PDF model. Radiation model is also taken into account since it is believed that one third of the thermal energy gone by radiation (Reference is given to private communications made with R. Koch). The inlet boundary is given at the burner exit while it is tuned with experimental data at 5mm above of the burner exit. Investigated results show that, numerical solutions create an open recirculation zone while it is closed in the experimental data. Author tried to do the simulation with different turbulence and combustion models but failed to generate a closed recirculation zone. Comparing of the simulation data and experimental data is shown in Figure 9.

Connected to this work, another study presented in TNF5 shows the velocity profiles and mass fractions of the 2D axis-symmetry solutions. From the results of the simulations, it can be seen thatthe velocity profiles near to the burner exit are very close to experimental results. ON the other hand, the results at the downstream of the chamber are not identical with the experimental values. This is because; inlet velocity is defined by the values of experimental data close to burner exit. The rest of the domain is computed inaccurately [39]. Calculations for a similar non-premixed TECFLAM burner are made by S. Repp et al. [35]. Performance of presumed β-PDF and Monte-Carlo scalar PDF models are compared. It is shown that both models give similar accuracy in the mean field while presumed PDF need much less computational power and Monte-Carlo PDF allows to capture well the turbulence-chemistry interactions and strong finite-chemistry effects like local extinction.

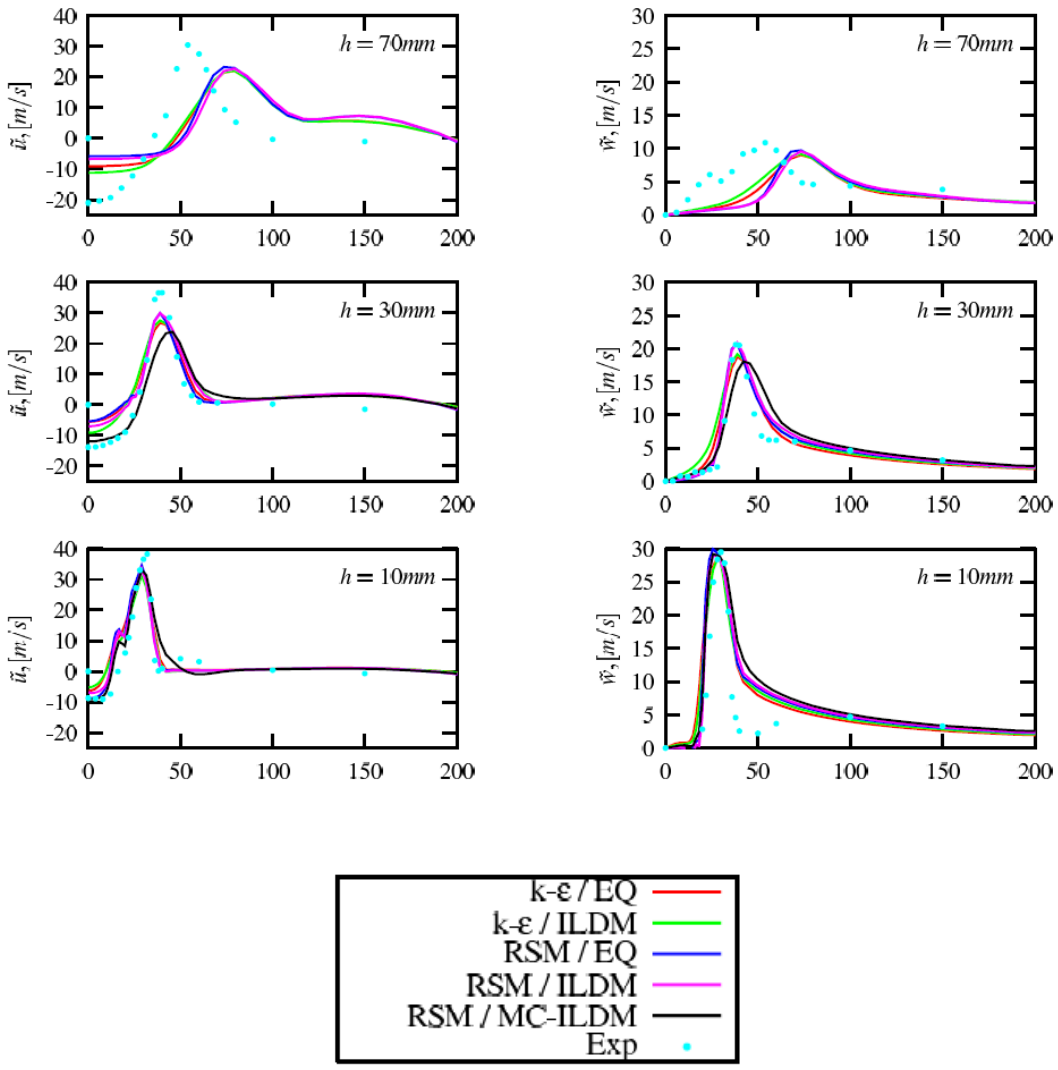

Figure 10. Velocity profiles of 2D Axis-symmetry simulation results done by Meier et al. presented in TNF5 [39]

A study made by W. Yand and J. Zhang [36] proposes two PDF models for methane-air combustion. Both PDF models are formulated by using four-step reaction mechanism. The First reaction mechanism includes 22 species while the second one includes 18 species. Results are obtained by simulating TECFLAM S09C test case where the flame is non-premixed, thermal power is 150kW and swirl number S is 0.9. Steady calculations are performed with 2D axis-symmetry grid. Very similar results are gathered with two of the presumed PDF models. Almost no differences is observed between two models.

The study made by Meier [24] is restudied by Frassoldatiet. al. [32] in 2004 by using a newer version of commercially available code Fluent 6.0. Similar approaches are made such as 2Daxis-symmetry solution by using k-epsilon turbulence model. Except all other settings, two-step finite rate eddy dissipation model is used as chemical approach. In this approach, methane burns it two steps. Results show good agreement with experiments. The recirculation loop is closed and temperature isolines nearly attached. Figure 11 shows temperature distribution of this new calculation and experimental data.It can be seen that recirculation zone is a bit longer in calculated data. Since the solution is mesh density independent, this may be because of missing tangential effects and the weakness of k-epsilon turbulence model in swirling flows.

Similar approach is made by A. Khelil et al. [34]. The pollutant emissions NOx are predicted with Reynolds Stress Model by presumed β-PDF model. Although Meier et al. could not see any significant difference between turbulence models and failed to predict CRZ in their past studies [24,39],Khelil et al. was able to capture CRZ by using RSM and PDF models. Temperature field comparison between experimental data and 2D axis-symmetry steady simulations can be seen inFigure 12. A, B and C indicate with same order: CRZ, mixing zone and outer recirculation zone.

The study made by Frassoldati and Khelil shows that, a 2D axis-symmetry solution by using RANS model gives identical solutions if only right boundary conditions can be applied. However, boundary conditions cannot be known in such details. In order to overcome this problem, the approaches made to solve the problem should be less independent from experimental data. 3D calculations should be performed by including swirler calculations. By performing 3D calculations, tangential effects can be observable also.

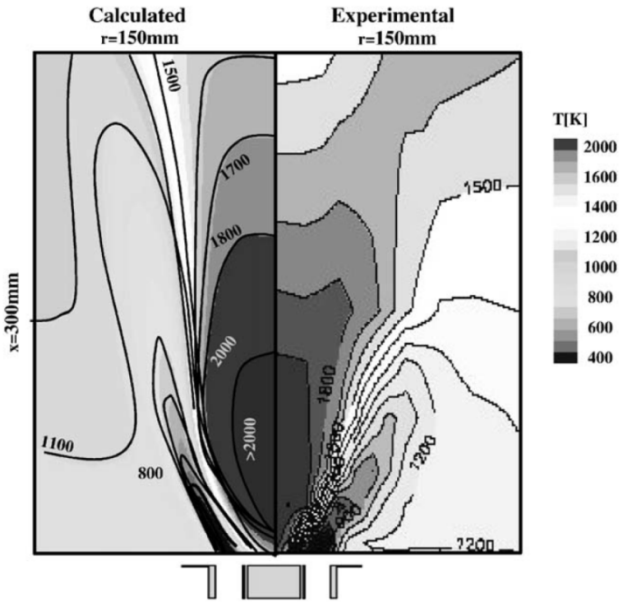

Figure 11.Favre-averaged temperature field calculated by 2D axis-symmetry, k-ε turbulence model and 2-step finite rate approach. Left side: Simulation, Right side: Experimental data [32]

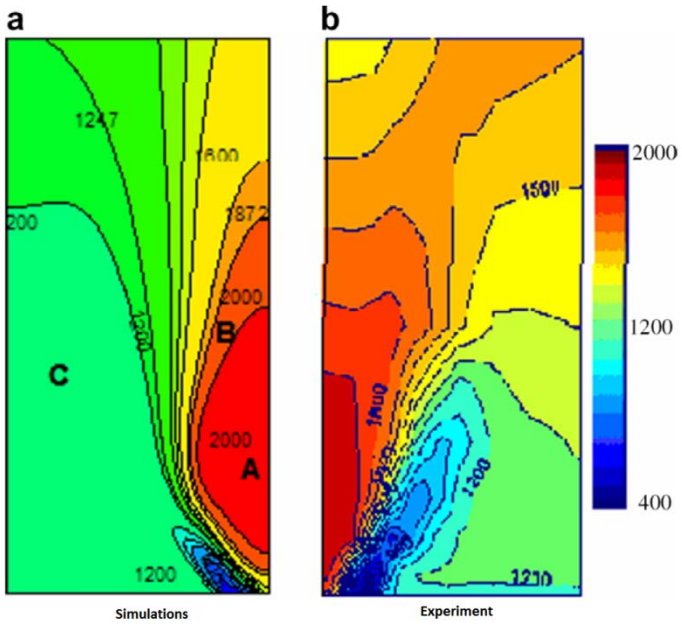

Figure 12. Favre-Averaged temperature field of 2D axis-symmetry simulations done by RSM turbulence model and presumed β-PDF combustion model (Left simulations, Right Experiment) [34]

Assessment of unsteady 3D RANS is performed by B. Wegner et al. [30]. A premixed version of TECFLAM is studied whose swirl number is 0.75 and thermal power is 30kW. Unsteady-RANS (U-RANS) calculations are made by comparing the results with LES results and experimental data. Standard k-epsilon model and second order closure is employed by using second order accurate implicit Crank-Nicolson scheme. For LES calculations, a Smagorinsky model with dynamic procedure according to Lilly was used. No special wall treatment is included in the subgrid-scale model. The author tried to perform calculations without the burner. The PVC could not be observed. Since one of the objectivesof the study was observing PVC and seeing the hydrodynamic instabilities, the burner was meshed. 8 grid points and 16 grid points in radial direction are studied. Unstable behavior is observed in both meshes but, the results were unsatisfactory near nozzle exit for course mesh. Total elements are counted nearly 800000 for fine mesh. Time step size is chosen by keeping Cell Courant Number (CFL number) order of five for U-RANS. For Large Eddy Simulations, time step size is decreased by a factor of ten. So called PVC is captured by this set of simulation which is shown inFigure 13. Results showed that, U-RANS gives better agreement with experimental data for the mean velocity field. Author refers it low mesh quality.

A. Sadiki [38] extended this work by performing LES to Sandia flame D [40], and DLR Standard Flame(Sydney flame) [41,42]. It is understood that, to perform LES, a fine mesh structure not only for flow direction but for all directions is required while URANS still gives satisfactory results with a moderate mesh. LES is good for solving large flow structures. On the other hand, very fine mesh shall be used for near wall treatments. Since the wall functions are applicable and gives pretty fine solutions, URANS is less mesh dependent near wall solving if nothing happens in the wall. In order to increase the results quality, hybrid LES-URANS may be used in which RANS is used near wall treatment and LES is used for rest of the domain.

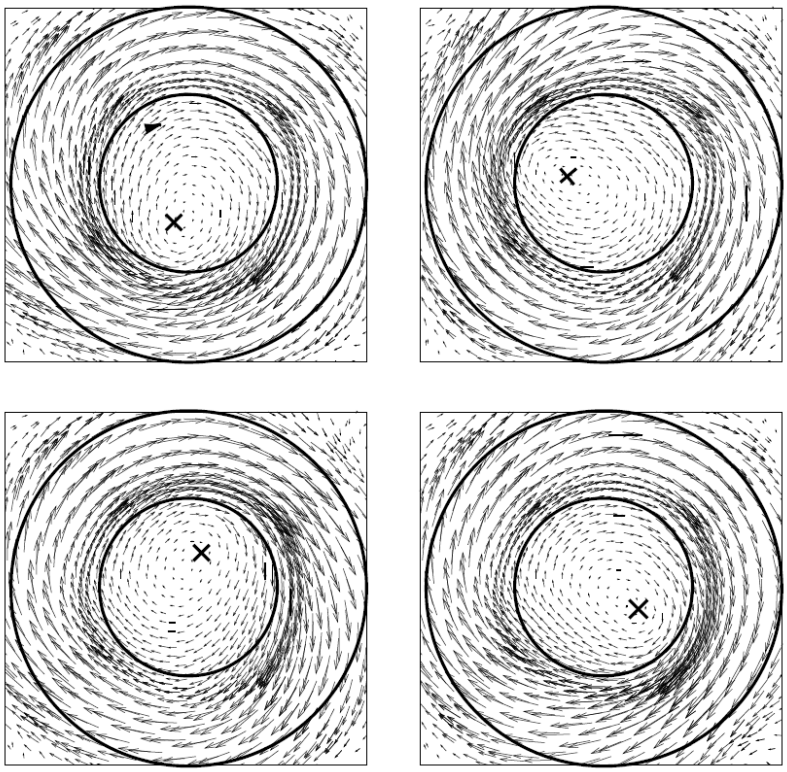

Figure 13. Sequence of snap shots taking from U-RANS of 30kW premixed case showing vector plot of velocity in a plane axial location=30mm. The Swirler annulus is indicated by the two concentric circles. The approximate instantaneous vortex center and precession direction are also indicated [31]

Another study is made by E. Schneider et al. [37] to compare the solver configurations by applying U-RANS for solving premixed TECFLAM burner whose swirl number is 0.75. Reynolds Stress Model (RSM) and k-epsilon model are compared for turbulent models. For flame front capturing G-equation model and Bray-Moss-Libby (BML) model are compared. For chemistry, ILDM method, CPVA method and Equilibrium method are used. Effect of radiation is also tested for equilibrium chemistry. Author realized that, no specific advantage between combustion models is observed. For flame front capturing models, no remarkable results between G-equation model and BML model while BML approaches are one third times shorter than G-equation approaches. Both turbulence models showed comparable performance. It is noted that, no remarkable advantages of second-moment turbulence closure is noticed in results of mean flow and turbulence characteristics. Radiation is observed to have no effect on flow field but it affects

temperature distribution. Study is continued with a model GT combustion chamber analyses. Grid independent solutions are gathered with 55000 elements for U-RANS. Results showed that, k-epsilon model damps radial and tangential effects of the flow in forward axial locations. High turbulent diffusion causes fast homogenization and results with too smooth velocity profile in upper position of the burner exit. Both turbulent models under estimates turbulent kinetic energy near to burner exit locations. Since kinetic energy agrees better by increasing axial position this may be a result of logarithmic law wall function which is applied in computations. BML approach for different cases shows better performance.

One of the study including non-premixed TECFLAM test case is done recently by Simon Ayache as a part of PhD Thesis who advised by E. Mastorakos [3]. The aim of the thesis is to perform validation simulations for CMC combustion model derived by Selwyn Collage of Cambridge. Large Eddy Simulations are done for TECFLAM S09C test case. In this test case, a swirled non-premixed combustion chamber, whose swirl number is 0.9 mean length of the chamber is 1200mm, diameter of the chamber is 500mm and thermal power is 150kW, is taken into account. Measurements are taken through a window by traversing the burner in axial direction. Velocity data are taken with LDV at the EKT (Energie und Kraftwerstechnik) University of Darmstadt by Christoph Schneider, Andreas Dreizler, E.P. Hassel, Johannes Janicka [28,39,43]. Laser based imaging measurements are done at the PCI (Physikalisch-ChemischesInstitut) University of Heidelberg by Stefan Böckle, Jan Kazenwadel, Thomas Kunzelmann, Christof Schulz, Jürgen Wolfrum [23-28,44].Raman scattering is applied at the DLR [23,24].

In Ayache's PhD thesis, the whole combustion chamber has not beenmodeled. Instead, 350mm of the combustion chamber is taken into account by applying nearly 7.9million (303x162x160)O-grid mesh which is very fine near to the burner exit. Swirl burner is also taken into account in order to investigate PVC. Large Eddy Simulations are performed for non-reacting and reacting cases by using code Precise. 0-D and 3D CMC combustion models are applied. The mechanism of the CMC code is illustrated in Figure 14. Further information about CMC solvers and code Precise can be found in Ref. [45,46].Reduced ARM2 derived from detailed GRI-Mech3.0 mechanism is used which contains 19 species and 15 reactions [47]. There is very

little information about boundary condition implementation which is very important to get meaningful results. However, it is stated that, inlet air boundary conditions are defined by an extensive parametric study. During experiments,the closest data taken near to the burner exit is from 1mm above the burner exit. The inlet boundary definitions at the air swirler inlet portsare made by using this data. 3D-CMC calculations are performed at each LES iteration with a structured grid (25x25x30) which can be seen in Figure 15. Time step for both combustion models is 5x10-6s. The CFL number for this time step is varying around 0.35. It is noted that time averaging has been done for 195ms in 0D-CMC calculations while for 3D-CMC calculations, averaging started after 15ms and conducted for 45ms. Almost the same computation power is used for both cases. For 0D-CMC, 1ms has achieved by 93minutes computation whileit takes 253minutes for 3D-CMC model. There are no mean contours for 3D-CMC calculations in the thesis.

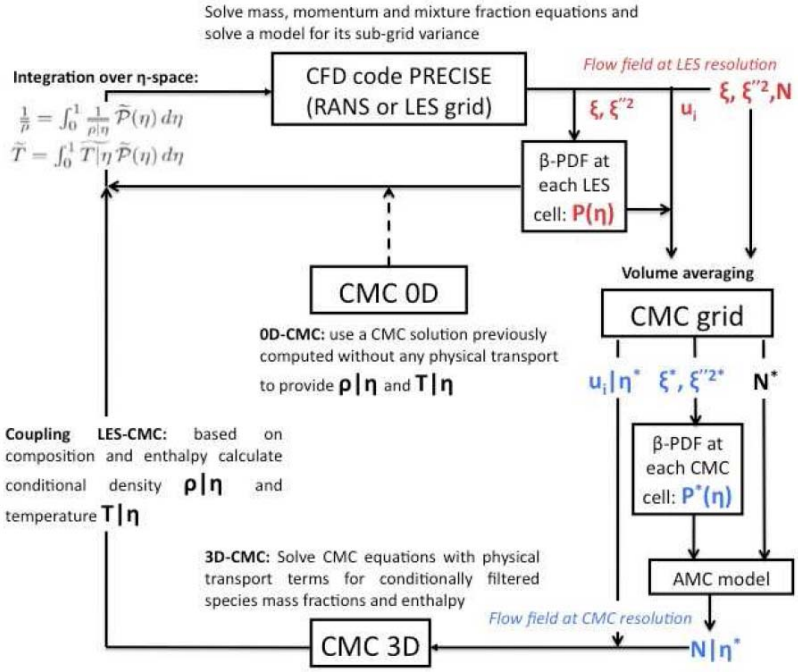

Figure 14. Schematic showing of the coupling of the CFD and CMC solvers according to the type of computation: 0D-CMC or 3D-CMC [3]

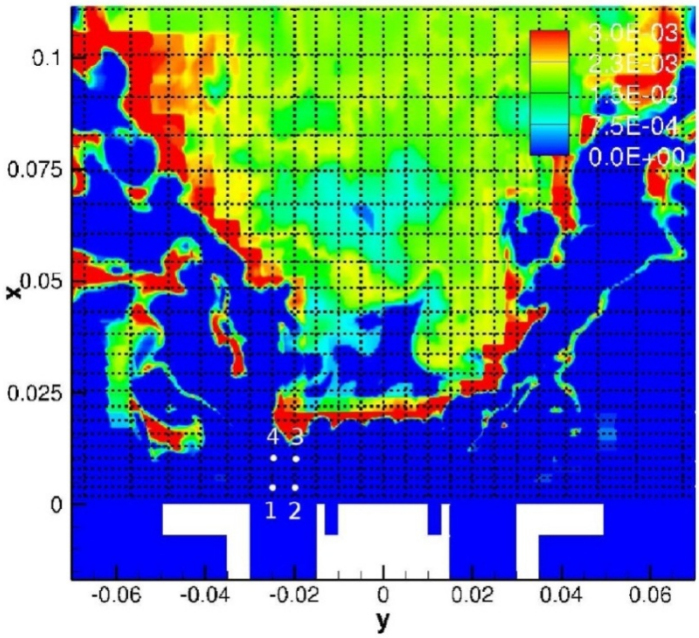

Figure 15. Mesh used for 3D-CMC calculations performed by S. Ayache [3](Axis in meter).

From results given in the thesis, it can be seen that not an exact mean data could be gathered for 0D-CMC simulation since the mean axial velocity contour is not symmetric. This may be because of problems nature, or most probably short computation duration or some numerical errors. It should be noted that, there is no mean contours for 3D-CMC simulation which is done for 45ms flow time. From the mean velocity contours, one can see thatzero axial velocity isolines ends at very before the computational domain's outlet. Another recirculation zone also occurs very near to chamber's upper side. This may indicates that flow is not formed in this short domain. From velocity gradients given in the thesis, one can say that, LES was not able to predict the central recirculation zone satisfactorily. 0D-CMC model was able to capture peak points of the flow velocity. However, at 70mm axial direction, both models failed to predict the peak velocity where 3D-CMC underestimates the magnitude and 0D over estimates it. 0D CMC model takes shorter time while giving better results in velocity distribution. On the other hand, temperature distribution could be captured better compared to 3D CMC model. 0D CMC simulations calculate a reaction zone in the burner exit middle which is not true. Higher temperature values at radial direction may be the cause lack of radiation model.

The scope of this work is to investigate the effect of combustion chamber modeling. A faster strategy is desired in industry calculations since a very limited computational power exist. RANS based models will be used instead of long time needed LES calculations. Thus, a solution with coarser mesh will be investigated by using different turbulence and combustion models. Further study will be done for denser mesh in order to see the effects of numerical diffusion. Unsteady RANS will be performed to capture PVC and instability effects. Length of computational domain will also be investigated to see if there is any unclosed recirculation occurs and if they affect the primary zone or not. To see the effect of combustion model, presumed PDF model and species transport models are performed. Study is done in currently available ANSYS Fluent code.

CHAPTER 2

MATHEMATICAL MODELING

2.1 Governing Equations

The molecular structure of fluids shows no resistance to external shear forces. Therefore, every single action creates a motion for fluid substances. By continuum assumption, all fluids shall obey the laws of motion. Thus, conservation of mass, momentum and scalars (energy, species etc.) should be sustained for a control volume. Conservation equations for Cartesian coordinates can be written as followings [48-50]:

For conservation of mass:

$$\frac{\partial \rho}{\partial t} + \frac{\partial (\rho u_i)}{\partial x_i} = \frac{\partial \rho}{\partial t} + \frac{\partial (\rho u_x)}{\partial x} + \frac{\partial (\rho u_y)}{\partial y} + \frac{\partial (\rho u_z)}{\partial z} = 0 \tag{2.1}$$

For conservation of momentum:

$$\frac{\partial (\rho u_i)}{\partial t} + \frac{\partial (\rho u_j u_i)}{\partial x_j} = \frac{\partial \tau_{ij}}{\partial x_j} - \frac{\partial p}{\partial x_i} + \rho g_i \tag{2.2}$$

For conservation of scalars:

$$\frac{\partial (\rho \phi)}{\partial t} + \frac{\partial (\rho u_j \phi)}{\partial x_j} = \frac{\partial}{\partial x_j}\left(\Gamma \frac{\partial \phi}{\partial x_j}\right) + q_\phi \tag{2.3}$$

2.2 Turbulence Modeling

Many problems encountered in engineering problems are turbulent flow [48-50]. Turbulent flows show same characteristics for different flows. Parametric studies like Reynolds Numbers guides engineering approaches for the problems encountered. Whether turbulence is known for its existence, it is the last unexplained problem of

classical physics. Thus, it needs to be modeled. Unfortunately there is still no approach which covers all the problems. Instead, different solving approaches shall be applied for every kind of problem. Models used in this study will be explained under this title.

Depending on the problem turbulence is either wanted or unwanted phenomena. In sense of non-premixed combustion problems, due to mixing that turbulence sustain, it is most desired. However, an engineer should be aware of its effects to achieve good designs. There are some characteristic properties of turbulent flows. Turbulent flows, for example, are both 3D and unsteady. They contain a great deal of vorticity. These vorticities are called eddies. An eddy contains momentum and kinetic energy. An eddy which contains high kinetic energy, break downs into smaller eddies due to viscous forces. Smaller eddies splits into more smaller ones. This action continues until the smallest eddies are created. An eddy, whose turnover energy is equal to the energy lost by viscous forces, is called the smallest eddy. Thus, the smallest eddies dissipates into internal energy. This mechanism called eddy break up mechanism or Kolmogorov cascade named after Russian mathematician Andrey Kolmogorov. The strength of the turbulence is generally described with its intensity. Intensity is the ratio between root mean square of the fluctuations and mean value which is defined as:

$$I = \frac{\sqrt{\overline{\phi'^2}}}{\bar{f}} \tag{2.4}$$

Where ϕ is any property and can be split into mean and fluctuations:

$$\phi = \overline{\phi} + \phi' \tag{2.5}$$

The largest scale in the turbulent flow is called integral length scale, l_t. The largest scale is generally geometry dependent and usually close to characteristic size of the flow. The smallest eddy is defined by Kolmogorov and also called Kolmogorov scale, η:

$$\eta_k = \left(\frac{\nu^3}{\varepsilon}\right)^{1/4} \tag{2.6}$$

Eddy break up mechanism is first introduced by Kolmogorov [51]. Energy from bigger scale to smaller scale is calculated by dissipation of kinetic energy. The dissipation of the energy is simply the ratio of the kinetic energy dived by the time scale. For any length scale, the characteristic velocity of the length scale is defined as

$$u = u'(r) \tag{2.7}$$

Where r is the size of length scale. Then the ratio of inertia to viscous forces is defined as:

$$Re(r) = \frac{u'(r)r}{\nu} \tag{2.8}$$

Where ν is flow kinematic viscosity. It is obvious that the largest scales in a turbulent flow are not affected significantly by viscous dissipation. The inertial motion is much more dominant. However, for the Kolmogorov length scale, the inertia is equal to viscous dissipation by definition. The definition of dissipation is:

$$\varepsilon = \frac{k}{t} = \frac{(u'(r))^2}{r/u'(r)} = \frac{u'(r)^3}{r} \tag{2.9}$$

For simulation of a turbulent flow, one should check the ratio of largest scale to smallest scale. It is theoretically expressed as:

$$\frac{l_t}{\eta_k} = \frac{u'^3/\varepsilon}{(\nu^3/\varepsilon)^{1/4}} = \left(\frac{u' l_t}{\nu}\right)^{3/4} = {Re_t}^{3/4} \tag{2.10}$$

Where Re_t is the Reynolds number of the largest scale which is usually high (100 to 2000 in most combustion devices)

A difficulty dealing with turbulent flows is their broad range of length and time scales. The large scales generally geometry dependent. Random components of the fluctuations depending on the problem also create differences. Thus, studying turbulence is also problem dependent issue which narrows the usage of a DNS result. On the other hand, it is observed that somehow, small scales show similarities. Since eddy break up mechanism continues until to the smallest scales, there is a common behavior for diffusion. Large Eddy Simulations offer a 'cut off' method. As it can be seen in Figure 16, DNS computes every fluctuation of the flow. LES computes problem based part of the flow and models the homogeneous eddies while Reynolds

Averaged Navier-Stokes (RANS) models every part of turbulence assuming isotropy. More the modeling exist in solution, less the computational power is needed. Thus, RANS based solutions needs very little computational resource compared to DNS. Source needed for LES depends on chosen cut off wavelength. In another word, the fewer the eddies resolved, more the computation power is needed. Either way, power needed for LES is between that needed for RANS and for DNS. For industrial applications, RANS is the best available solution. LES can also be performed for industrial applications but only for simple cases. For more complex flows, it is only a solution method for academic studies. Further, LES is still can not be applicable for very complex physical processes such as sprays and granular flows. According to Pope, LES is an applicable solution method for some years [52].

It is noted that, the advances in numerical approaches, the difference in attitudes and practices make LES cheaper than it was. A sketch of the computer power and that needed for LES is shown in Figure 17.

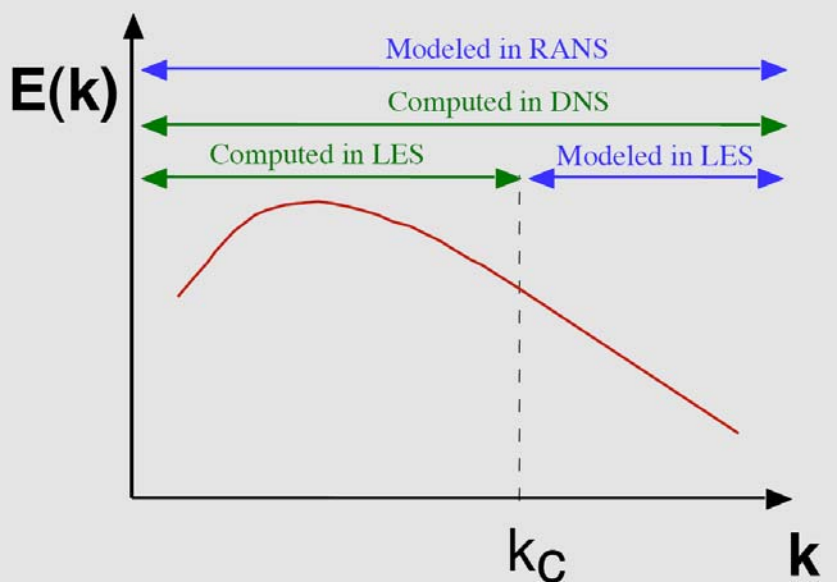

Figure 16. Energy spectrum and cut off wavelength [53]

Modeling of a part of the flow, make the whole picture a bit blurry. Sketch shown in Figure 18 for a channel flow shows the difference of a DNS resolution and LES resolution. As it is seen, large eddies are resolved with LES and smaller ones modeled. Since the little fluctuations are not resolved, the effects of them can not be seen in results. On the other hand, RANS based solutions models also the large

structures and brings just the averaged values. A sketch of velocity transition for the three types of simulations is shown in Figure 19. It can be seen that RANS is only dealing with averaged values while LES aims to capture large fluctuations. Following sections will bring short description about the simulation types.

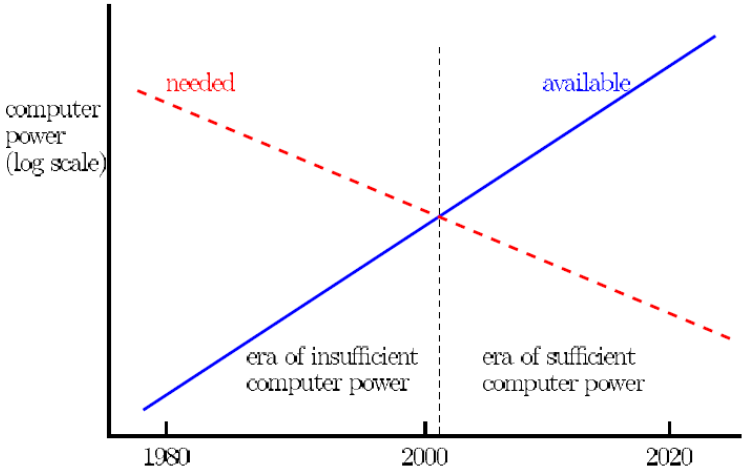

Figure 17. Sketch of the computer power available and that needed for LES as a function of time [52]

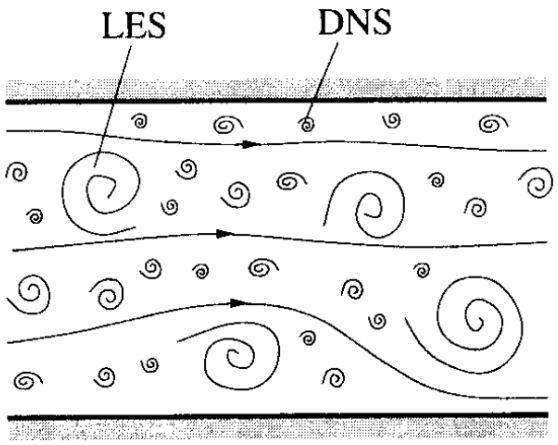

Figure 18. A Schematic view of comparison between LES and DNS [54]

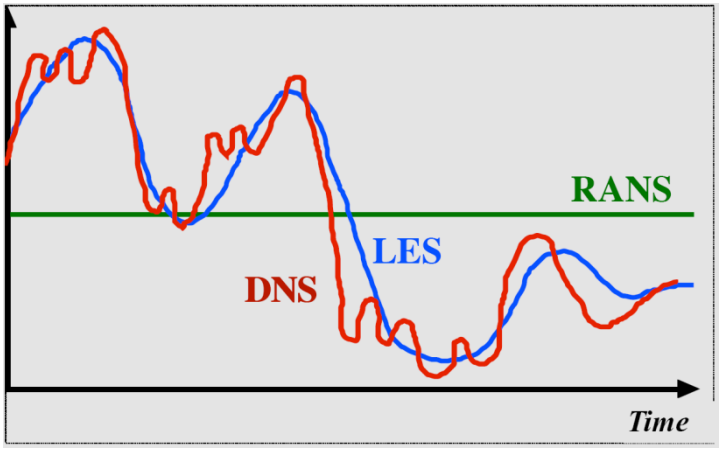

Figure 19.A sketch of velocity transition estimated by three types of simulations [53].

2.2.1 Reynolds Averaged Navier-Stokes Simulations (RANS)

This method is created because of drastic computation power needed for DNS. Instead of treating Navier-Stokes equations directly and get solutions after hundred years, engineers have chosen the way of getting mean values of the equations and having a solution soon. This method requires a splitting for average and fluctuation values. This is called Reynolds Averaging where mean values of the flow and fluctuation ones can be treated separately. Continuity equation written by Reynolds Averaging is as following:

$$\frac{\partial \bar{\rho}}{\partial t} + \frac{\partial}{\partial x_i}(\overline{\rho u_i}) = \frac{\partial \bar{\rho}}{\partial t} + \frac{\partial}{\partial x_i}(\bar{\rho}\bar{u_i} + \overline{\rho' u_i'}) = 0 \tag{2.11}$$

By constant density assumption, the equation can be simplified as:

$$\rho' = 0$$

$$\rho = \bar{\rho}$$

$$\frac{\partial \rho}{\partial t} + \frac{\partial(\rho \overline{u_i})}{\partial x_i} = 0 \tag{2.12}$$

And the momentum equation is:

$$\frac{\partial(\rho \overline{u_i})}{\partial t} + \frac{\partial}{\partial x_j}\left(\rho \bar{u}_i \bar{u}_j + \rho \overline{u'_i u'_j}\right) = -\frac{\partial \bar{p}}{\partial x_i} + \frac{\partial \bar{\tau}_{ij}}{\partial x_j} \tag{2.13}$$

Where the $\bar{\tau}_{ij}$ are the mean viscous stress tensor components:

$$\bar{\tau}_{ij} = \mu\left(\frac{\partial \bar{u}_i}{\partial x_j} + \frac{\partial \bar{u}_j}{\partial x_i}\right) \tag{2.14}$$

And the mean of a scalar quantity ϕ can be written:

$$\frac{\partial(\rho\bar{\phi})}{\partial t} + \frac{\partial}{\partial x_j}\left(\rho\bar{u}_j\bar{\phi} + \rho\overline{u'_j\phi'}\right) = \frac{\partial}{\partial x_j}\left(\Gamma\frac{\partial\bar{\phi}}{\partial x_j}\right) \tag{2.15}$$

For flows which are not incompressible, Favre averaging should be applied to avoid the difficulty of unclosed terms.

2.2.1.1 Favre Averaging

For flows where density is variable, the term $\overline{\rho' u_i'}$ appears. Thus, a correlation between density and velocity fluctuations is needed. Favre averaging, offers an averaging technique which is mass-weighted. For a quantity ϕ, Favre averaging is as follows:

$$\phi = \tilde{\phi} + \phi'' \tag{2.16}$$

Where $\tilde{\phi}$ is mean part and ϕ'' is fluctuating part. And the Favre mean of fluctuating component is:

$$\widetilde{\phi''} = 0$$

The relationship between Favre averaging and Reynolds analogy is:

$$\tilde{\phi} = \frac{\overline{\rho\phi}}{\bar{\rho}} \tag{2.17}$$

Using this definition, Navier-Stokes equations are rearranged as following:

Continuity:

$$\frac{\partial\bar{\rho}}{\partial t} + \frac{\partial}{\partial x_i}(\bar{\rho}\tilde{u}_i) = 0 \tag{2.18}$$

Momentum:

$$\frac{\partial\bar{\rho}\tilde{u}_i}{\partial t} + \frac{\partial}{\partial x_i}\left(\bar{\rho}\tilde{u}_i\tilde{u}_j\right) + \frac{\partial\bar{p}}{\partial x_j} = \frac{\partial}{\partial x_i}\left(\bar{\tau}_{ij} - \bar{\rho}\widetilde{u''_i u''_j}\right) \tag{2.19}$$

Chemical Species:

$$\frac{\partial(\bar{\rho}\tilde{Y}_k)}{\partial t} + \frac{\partial}{\partial x_i}\left(\bar{\rho}\tilde{u}_i\tilde{Y}_k\right) = -\frac{\partial}{\partial x_i}\left(\overline{V_{k,\imath}Y_k} + \bar{\rho}\widetilde{u_\imath'' Y_k''}\right) + \overline{\dot{\omega}_k} \qquad (2.20)$$

Where Y_k is species mass fraction, $V_{k,i}$ is the diffusion velocity of the species, and $\dot{\omega}_k$ is reaction rate. Then the energy equation for a combustion system is:

$$\frac{\partial\bar{\rho}\tilde{h}_s}{\partial t} + \frac{\partial}{\partial x_i}\left(\bar{\rho}\tilde{u}_i\tilde{h}_s\right) =$$

$$\overline{\dot{\omega}_T} + \frac{\overline{Dp}}{Dt} + \frac{\partial}{\partial x_i}\left(\overline{\lambda\frac{\partial T}{\partial x_\imath}} - \overline{\rho u_\imath'' h_s''}\right) + \overline{\tau_{\imath\jmath}\frac{\partial u_\imath}{\partial x_\jmath}} - \frac{\partial}{\partial x_i}\left(\overline{\rho\sum_{k=1}^{N} V_{k,\imath}Y_k h_{s,k}}\right) \qquad (2.21)$$

Where h_s is enthalpy and $\frac{DP}{Dt}$ is:

$$\frac{\overline{Dp}}{Dt} = \frac{\partial\bar{p}}{\partial t} + \overline{u_\imath\frac{\partial p}{\partial x_\imath}} = \frac{\partial\bar{p}}{\partial t} + \tilde{u}_i\frac{\partial\bar{p}}{\partial x_i} + \overline{u_\imath''\frac{\partial p}{\partial x_\imath}} \qquad (2.22)$$

This technique offers a simple and efficient route for reacting flows. However, it should be noted that there is no simple relation between Favre averaged and Reynolds averaged values. Therefore, one must take care when comparing any data.

Unclosed terms such as Reynolds stresses, species turbulent fluxes, enthalpy turbulent fluxes and laminar diffusive fluxes for species and enthalpy appear when using these approaches. Anyone who wants to solve the Averaged Navier Stokes Equations should deal with the unclosed terms. Some assumptions or modeling are required for the unclosed terms.

Assuming large turbulence level (which means large Reynolds numbers limit) helps to make some further assumptions. Molecular terms are neglected since a large turbulence level is assumed. Therefore, Laminar diffusive fluxes for species or enthalpy are dropped. However, they can also be modeled which is generally as:

$$\overline{V_{k,\imath}Y_k} = -\overline{\rho D_k\frac{\partial Y_k}{\partial x_\imath}} \approx -\bar{\rho}\bar{D}_k\frac{\partial\tilde{Y}_k}{\partial x_i} \qquad (2.23)$$

Where$\bar{D}_k$ is a mean species molecular diffusion coefficient. And the laminar heat diffusion flux in the enthalpy equation is rewritten as:

$$\overline{\lambda\frac{\partial T}{\partial x_\imath}} = \bar{\lambda}\frac{\partial\tilde{T}}{\partial x_i} \qquad (2.24)$$

The species and enthalpy turbulent fluxes can be closed by using classical gradient assumption:

$$\bar{\rho}\widetilde{u_i''Y_k''} = -\frac{\mu_t}{Sc_{kt}}\frac{\partial \tilde{Y}_k}{\partial x_i} \tag{2.25}$$

Where Sc_{kt} is turbulent Schmidt number for species k, μ_t is turbulent viscosity. Schmidt number is a dimensionless number which defines the ratio of momentum (viscous) diffusivity to mass diffusivity. It can be written as:

$$Sc_k = \frac{\mu}{\rho D_k} \tag{2.26}$$

And the turbulent viscosity comes from turbulence models. Turbulence models are needed in order to close the Reynolds stresses terms, $\widetilde{u_i''u_j''}$. High Reynolds number assumption gives right to assume homogeneous and isotropic turbulence which is proposed by Boussinesq [50]. For Newtonian fluids, using viscous tensor τ_{ij} expression, Reynolds stresses are described as:

$$\overline{\rho u_i'' u_j''} = \bar{\rho}\widetilde{u_i''u_j''} = -\mu_t\left(\frac{\partial \tilde{u}_i}{\partial x_j} + \frac{\partial \tilde{u}_j}{\partial x_i} - \frac{2}{3}\delta_{ij}\frac{\partial \tilde{u}_k}{\partial x_k}\right) + \frac{2}{3}\bar{\rho}k \tag{2.27}$$

Where δ_{ij} is the Kronecker symbol and k is turbulent kinetic energy. Turbulent kinetic energy is described as:

$$k = \frac{1}{2}\sum_{k=1}^{3}\widetilde{u_i''u_j''} \tag{2.28}$$

Viscosity of the flow is redefined as:

$$\mu_{eff} = \mu + \mu_t \tag{2.29}$$

Now a definition is needed for turbulent viscosity, μ_t, and it lies in turbulence model.

The one of the most important parameters, which should be closed, in turbulent combustion models are species chemical reaction rates $\overline{\dot{\omega}_k}$. Closure of this parameter will be investigated in combustion modeling part.

2.2.1.2 Standard k-epsilon Turbulence Model

k-epsilon or k − ε model is first introduced by Jones and Launder in 1972 [55]. The idea of the model is describing the turbulent viscosity by the production and destruction equations of turbulence. Empiric relationships are constructed by the help of experimental data. For k − ε model, turbulent viscosity is defined as:

$$\mu_t = \bar{\rho} C_\mu \frac{k^2}{\varepsilon} \tag{2.30}$$

Where ε is the dissipation of turbulent kinetic energy.k and ε are described by closure of two balance equations:

$$\frac{\partial}{\partial t}(\bar{\rho}k) + \frac{\partial}{\partial x_i}(\bar{\rho}\tilde{u}_i k) = \frac{\partial}{\partial x_i}\left[\left(\mu + \frac{\mu_t}{\sigma_k}\right)\frac{\partial k}{\partial x_i}\right] + P_k - \bar{\rho}\varepsilon \tag{2.31}$$

$$\frac{\partial}{\partial t}(\bar{\rho}\varepsilon) + \frac{\partial}{\partial x_i}(\bar{\rho}\tilde{u}_i \varepsilon) = \frac{\partial}{\partial x_i}\left[\left(\mu + \frac{\mu_t}{\sigma_\varepsilon}\right)\frac{\partial \varepsilon}{\partial x_i}\right] + C_{\varepsilon 1}\frac{\varepsilon}{k}P_k - C_{\varepsilon 2}\bar{\rho}\frac{\varepsilon^2}{k} \tag{2.32}$$

The source term P_k is given by:

$$P_k = -\bar{\rho}\widetilde{u''_i u''_j}\frac{\partial \tilde{u}_i}{\partial x_j} \tag{2.33}$$

The standard model constants are listed inTable 1. Since these constants are derived from experimental data, standard k − ε model is comparably accurate for a wide range of wall bounded and free shear flow types. However, improvements shall be made for other types of flows such as swirling flows. Therefore, RNG k − ε model and Reliazable k − ε model are derived.

Table 1.Constant values used in standard k − ε turbulence model

$C_{\varepsilon 1}$	1.44
$C_{\varepsilon 2}$	1.92
C_μ	0.09
σ_k	1.0
σ_ε	1.3

2.2.1.3 Realizable k-epsilon Turbulence Model

The realizable $k-\varepsilon$ model threats ε in a different way. Exact equation for the transport of the mean-square vorticity fluctuation has been derived for ε transport equation. Further, realizable model contains an alternative formulation for turbulent viscosity. This idea comes from the mathematical constrains. By these modifications, the transport equation of k (2.31) kept the same with standard model, but ε is redefined as:

$$\frac{\partial}{\partial t}(\bar{\rho}\varepsilon) + \frac{\partial}{\partial x_i}(\bar{\rho}\tilde{u}_i\varepsilon) = \frac{\partial}{\partial x_i}\left[\left(\mu + \frac{\mu_t}{\sigma_\varepsilon}\right)\frac{\partial \varepsilon}{\partial x_i}\right] + \bar{\rho}C_1\tilde{S}\varepsilon - \rho C_2\frac{\varepsilon^2}{k+\sqrt{\nu\varepsilon}} \tag{2.34}$$

Where

$$C_1 = max\left[0.43, \frac{\eta}{\eta+5}\right]$$

$$\eta = \tilde{S}\frac{k}{\varepsilon}$$

$$\tilde{S} = \sqrt{2\widetilde{S_{ij}}\widetilde{S_{ij}}}$$

$$\tilde{S}_{ij} = \frac{1}{2}\left(\frac{\partial \tilde{u}_i}{\partial x_j} - \frac{\partial \tilde{u}_j}{\partial x_i}\right)$$

And the viscosity is defined as:

$$\mu_t = \rho C_\mu \frac{k^2}{\varepsilon}$$

Where C_μ is no more constant. T is computed from:

$$C_\mu = \frac{1}{A_0 + A_s\frac{kU^*}{\varepsilon}}$$

Where

$$U^* \equiv \sqrt{\tilde{S}_{ij}\tilde{S}_{ij} + \widetilde{\Omega}_{ij}\widetilde{\Omega}_{ij}}$$

And

$$\tilde{\Omega}_{ij} = \Omega_{ij} - 2\varepsilon_{ijk}\omega_k$$

$$\Omega_{ij} = \overline{\Omega_{ij}} - \varepsilon_{ijk}\omega_k$$

Where $\overline{\Omega_{ij}}$ is the mean rate of rotation tensor viewed in a moving reference frame with the angular velocity ω_k. The model constants A_0 and A_s is given by

$$A_0 = 4.04$$

$$A_s = \sqrt{6}cos\phi$$

Where

$$\phi = \frac{1}{3}cos^{-1}(\sqrt{6}W)$$

$$\widetilde{W} = \frac{\tilde{S}_{ij}\tilde{S}_{jk}\tilde{S}_{ki}}{\tilde{S}^3}$$

Therefore, C_μ is a variable parameter which is a function of strain and vorticity. The other constants used in the model are listed in Table 2 which are slightly different from the values of the standard model.

Table 2.Constant values used in Realizable k − ε turbulence model

$C_{1\varepsilon}$	1.44
C_2	1.9
σ_k	1.0
σ_ε	1.2

2.2.2 Detached Eddy Simulation (DES)

In DES approach, hybrid of RANS / LES combination is applied to computations. Unsteady RANS solverhandles to near wall regions where a high resolution is needed for LES. And, LES is applied where large structures appear. The large scales in the domain play dominant role in the flow. Therefore, using hybrid model brings advantages in computations.

DES is specifically designed for high Reynolds number flows. Applying LES would generate a need of very fine mesh at near wall regions and increase the computation source need highly. Instead, applying less power needed Unsteady RANS will decrease the costs. Since then, the application of DES needs less computational

power compared to LES. On the other hand, the needed power is greater compared to RANS.

2.2.3 Large Eddy Simulation (LES)

Instead of solving all of the eddies, large eddy simulation offers to model small ones. While DNS deals with all spatial frequencies in the spectrum, LES puts a cut-off wave number, k_c, and solves the scales whose frequency wave number, k, is lower than the k_c . Scales whose frequencies higher than k_c are modeled. These are called subgrid scales and need to be treated carefully since they confine the conservation. Also the quality of the solution is highly dependent to the effects of small scales. In a flow, the large scales contain the most of the conserved properties. Thus, the small scales provide little transport of these properties. LES appears as a very promising approach for combustion simulations because of combustion instabilities and mixing zone determination. However, it is still a bit far away from being the routine approach as a design tool in industry.

2.2.4 Direct Numerical Simulation (DNS)

Solving Navier-Stokes equations numerically is a way of solving turbulence. Even the errors due to discretization still exist; this approach is the most accurate approach to turbulence simulation. It is also referred as a pure experiment whose results contain no experimental errors. Thus a result of a DNS gives much more extensive and more reliable data than an experimental data. However, the source needed for this approach is extremely high. In order to perform a Direct Numerical Simulation, one must put more than two grid points to the smallest eddy location. The size of a time step must be smaller than this smallest eddy turnover time which constructs a relationship between grid size and time step size. The scale of cost of a simulation can be described with third order of the Reynolds number of the largest scale which is Re_t^3. Therefore, DNS is only available for academic researches. Nowadays some basic flows whose Reynolds number is in the order of 1000 can be resolved.

2.3 Non-Premixed Combustion Modeling

Turbulent non-premixed flames are usually encountered in engineering applications. While diesel engines or industrial burners are some examples of non-premixed

combustion, it is also favorite for aerial applications. Although the applied area is very wide, it is still hard to model and inaccurate solutions are very common for most of the times. Under this topic, the used models will be outlined and summarized.

The models are differs due to their approach to chemical reactions. One of the assumptions is infinitely fast chemistry. This assumption can be made while turbulence level is high and chemical reactions very fast compared to flow speed. Although assuming high turbulence level is not wrong, this assumption generally gives inaccurate solutions. The other approach, which is more realistic, is the finite rate chemistry. However, the parameters used for finite rate chemistry varies with turbulence interaction and this is not modeled. The problem is tried to be simulated by using either ways.

The approaches for modeling of the non-premixed methane-air flame are categorized under two subtitles:

- Species Transport Model
- Presumed Probability Density Function Model

2.3.1 Species Transport Models

Species transport models are based on transporting molecules information which brings extra transport equations to simulations. Because of computational costs, only limited numbers of molecules can be tracked while reaction mechanism of a CH4 (methane) molecule includes much more. However, most of the reactions are very fast compared to others and are not determinants. Reduction mechanism is always applied for reactions. Kenneth Kuo [4] and many others explained the underlying theory and applying procedure in text books or in publications. A reduced CH4 oxidation for 15 species and 41 reactions can be seen in Figure 20.

The computation effort increases with the number of reaction steps and the number of species. In this thesis, one step and two step reactions are performed which are feasible for available computation sources. The reaction schemes are given in Table 3. In the species transport based models, the fraction of the species located in Table 3 are transported. Therefore, 5 or 6 transported variable (depending on the chosen

reaction scheme) added in flow solver computations. Following subsections will describe the computation methodology.

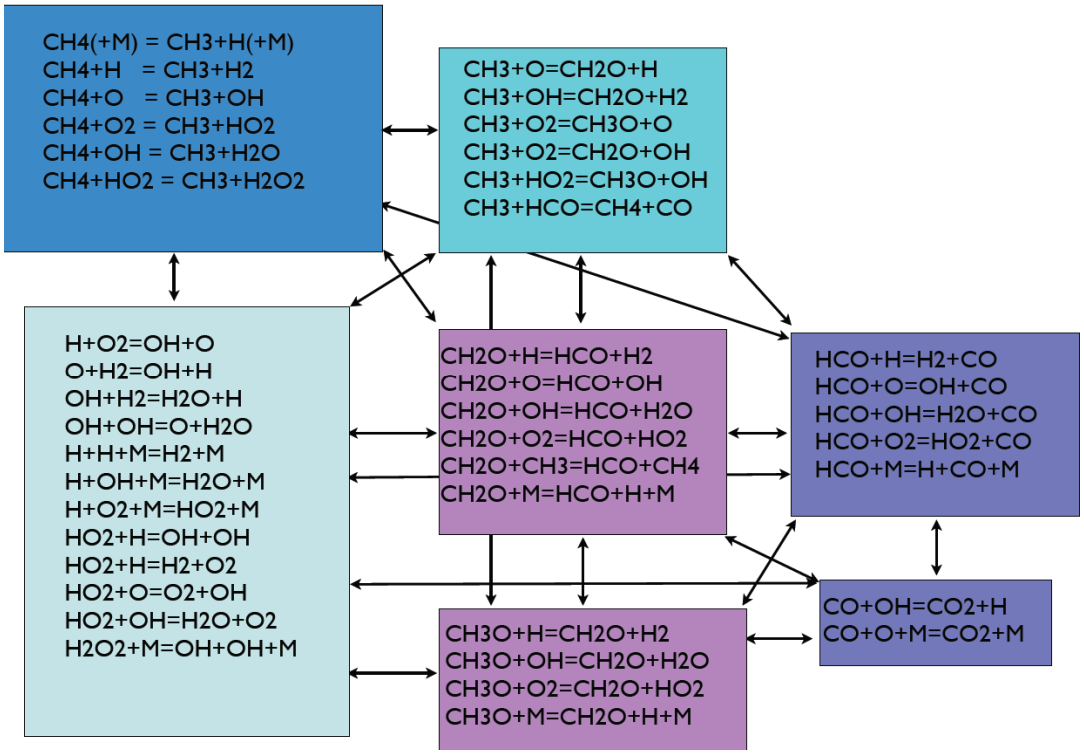

Figure 20. A reaction mechanism of CH4 oxidation [56]

Table 3. Reaction schemes used in species transport based simulations

One-Step	$CH_4 + 2O_2 \rightarrow CO_2 + 2H_2O$	
Two Step	I)	$CH_4 + {}^3/_2\, O_2 \rightarrow CO + 2H_2O$
	II)	$CO + {}^1/_2\, O_2 \rightarrow CO_2$

2.3.1.1 Eddy Dissipation Model

Eddy Dissipation Model (EDM) is derived from Eddy Break up Model which is proposed for Premixed Combustion Modeling by Spalding [57]. The derivation for non-premixed combustion modeling is made by Magnussen and Hjertager [58] in 1976. The burning rate which remained unclosed is defined as:

$$\overline{\rho\dot{\omega}_k} = C_{mag}\bar{\rho}\frac{1}{\tau_t} min\left(\tilde{Y}_F, \frac{\tilde{Y}_O}{s}, \beta\frac{\tilde{Y}_P}{(1+s)}\right) \quad (2.35)$$

Where C_{mag} and β are model constants. $\tilde{Y}_F$, $\tilde{Y}_O$, $\tilde{Y}_P$ are mean mass fractions of fuel, oxidizer and products. s is Turbulent mixing time, τ_t, plays a determinant role. It is estimated from integral length scales. It is defined as:

$$\tau_t = \frac{k}{\varepsilon} \tag{2.36}$$

After it, the burning rate definition is reconstructed as:

$$\overline{\rho\dot{\omega}_k} = C_{mag}\bar{\rho}\frac{\varepsilon}{k} min\left(\tilde{Y}_F, \frac{\tilde{Y}_O}{s}, \beta\frac{\tilde{Y}_P}{(1+s)}\right) \tag{2.37}$$

The idea of the Eddy Dissipation Model is based on the assumption of high turbulence level. Mixing velocity due to turbulence is assumed much more compared to diffusion velocity of the chemicals. By this approach, the model burns the fuel as soon as it meets with oxidizer. In other word, this is an infinitely fast chemistry model. Therefore, the model is not proper for ignition problems or can not capture lifted flames. In order to ignite the flame for computations, all the radicals shall be patched to a volume where flame can reach to the fresh reactants.

2.3.1.2 The Laminar Finite-Rate Model

Instead of assuming infinitely fast chemistry, this model offers a finite rate chemistry which is more real, but more proper for laminar flames [59]. However, experiments in jet flames and direct numerical simulations suggest that, chemistry is fast but may not the be infinitely fast for burners [11]. Therefore, finite rate chemistry should be taken into account. Damköhler number is a determinant parameter which indicates the ratio of diffusive time and chemical time. It is defined as:

$$Da^* = \frac{Diffusive\ time}{Chemical\ time} = \frac{\tau_{\boldsymbol{x}}}{\tau_c} \approx (\tau_c \boldsymbol{\chi_{st}})^{-1} \tag{2.38}$$

Damköhler variations with burning rate leads to so called “S” curve which can be seen in Figure 21.

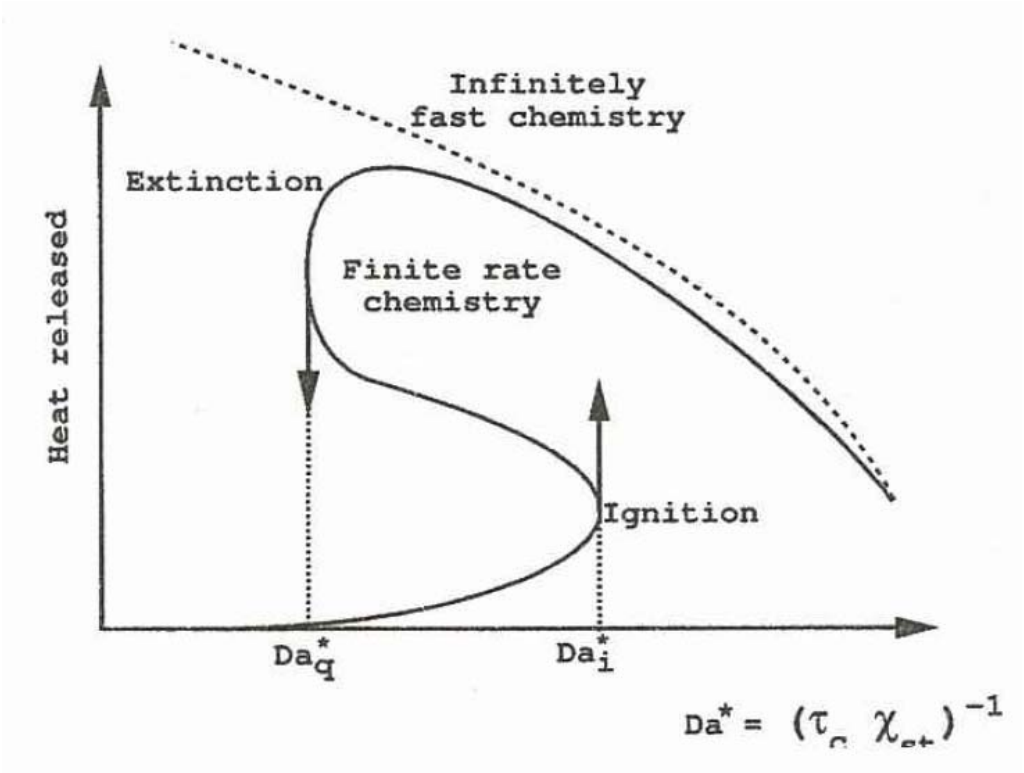

Figure 21. Generic response of heat released by one dimensional strained diffusion flame versus Damköhler number [11]

The laminar finite rate model in ANSYS fluent uses non-linear Arrhenius chemical kinetics. The net rate of the production of the species is defined as:

$$R_i = M_{w,i} \sum_{r=1}^{N_R} \hat{R}_{i,r} \tag{2.39}$$

Where $M_{w,i}$ is molecular weight of species i, $\hat{R}_{i,r}$ is the Arrhenius molar rate of creation/destruction of species i in reaction r and N_R is total reaction number. And the reactions equation is:

$$\sum_{i=1}^{N} sc'_{i,r} \boldsymbol{M_i} \xrightleftharpoons{k_{b,r} k_{f,r}} \sum_{i=1}^{N} sc''_{i,r} \boldsymbol{M_i} \tag{2.40}$$

Where N number of species in the system, $sc'_{i,r}$ is stoichiometric coefficient for reactant i in reaction r, $sc''_{i,r}$ is stoichiometric coefficient for product i in reaction r. $\boldsymbol{M_i}$ is symbol denoting species i. kf and kb are forward rate and backward rate constants for reaction r.

For a reversible reaction, molar rate of creation/destruction is given as:

$$\hat{R}_{i,r} = \theta(sc''_{i,r} - sc'_{i,r})\left(k_{f,r}\prod_{j=1}^{N}[C_{j,r}]^{\eta'_{j,r}} - k_{b,r}\prod_{j=1}^{N}[C_{j,r}]^{sc''_{j,r}}\right) \quad (2.41)$$

And θ is defined as

$$\theta = \sum_{j}^{N}\gamma_{j,r}C_j \quad (2.42)$$

Where $\gamma_{j,r}$ is third body efficiency of the j th species in reaction r. The Arrhenius expression is:

$$k_{f,r} = A_r T^{\beta_{re}-E_r/RT} \quad (2.43)$$

Where A_r is pre-exponential factor, β_r is temperature exponent, E_r is activation energy for the reaction and R universal gas constant. $k_{b,r}$is computed from $k_{f,r}$ and one may see Ref. [59] for further information. The constants of Arrhenius expression comes from ANSYS Fluent data base.

2.3.1.3 Finite Rate / Eddy Dissipation Model

In finite rate / Eddy Dissipation combustion model, both Arrhenius and Eddy Dissipation reaction rate equations are calculated. Minimum of these two rates are taken. Therefore, any reaction latency can be estimated.

2.3.2 Presumed Equilibrium PDF Model

Another "mixed is burnt" model is presumed Equilibrium PDF model. Instead of transporting all the molecules information mixture fraction and mixture fraction of fuel and oxidizer and its variance are carried.Mixture fraction is defined as:

$$z = \frac{\emptyset}{r+\emptyset} \quad (2.44)$$

Where $\emptyset$ is equivalence ratio and defined as:

$$\emptyset = \frac{(fuel/air)_{actual}}{(fuel/air)_{stoichiometric}} \quad (2.45)$$

$$\emptyset F + rO \rightarrow (\emptyset + r)P \quad (2.46)$$

Where F is for fuel, O is for oxidizer and P is for products. The mixture fraction can be split into its mean and variance values:

$$z = \tilde{z} + \widetilde{z''^2} \tag{2.47}$$

Where $\tilde{z}$ is local mean fuel/air mixture and $\widetilde{z''^2}$ is its variance. Therefore, the classical gradient transport closures for turbulent fluxes are defined as:

$$\bar{\rho}\frac{\partial \tilde{z}}{\partial t} + \bar{\rho}\tilde{\boldsymbol{u}} \cdot \nabla \tilde{z} = \nabla \cdot \left(\bar{\rho} v_t \nabla \tilde{Z}\right) \tag{2.48}$$

For variance:

$$\bar{\rho}\frac{\partial \widetilde{z''^2}}{\partial t} + \bar{\rho}\tilde{\boldsymbol{u}} \cdot \nabla \widetilde{z''^2} = \nabla \cdot \left(\bar{\rho} v_t \nabla \widetilde{z''^2}\right) + 2\bar{\rho} v_t |\nabla \tilde{z}|^2 - 2\bar{\rho}\tilde{\boldsymbol{\chi}} \tag{2.49}$$

The first term on the right hand side (RHS) of the equation (2.49) is the turbulent transport, second term is the production of the fluctuations by the mean of gradients, the last is the scalar dissipation rate which is defined as:

$$\bar{\rho}\tilde{\boldsymbol{\chi}} = 2\overline{\rho D \frac{\partial z}{\partial x_\iota}\frac{\partial z}{\partial x_\iota}} \tag{2.50}$$

The widely used linear relaxation model for the equilibrium condition is:

$$\tilde{\boldsymbol{\chi}} = \frac{\widetilde{z''^2}}{(k/\varepsilon)} \tag{2.51}$$

Then the closed form of the mixture fraction variance equation is:

$$\frac{\partial \bar{\rho}\widetilde{z''^2}}{\partial t} + \frac{\partial}{\partial x_i}\left(\bar{\rho}\tilde{u}_i \widetilde{z''^2}\right) = \frac{\partial}{\partial x_i}\left(\frac{\mu_t}{\sigma_t}\frac{\partial \widetilde{z''^2}}{\partial x_i}\right) + C_g \mu_t \frac{\partial \tilde{z}}{\partial x_i}\frac{\partial \tilde{z}}{\partial x_i} - C_d \bar{\rho}\frac{\varepsilon}{k}\widetilde{z''^2} \tag{2.52}$$

Where σ_t, C_g, C_d are constants and assumed as 0.85, 2.86, 2.0 by ANSYS Fluent default [59].$\sigma_t$and C_g, constants can be calculated via turbulent Schmidt number also [8].

Since the equations are closed, the mean mixture fraction and its variance are calculated values from transport equations. By the existing information of mean mixture fraction, one can make an approach for temperature and density. The simplest approach is to create a lookup table at the beginning of the computation and make iterations for every mixture fraction value. Libby and Williams [60] offer a presumed beta function Probability Density Function (PDF). The presumed function, $\bar{p}(z^*: \underline{x}, t)$, is defined as:

$$\tilde{P}(z^*:\underline{x},t)=\frac{z^{*a-1}(1-z^*)^{b-1}}{\int_0^1 z^{+a-1}(1-z^+)^{b-1}dz^+} \quad (2.53)$$

Where

$$a=\tilde{z}\left(\frac{\tilde{z}(1-\tilde{z})}{\widetilde{z''^2}}-1\right)\geq 0$$

$$b=a\left(\frac{1}{\tilde{z}}-1\right)\geq 0$$

A tabulated look up data can be created by using beta function shape PDF. The presumed PDF should reproduce the mean of the mixture fraction and its variance. Algorithm lies under presumed PDF model for RANS calculations can be seen in Figure 22.

The presumed PDF is simple and useful if only the following assumptions can be made:

- The thermodynamic pressure is constant and Mach numbers are small.
- Species heat capacities are equal and constant.
- Lewis numbers are equal to unity.
- Turbulence level is very high as it controls the burning rate.

Like EDM, the presumed PDF model can not also predict ignition delay. Non-adiabatic definition brings H, enthalpy in to PDF as an unknown. Therefore, 3D look up table is calculated for max and min H and another interpolation is made during calculation which slows down the iterations.

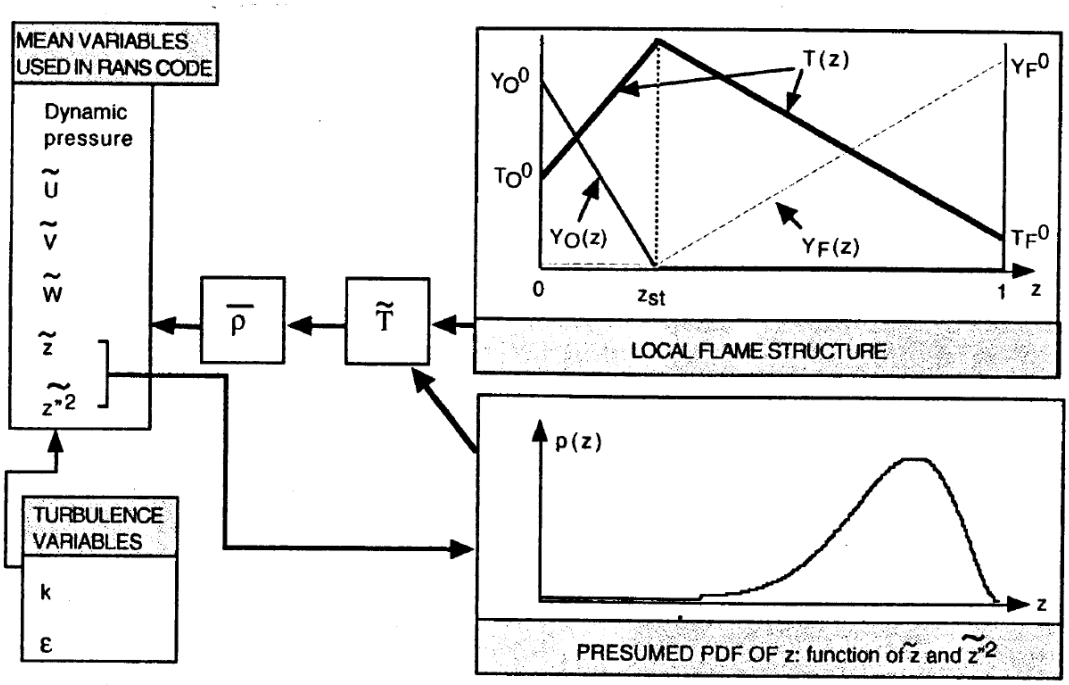

Figure 22. Presumed PDF method for infinitely fast chemistry [11]

2.4 Modeling Radiation

Radiation is one of three ways of heat transfer which is very important phenomenon in combustion applications. As it is stated in Chapter 1, one third of thermal power may goes to walls as heat source by radiation effect [24]. In order to simulate this effect Discrete Ordinates (DO) Radiation Model is used.

The theory of the discrete ordinates radiation model lies on solving the radiative heat transfer equation for a finite number of discrete solid angles. Each of the angles are associated with a vector direction. Therefore, DO model solves as many equations as there are directions $\vec{s}$. The radiation heat transfer is defined as [59]:

$$Q_{rad} = \sigma(T_2^4 - T_1^4) \tag{2.54}$$

Where σ is Stephan Boltzmann constant. And the DO model radiation equation is defined as[59]:

$$\nabla \cdot (I(\vec{r},\vec{s})\vec{s}) + (a+\sigma_s)I(\vec{r},\vec{s}) = an^2\frac{\sigma T^4}{\pi} + \frac{\sigma_s}{4\pi}\int_0^{4\pi} I(\vec{r},\vec{s})\Phi(\vec{s}\cdot\vec{s}')d\Omega' \tag{2.55}$$

Where $\vec{s}$ is direction vector, $\vec{r}$ position vector, a is absorption coefficient, σ_s is scattering coefficient, I is radiation intensity, Φ phase function, Ω' is solid angle, n is refractive index, $\vec{s}'$ is scattering direction vector. In 3D calculations, a total of $8N_\theta N_\phi$ directions are needed to be solved.

There may be also different wavelength bands in a radiative region. It can be modeled by defining new spectral absorption coefficient and black body intensity. However, the total equation numbers are increased which increases the calculation time drastically.

DO radiation model is moderate cost and a proper model for combustion problems which allows to solve problems ranging from surface to surface radiation to participating radiation[59].

2.5 Numerical Methodology

2.5.1 Finite Volume Method

Finite volume method is the most used method in Computational Fluid Dynamics (CFD) area. The control volume domain subdivided into a finite number of contiguous control volumes which are named as cells. Conservation equations are used as in their integral form and applied to each cell. Each cell has a computational node at the center of the geometry. Information between cell center node and face are being calculated by interpolation. Unlike finite difference method, finite volume method uses control volume boundaries instead of computational nodes.The integral form of conservation equations is:

$$\frac{\partial}{\partial t}\int_\Omega \rho\phi d\Omega + \int_S \rho\phi\vartheta \cdot ndS = \int_S \Gamma grad\phi \cdot ndS + \int_\Omega q_\phi d\Omega \qquad (2.56)$$

Approximation of surface and volume integrals shall be done for numerical solutions. The code used for analysis stores the information at cell center. For spatial and temporal information exchange, interpolations must be done. The following sections describe the methods of interpolation.

2.5.2 Solving Theory

By default, ANSYS Fluent stores the information at cell center.Two methods are used for computation:

- Pressure Based Solving
- Density Based Solving

For both solving methodology, velocity field is extracted from momentum equation. The pressure based solver manipulates continuity and momentum equations in order to solve pressure field. The density based solver obtains density field by continuity equation and pressure field determined from equation of state.

In the beginning, pressure based solving methodology is derived for low speed incompressible flow problems while density based solving methodology is derived for high speed compressible flow problems. Now, both methodologies can be applied for all kind of problems. As mentioned in previous chapter, swirling flows include high pressure gradients. In this scope of thesis, pressure based solving methodology is applied in order gain numerical advantage of this pressure gradient.

2.5.2.1 Pressure Based Methodology

Two pressure based algorithm exist in ANSYS Fluent:

- Segregated Algorithm
- Coupled Algorithm

For both of the algorithms, the pressure equation is derived from momentum and continuity equations. Then, velocity field is corrected by calculated pressure by satisfying continuity. In segregated solver algorithm, variables are computed one after other while in coupled algorithm, all variables computed together. The difference between two algorithms results with memory usage. Since all the equations solved separately, segregated algorithm needs nearly half of the memory which is needed for coupled solver. However, the convergence of the coupled algorithm needs less iteration. Overview of algorithms in ANSYS Fluent is shown in Figure 23. So called projection method is used for pressure-velocity correction.

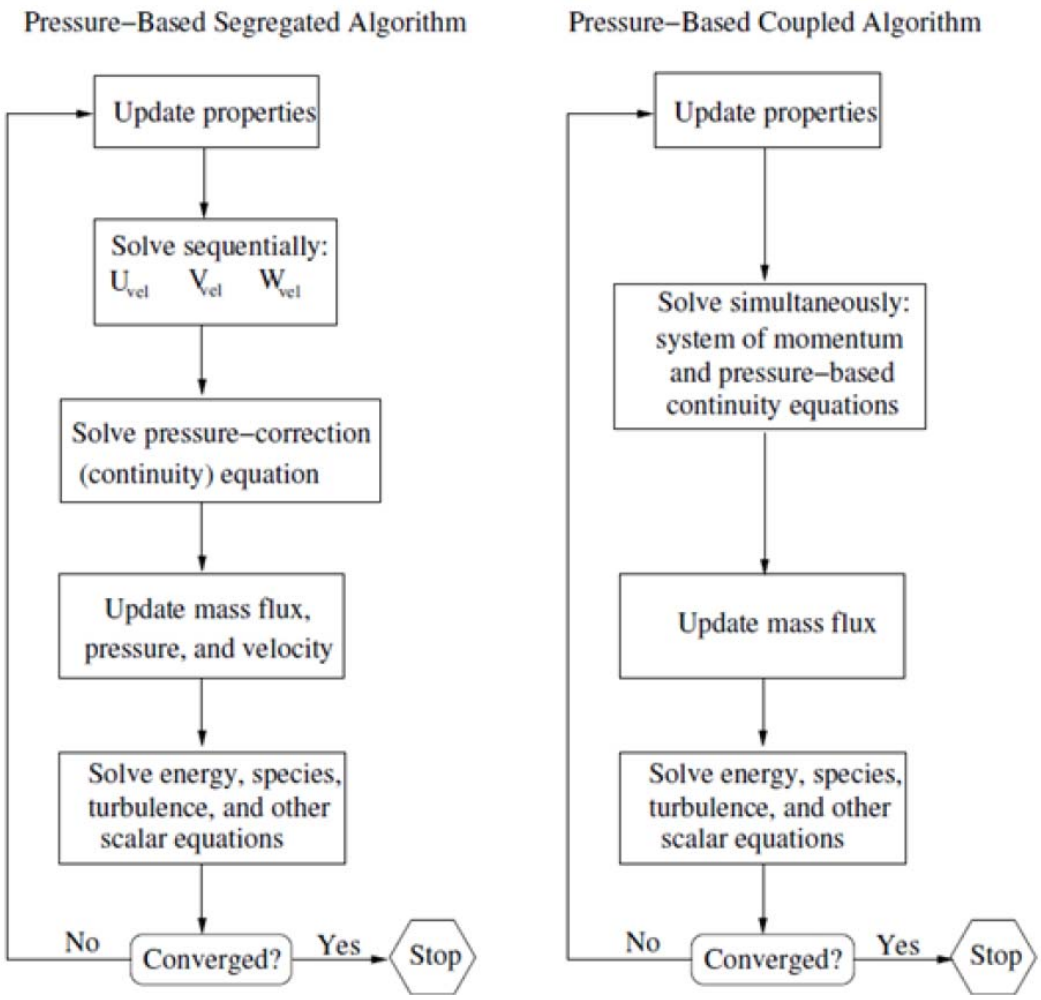

Figure 23. Algorithms for pressure based solver in ANSYS Fluent

According to this algorithm, face mass flux and pressure field shall be obtained in order to solve the other quantities.

2.5.3 Discretization Schemes

2.5.3.1 Spatial Discretization

A schematic view of 2D cells can be seen in Figure 24. In this section, first order upwind, second order upwind and QUICK discretization will be explained by respect to the notation.

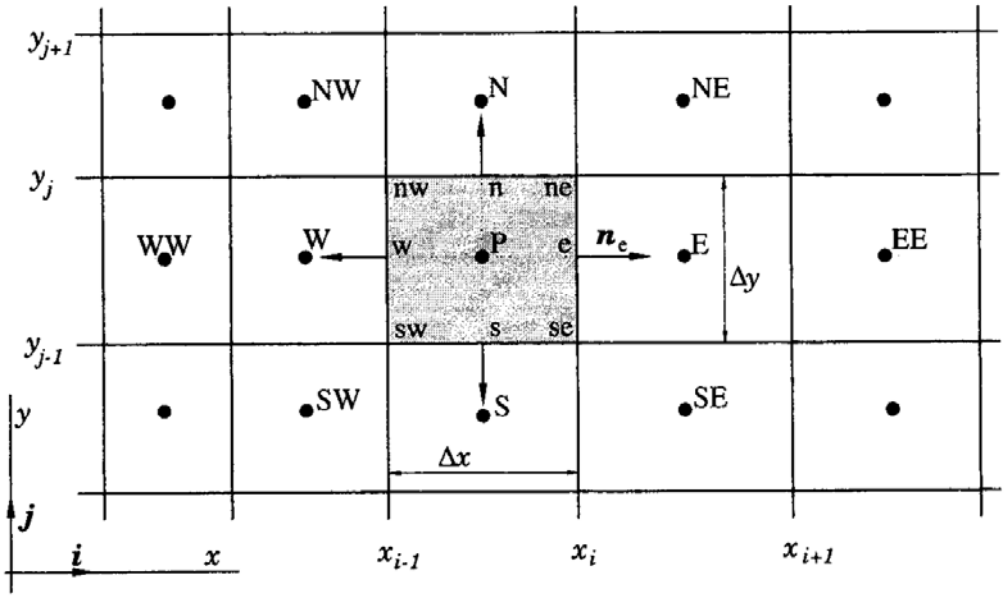

Figure 24.A typical cell notations for a 2D control volume grid [54]

2.5.3.1.1 First Order Upwind Interpolation

In order to solve the integral forms of the finite volume integrations, Taylor series expansion is applied. Taylor series expansion for Cartesian grid about P gives:

$$\phi_e = \phi_P + (x_e - x_P)\left(\frac{\partial\phi}{\partial x}\right)_P + \frac{(x_e - x_P)^2}{2}\left(\frac{\partial^2\phi}{\partial x^2}\right)_P + H \qquad (2.57)$$

Where H denotes higher-order terms. The name first order comes from that only the first term remains at the right hand side of the equation. The idea comes from assuming homogenous distribution for whole cell. Thus, the value at the cell face and at the cell center are equal.Rest of the expansion of the series leads to truncation error. Because only the first term is calculated, first order interpolation is diffusive.

According to the notation given in Figure 24 this formulation can be both forward difference and backward difference depending on flow direction. In both cases it is upwind differencing. For further information about naming and notations, one can see Ref. [54]. This method is used for primary convergence iterations for most of the work. Second order upwind discretization schemes are applied for final state of the results.

2.5.3.1.2 Second Order Upwind Interpolation

As it is explained in the previous section, upwinding idea is the same for second order upwind interpolation. However, since it is second order accurate, second term at the right hand side of Taylor Series expansion is also included in Second Order Upwind Interpolation.

$$\phi_e = \phi_P + \nabla\phi_P\vec{r} \tag{2.58}$$

In order to solve the equation, gradient$\nabla\phi$ shall be determined for each cell.

Discretization schemes other than first order may produce oscillatory solutions. This is because the truncation error is second order. In order to damp this error, first order diffusive scheme is used for primary convergence. Higher order schemes are used for final state of the most of the solutions.

2.5.3.1.3 Quadratic Upwind Interpolation (QUICK)

The name 'QUICK' represents the short form of 'Quadratic Upwind Interpolation for Convective Kinematics'. This interpolation constructs a parabola between two cell centers in order to approximate variable profiles between them. The computation method is as following:

$$\phi_e = \phi_U + g_1(\phi_D - \phi_U) + g_2(\phi_U - \phi_{UU}) \tag{2.59}$$

Where D, U and UU represents for downstream, upstream and second upstream cell centers. Assume that flow is from W to E direction, than D, U and UU are P, E and EE.

The coefficients g_1 and g_2 comes from coordinate allocations.

$$g_1 = \frac{(x_e - x_E)(x_e - x_{EE})}{(x_P - x_E)(x_P - x_{EE})}$$

$$g_2 = \frac{(x_e - x_E)(x_P - x_e)}{(x_E - x_{EE})(x_P - x_{EE})}$$

This algorithm is third order accurate. However it is designed for Cartesian grid only, ANSYS Fluent uses second order upwind interpolation where grid is not

hexahedral(or quad for 2D). For parallel solving, second order upwind interpolation is against used at partition boundaries.

2.5.3.1.4 Second Order (Linear) Interpolation (CDS)

Central differencing scheme is used for momentum equations in LES calculations. It is noted as providing improved accuracy for LES calculations.

$$\phi_e = \phi_E \lambda_e + \phi_P (1 - \lambda_e) \tag{2.60}$$

Where the linear interpolation factor is defined as:

$$\lambda_e = \frac{x_e - x_P}{x_E - x_P}$$

2.5.3.1.5 Pressure Interpolation Scheme

There are five schemes that ANSYS Fluent uses for pressure interpolation.

2.5.3.1.5.1 Standard

Using momentum equation coefficients, the code interpolates pressure values at the cell faces.

2.5.3.1.5.2 Linear

This method assumes that the changing is linear and computes the face pressure as the average of pressure values in adjacent cells.

2.5.3.1.5.3 Second Order

Second order accurate upwind scheme is applied for face pressure calculation.

2.5.3.1.5.4 Body-Force-Weighted

When the body forces are dominant in flow, body-force-weighted scheme is suitable for pressure calculations. This method assumes normal gradient of the difference between pressure and body forces is constant.

2.5.3.2 Temporal Discretization

Fourth coordinate direction for a solution is time. Thus, like discretization applied to space, an interpolation method shall also be applied to time marching.

A generic expression for the time evolution of a variable ϕ is given by

$$\frac{\partial \phi}{\partial t} = F(\phi) \tag{2.61}$$

The function F change by the method applied.

2.5.3.2.1 Implicit Time Integration

One method for evaluating the function F is implicit method. Value of the variable is calculated by neighboring cell. Iterations are done before moving to the next time step. Thus, convergence for each time step is needed.

$$\frac{\phi^{n+1}-\phi^{n}}{\Delta t} = F(\phi^{n+1}) \tag{2.62}$$

Implicit time integration can be done either by first order Euler implicit or second order Crank-Nicolson implicit.

2.5.3.2.1.1 First Order Euler Implicit

This method is unconditionally stable with respect to time step size. If the stability is the prime requirement, first order Euler implicit method is suggested. For studying steady flows or a flow with slow transition, arbitrary large time steps can be applied without subjected to any stability problem. This method creates first order truncation error. And each variable equation should be solved for each time step and each inner iteration. This algorithm requires extra time and huge storage. However, large time step marching can change the drawbacks to an advantage.

Initial guess for inner iterations is the converged solution of the previous time step. One may use single inner iteration if only the latest data is important.

2.5.3.2.1.2 Second Order Crank-Nicolson Implicit

This scheme needs a very little more computational effort compared to first order Euler method. Truncation error is second order. Von Neumann stability analysis showed that it is unconditionally stable. However, oscillatory solutions are possible

for large time steps. Whether choosing stable time step is a problem dependent issue, following equation derived for CDS may be used for an initial guess which guarantees for positive coefficient calculation included in the algorithm.

$$\Delta t < \frac{\rho(\Delta x)^2}{\Gamma} \tag{2.63}$$

Where Γ is diffusivity for the quantity ϕ. Thus the inequality shows simply the time required for a disturbance to be transmitted by diffusion over a distance Δx.

For further information about implicit algorithms, one can see Ref. [54,59].

2.5.3.2.2 Explicit Time Integration

First order Euler explicit method is the most used explicit time integration method. This method needs very small time step size. Courant number (also known as CFL number) must be below unity which is defined as:

$$c = \frac{u\Delta t}{\Delta x} \tag{2.64}$$

This rule restricts a particle not to move more than one grid point in a time step. This is simply the ratio of time step to characteristic convection time, time required for a disturbance to be converted to a distance Δx. Since this is a requirement, diffusivity factor should also be checked. Unlike Crank-Nicolson criteria, diffusivity transmission should be two times slower (thus, time step should be two times smaller) for Euler Explicit method. However, this criteria is just for the problems where diffusion is not negligible compared to convection.

Explicit method is suitable for compressible flows. It is less expensive and more accurate while dealing with moving waves such as shocks. Explicit scheme should not be used for incompressible flows since incompressible flows needed to be iterated and converged for each time step.

2.5.3.3 Pressure-Velocity Coupling

If the solver does not solve the variables in a coupled manner, pressure-velocity coupling should be done. ANSYS Fluent offers four pressure-velocity coupling algorithms for segregated pressure based solver:

- SIMPLE
- SIMPLEC
- PISO
- Fractional Step Method (FSM)

The concept of the projection method is to project out the divergence-producing part of the field.

2.5.3.3.1 SIMPLE

Velocity values are computed from linearized momentum equations and the pressure value is guessed for initial step. The velocity and pressure definition are made as:

$$u_i^m = u_i^{m*} + u'$$

$$p^m = p^{m-1} + p'$$

Where u_i is any velocity component, m is the final value (taken also as iteration indicator), m* is predicted value, u' and p' are velocity and pressure correction values.

The algorithm of the SIMPLE based methods are the same. For time based solutions, the steps are listed:

1. For new time step t_{n+1} , u_i^n and p^n are used as initial guesses of inner iterations.
2. Linearized momentum equations are solved in order to obtain u_i^{m*}.
3. Pressure correction equation is solved in order to obtain p'.
4. Continuity equation is solved to find new u_i^m and p^m values.
5. As inner iteration continues, recalculation is made to obtain new u_i^{m*}, p', u_i^m and p^m by using same order.
6. At the end, advancing to a next time step is done by saving last values.

The velocity at node P can be expressed as:

$$u_{i,P}^{m*} = \frac{Q_{u_i}^{m-1} - \sum_l A_l^{u_i} u_{i,l}^{m*}}{A_P^{u_i}} - \frac{1}{A_P^{u_i}} \left(\frac{\delta p^{m-1}}{\delta x_i} \right)_P \qquad (2.65)$$

Where l neighbor point. The source term Q contains all of the terms that may be explicitly computed in terms of u_i^nas well as body force or other linearized terms that may depend on the u_i^{n+1} or other variables at the new time level. The first term on the right hand side of the equation is called $\tilde{u}_{i,P}^{m*}$.

Velocity $u_{i,P}^{m*}$ is predicted value and not the final state of the velocity value which does not satisfies the continuity equation. Before applying the continuity equation, correction value equations embedded into the momentum equation. A new definition for correction is obtained as:

$$u'_{i,P} = \tilde{u}'_{i,P} - \frac{1}{A_P^{u_i}}\left(\frac{\delta p'}{\delta x_i}\right)_P \tag{2.66}$$

Where $\tilde{u}'_{i,P}$ is defined as:

$$\tilde{u}'_{i,P} = -\frac{\sum_l A_l^{u_i} u'_{i,l}}{A_P^{u_i}}$$

The velocities satisfy the continuity equation which is defined as:

$$\frac{\delta(\rho u_i^m)}{\delta x_i} = 0$$

When the continuity equation is used for correction definitions, the following pressure-correction equation is produced:

$$\frac{\delta}{\delta x_i}\left[\frac{\rho}{A_P^{u_i}}\left(\frac{\delta p'}{\delta x_i}\right)\right]_P = \left[\frac{\delta(\rho u_i^{m*})}{\delta x_i}\right]_P + \left[\frac{\delta(\rho \tilde{u}_i')}{\delta x_i}\right]_P \tag{2.67}$$

A very important note that, the inner differential equations are discretized by respect to momentum discretization selection, while the outer differential equations are discretized by respect to continuity equation. In SIMPLE method, the unknown velocity correction $\tilde{u}_i'$ is neglected. Then the corrected velocities and pressure are linked by:

$$u_{i,P}^m = \tilde{u}_{i,P}^{m*} - \frac{1}{A_P^{u_i}}\left(\frac{\delta p^m}{\delta x_i}\right)_P \tag{2.68}$$

It is obvious that neglecting a term will affect the convergence of solution. This problem is solved by under relaxation parameter which is defined as:

$$p^m = p^{m-1} - \alpha_p p'$$

2.5.3.3.2 SIMPLEC

This method uses the very same algorithm with SIMPLE. However, the neglected $\tilde{u}_i'$ term is weighted by mean of the neighbor values by defining:

$$\tilde{u}_{i,P}' \approx -u_{i,P}' \frac{\sum_l A_l^{u_i}}{A_P^{u_i}} \tag{2.69}$$

Since the neglected term is modeled, this method does not need under relaxation parameter for pressure.

2.5.3.3.3 PISO

This method uses the very same algorithm with SIMPLE. However, the neglected $\tilde{u}_i'$ term is again neglected at first correction step. Then, it is calculated with another corrector step by defining:

$$u_{i,P}'' = \tilde{u}_{i,P}' - \frac{1}{A_P^{u_i}} \left(\frac{\delta p''}{\delta x_i}\right)_P \tag{2.70}$$

Since the neglected term is modeled, this method does not need under relaxation parameter for pressure.

2.5.3.3.4 Fractional Step Method (FSM)

This method is derived mainly for unsteady flows. The pressure becomes a mathematical variable than a physical one for incompressible flows. FSMis an approach that does not use pressure in the predictor step.Details of this method are not mentioned here. It should be noted that, SIMPLE type methods solve the pressure equation at each iteration while fractional step method solve the pressure equation once in a time step. Steady-state solutions do not need an accurate pressure correction for each step. It is only a matter for converged solutions. While for unsteady solutions need an accurate correction for every time step. Therefore, the

approach of the FSM is more convenient for time based solutions. On the other hand, large time steps may produce an error during solution.

2.5.3.4 Evaluation of Gradients and Derivatives

Gradients are needed for computing secondary diffusion terms ad velocity derivatives. They are also constructing values of a scalar at cell faces. ANSYS Fluent uses Green-Gauss theorem based methods.

2.5.3.4.1 Green-Gauss Cell Based Method

This method calculates gradients by evaluating neighboring face values.

2.5.3.4.2 Green-Gauss Node Based Method

This method calculates gradients by evaluating arithmetic average of nodal values.Although it costs more computational power, nodal values gives more reliable solutions for irregular unstructured meshes.

2.5.3.4.3 Least Squares Cell Based Method

This method assumes the solution varies linearly between cell centers. It constructs a solution matrix between cell values and evaluates more reliable solutions compared to Green-Gauss Cell Based method for irregular unstructured meshes. Since it is computationally less expensive compared to node based method, it is used for all calculations.

2.6 Thermal Power Calculation

In order to calculate the thermal power of a combustor, the mass flow rate of burnt fuel and its heat of reaction value must be known.

Heat of reaction value is the amount of heat released during reaction. To calculate the value for a specific fuel, heat of formations of all compounds and the enthalpy of all species in a reaction should consist of equality. The heat of reaction at standard state is defined as:

$$\Delta H_{reaction} = \sum_{i=1}^{N} v_i'' \Delta \mathcal{H}^{\circ}{}_{f,M_i} - \sum_{i=1}^{N} v_i' \Delta \mathcal{H}^{\circ}{}_{f,M_i} \qquad (2.71)$$

Which implies:

$$\Delta H_{reaction} = \sum \Delta H_{Products} - \sum \Delta H_{Reactants} \quad (2.72)$$

Where h [j/kg] is for enthalpy, R for reactants, P for products, N for number of species and $\Delta \mathcal{H}^{\circ}_{f}$ is enthalpy of formation. Therefore, heat of reaction for a constant pressure can simply calculated by calculating the enthalpy difference between reactants and products.Once the heat of reaction value is calculated, the thermal power can be found by multiplying the value with the amount of mass flow rate.

$$P_{combuster} = \dot{m}_{fuel} \Delta H_{reaction} \quad (2.73)$$

If the reaction does not occur at standard state, enthalpy difference between the states shall be calculated also. If the reaction occurs in constant volume, internal energy differences should be employed to calculate the heat of reaction.

Some of the products may be produced in multiple phases such as water. The formation enthalpy of liquid water is lower than the formation enthalpy of gaseous water which absorbs some part of combustion energy. Therefore, lower heating value is the value where water is produced as vapor. And, higher heating value is the value where water is produced as liquid.

For further information about chemical thermodynamics, one can refer to Ref.[4].

CHAPTER 3

PROBLEM DEFINITION& BOUNDARY CONDITIONS

In this part of the thesis, the investigated TECFLAM s09 confined non-premixed flame test setup is introduced.

3.1 Confined TECFLAM Setup

TECFLAM combustion chamber is a natural gas fueled and air oxidized test setup. It can be premixed, non-premixed or partially premixed depend on its configuration. The combustion chamber built with double wall. Diameter of the insider wall is 500mm. There is a water flow between two walls to keep the wall temperature constant. The length of the chamber is 1200mm. There is window for diagnostics in the chamber. Injector part is traversable in axial directionwhich creates an opportunity to take measurements from 1mm above injector exit to 450mm downstream of it. The exit of the chamber is an annulus and 30mm exit hole. A CAD view of the test setup can be seen inFigure 26.

Ten thermocouples are allocated in test setup in order to measure the temperature of inflow gasses. Three temperature sensors are allocated at different locations of water loop which are for checking the water temperature. Sensing overheating at any of the sensors, stops the fuel inlet. There is also an UV sensor in order to stop the fuel inlet if the flame blows off. The top of the chamber is covered with an annulus which has 30mm exit holes for chamber gases. The burnt gas is analyzed for content of O2, CO2, CO, SO2, NO, NO2 and temperature. Thus the operating conditions can be checked and system can be balanced by energy. The schematic view of the test setup can be seen Figure 25. The standard thermal load of the test setup is 150kW while it can adjustable between 50kW to 350kW.

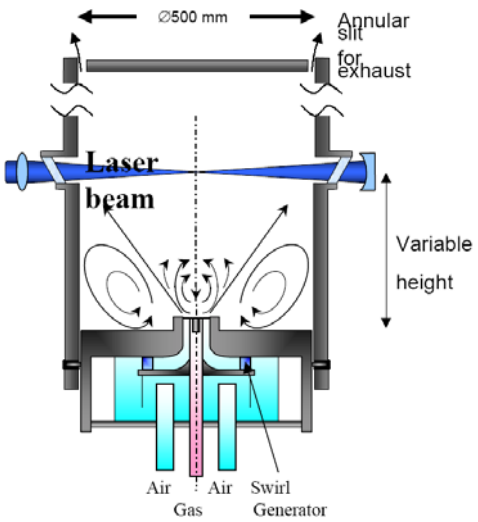

Figure 25. A Schematic view of the confined TECFLAM non-premixed flame test setup

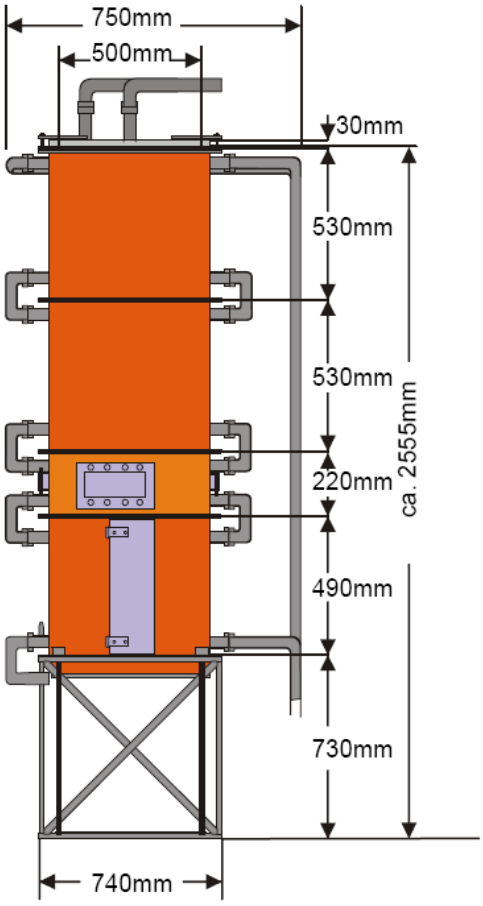

Figure 26.A CAD view of the confined TECFLAM test setup

3.2 Non-Premixed Movable Block Swirler

The air injector is a movable block swirler generator. The burner has a bluff body at the middle. There is a 3mm annulus surrounding the bluff body for fuel entrance to the combustion chamber. Then, there is a second annulus for air entrance which is fed through a swirler. The swirl number of the swirl burner generator is adjustable between S=0 to S=2. For the s09 configuration, the swirl number is S=0.9. A schematic cut view of the swirl burner can be seen in Figure 27.

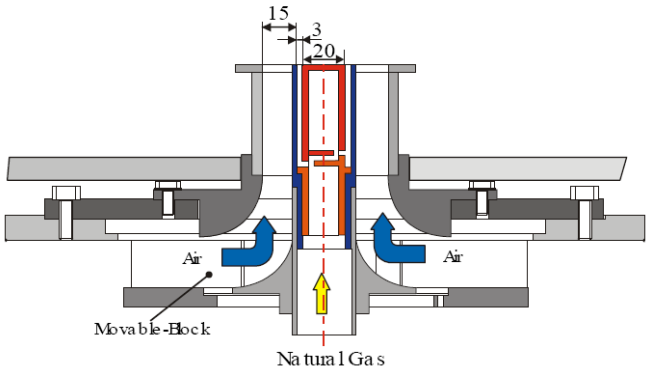

Figure 27. A schematic cut view of swirl burner injector

Dimensional properties of the swirl burner are listed inTable 4.

Table 4. Dimensional properties of the swirl burner

Fuel jet outer diameter [mm]	26
Coflowing air inner diameter [mm]	30
Coflowing air outer diameter [mm]	60
Chamber diameter [mm]	500
Mean chamber height [mm]	1200

3.3 Parameters for s09 Configuration

Test case named as “s09” has following properties listed in

Table 5. It is noted that air exit bulk velocity is 23m/s. Since the outer diameter of swirler is 60mm, Eddy Turnover time is calculated as:

$$\tau_{eddy\ time} = \frac{D_{swirler}}{U_{exit}} = \frac{0.06[m]}{23[m/s]} = 0.0026s$$

Table 5. List of parameters belongs to s09 TECFLAM configuration

Thermal Power [kW]	150
Swirl Number	0.9
Equivalence Ratio	0.83
Air to fuel ratio	1.2
Fuel	Natural Gas
Chamber pressure	Ambient Pressure
Exit bulk velocity: air [m/s]	23
Exit bulk velocity: fuel [m/s]	21
Reynolds Number: Air	42900
Reynolds Number: Fuel	7900
Temperature Cooling Water [°C]	80

Table 6. Measured quantities from TECFLAM, the methods of measuring and the groups

Quantity	Method	Author
Velocity	Laser Doppler Velocimetry	EKT, EBI [27,42]
Temperature, concentration of main species	Raman/Rayleigh	DLR [22,23]
Stable species	Probe sampling	EBI
Temperature (2-dim.)	Rayleigh	PCI [24-27,43]
Temperature	Thermocouple	EBI
Radiation	Spectrally resolved emission measurements	ITS
Intermediates OH, NO,CH2O	PLIF	PCI [24-27,43]

Table 7. The expansion of abbreviations at author column in Table 6

Abbreviations	Institute	Corresponding Author
EBI	EnglerBunteInstitut, University of Karlsruhe	Prof. Bockhorn, Prof. Leuckel
EKT	Energie- und Kraftwerkstechnik, TU Darmstadt	Prof. Janicka
DLR	DeutschesZentrumfürLuft- und Raumfahrte.V., Stuttgart	Dr. Stricker
ITS	InstitutfürThermischeStrömungsmaschinen, University of Karlsruhe	Prof. Wittig
PCI	PhysikalischChemischesInstitut, University of Heidelberg	Prof. Wolfrum

3.4 Experiment Methods and Authors

The investigation of the TECFLAM test setup is carried out by different scientific groups which are Darmstadt, Heidelberg, Karlsruhe and Stuttgart. Measured quantities and the groups are listed in Table 6.The expansion of abbreviations at author column in Table 6 is listed at Table 7.

3.5 Experimental Data

Experimental data are taken for various locations. A schematic view of available experimental data is given in Figure 28.

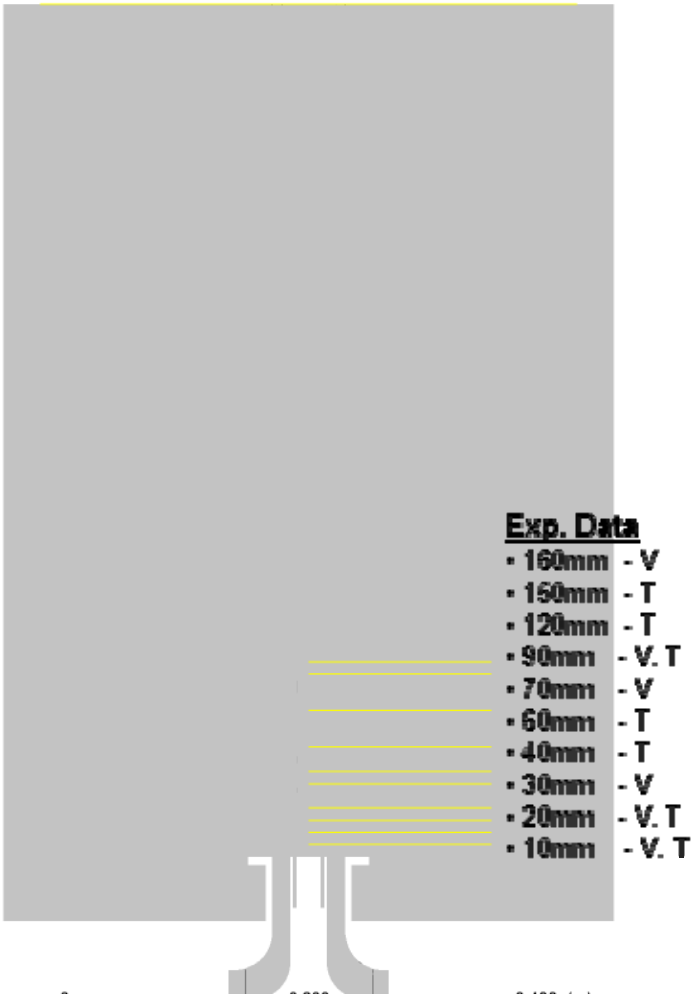

Figure 28. Measurement locations of LDV and Raman Scattering(*V* for velocity data, *T* for temperature data)

3.5.1 Velocity

3.5.1.1 Laser Doppler Velocimetry (LDV) Measurement

Two component Dantec LDV is used for velocity measurements. Argon-ion laser source is used with 4W power. The size of the probe volume is o.78mm in length and 0.094mm in diameter. Estimated statistical error for mean velocity is 5% and for fluctuation velocity 6%.

3.5.1.2 Measured Velocity Data

Measurements are done for 7 axial positions with variable radial positions. Mean and fluctuations of axial, radial and circumferential velocities are measured. Additionally the correlation between the axial and the radial velocities as well as the correlation between the axial and the circumferential velocities are measured. Graphics from measured mean velocity data for some locations are shown atFigure 29 and Figure 30.

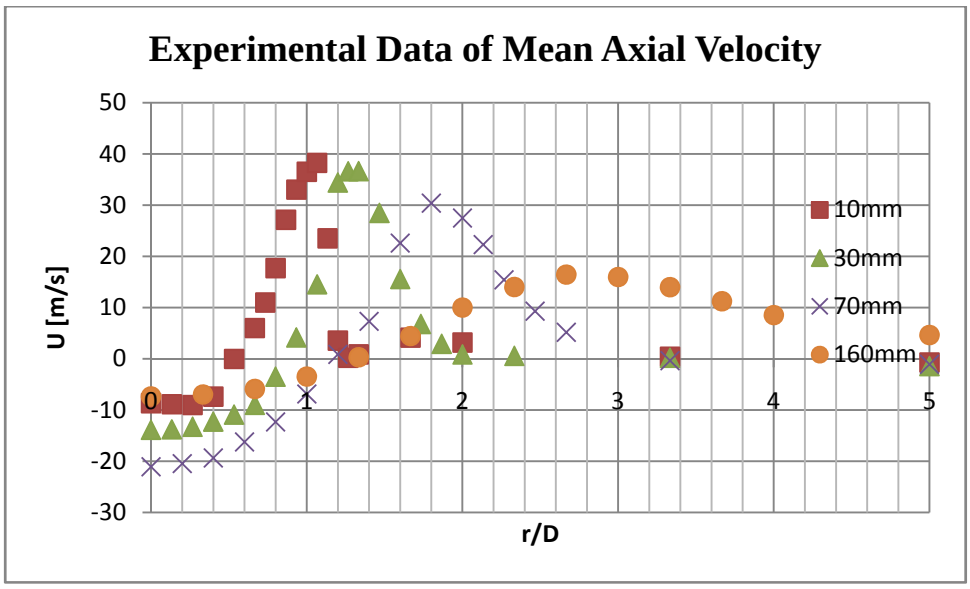

Figure 29. Experimental data of mean axial velocity for axial locations: 10mm, 30mm, 70mm and 160mm[27,42]

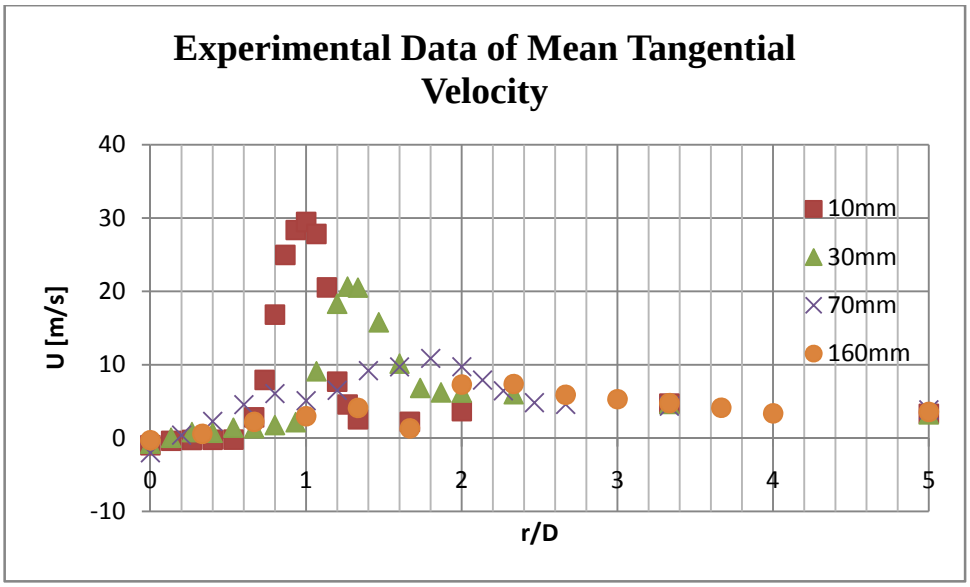

Figure 30. Experimental data of mean tangential velocity for axial locations: 10mm, 30mm, 70mm and 160mm[27,42]

3.5.2 Temperature and Species

3.5.2.1 Raman Scattering Measurements

For the simultaneous determination of temperature, mixture fractions and major species concentration, Raman scattering is applied. Series of 300 single-pulse with a spatial resolution of 0.6mm is recorded for 120 points in axial and radial directions. Estimated error for mean values are 2% and for fluctuations, 6%. Graphics from measured mean temperature data for some locations can be seen in Figure 31.

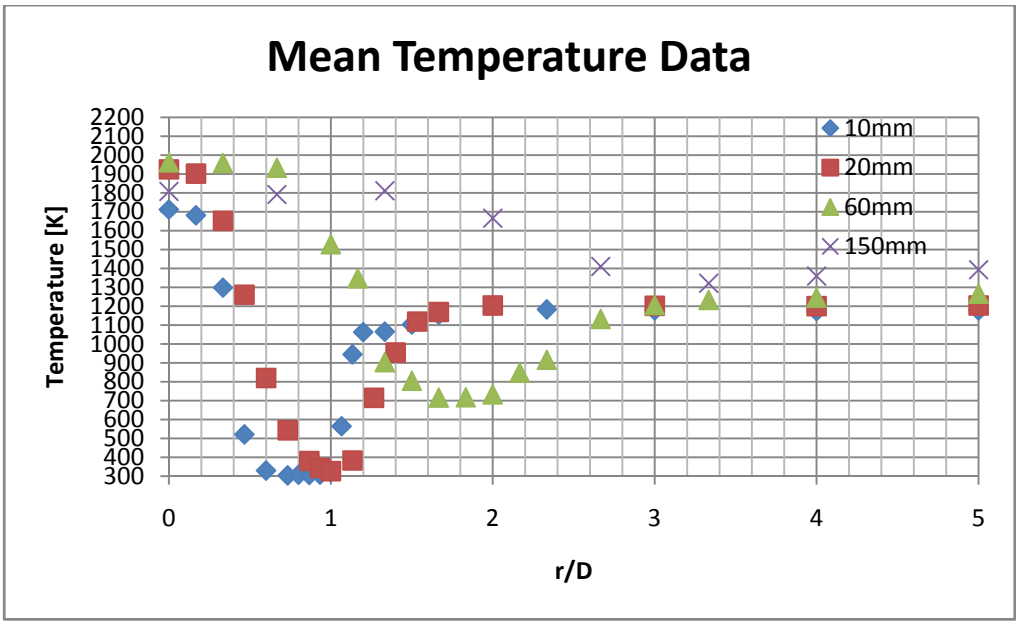

Figure 31. Experimental data of mean temperature for axial locations: 10mm, 20mm, 60mm and 150mm[24-27,43]

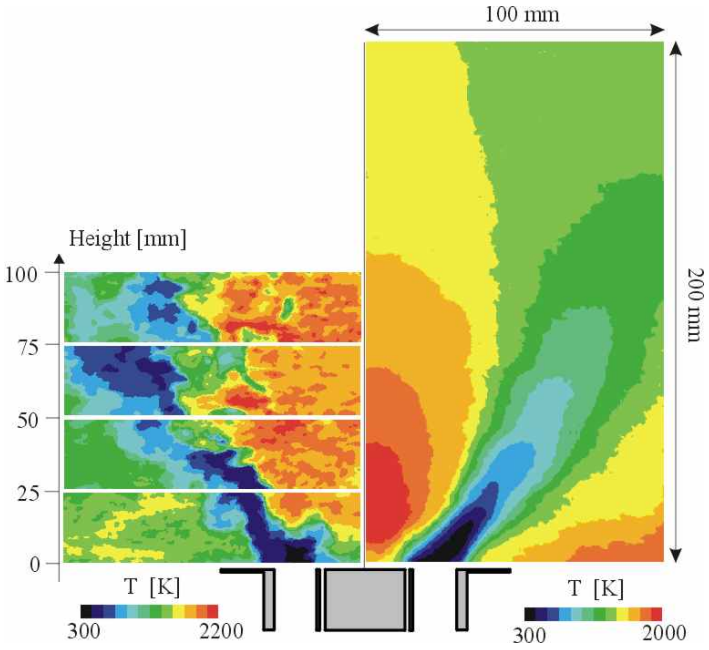

Figure 32.Temperature field in the s09 configuration. Left side instantaneous temperature field, right side averaged temperature field[24-27,43]

3.5.2.2 Planer Laser Induced Fluorescence Measurements

Rayleigh imaging thermometry is used for temperature measurements by exciting KrF laser at 248nm. Laser induced fluorescence is used for species concentration at different wave lengths.

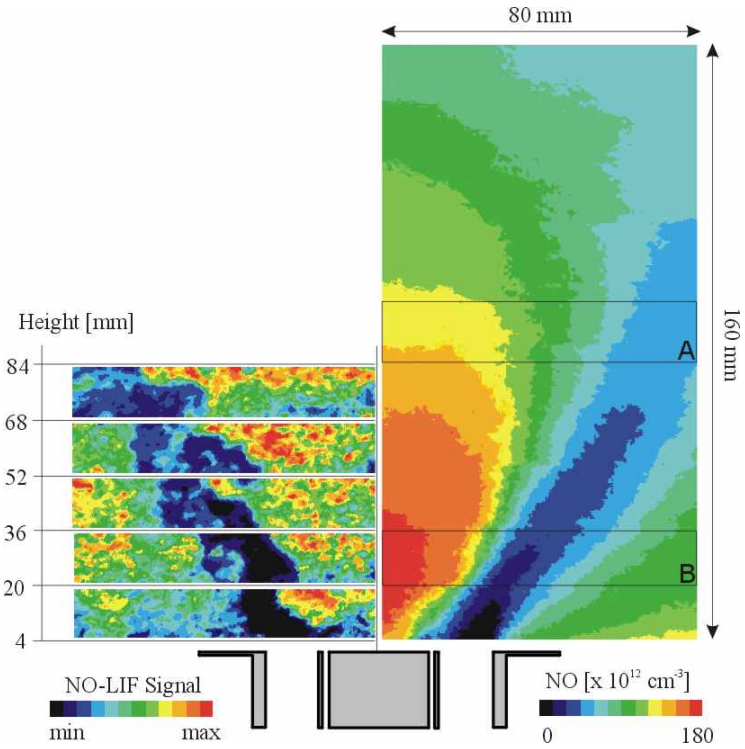

Figure 33. NO concentration in the s09 configuration. Left side single-shot images for different height, right side averaged temperature field[24-27,43]

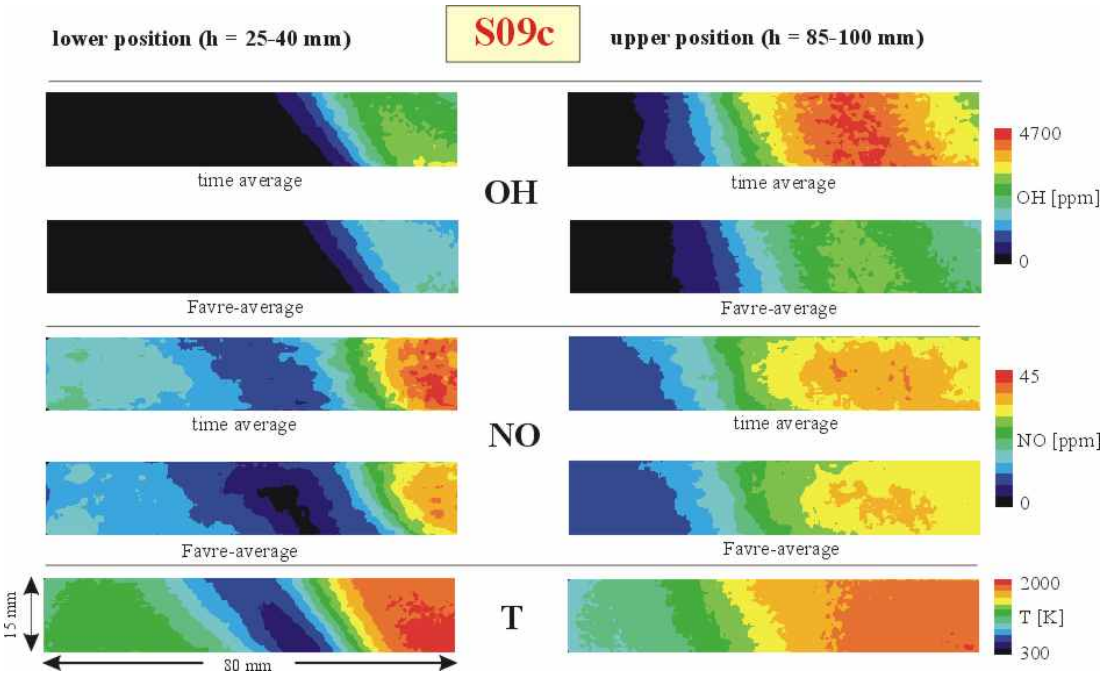

Figure 34. Results of simultaneous measurements of NO, T and OH. Operating condition S09. Comparison of Favre-averaged and temporally averaged concentration fields[24-27,43]

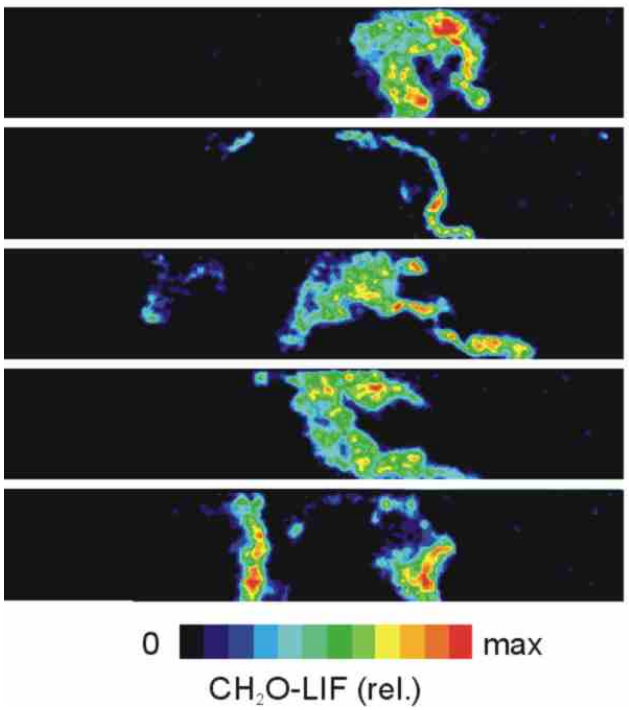

Figure 35. Single-shot images of CH2O-LIF distribution at operating condition S09[24-27,43]

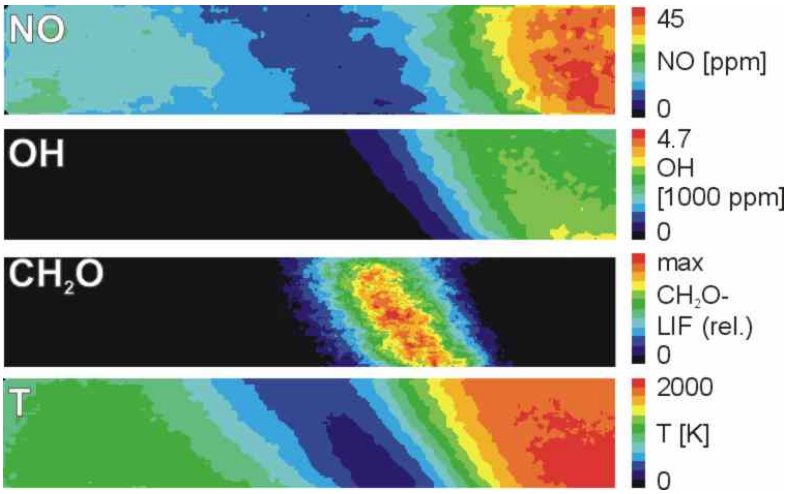

Figure 36. Averaged distribution of T, OH, NO and CH2O for the standard operating condition S09[24-27,43]

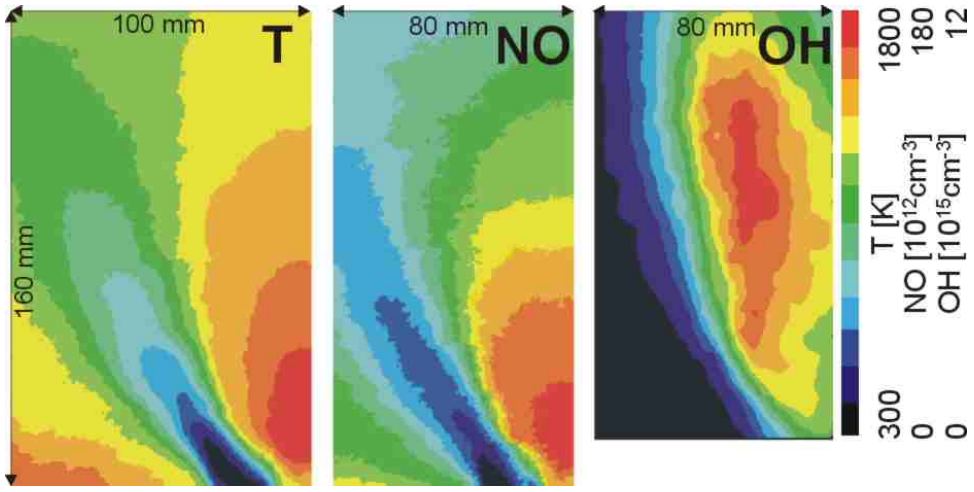

Figure 37. Comparison of the large-scale T, OH- and NO-fields in the swirl flame (operating condition S09). The images are assembled from numerous individual measurement positions to cover the whole height of the swirl flame[24-27,43]

3.6 Theoretical Thermal Power Calculation

Whether thermal power of the case is given reference [22-27,43] as 150kW, a calculation is made to be sure about the value.

In Chapter 2 Part 2.6, the calculation methodology for a reaction is defined. Whether the standard state definition is made for 298.16K and there is a temperature difference, it is low enough to neglect compared to 300K inlet temperature of test setup.

For the products, adiabatic flame temperature is calculated as 2040.84K for 0.83 equivalence ratio by using Cerfacs's Adiabatic Flame Temperature Calculator Tool[62].

The equation of reaction is:

$$0.83CH_4 + 2O_2 + 7.52N_2 \rightarrow 0.83CO_2 + 1.66H_2O + 7.52N_2 + 0.34O_2$$

$\Delta\mathcal{H}^\circ_f$ values of reactants and products are given inTable 8 where standard formation enthalpies of natural states (like elements) are zero.

Table 8. Calculated values of enthalpy of formation for products and reactants

	$\Delta\mathcal{H}^\circ_f$[kj/mol]	W[kg/kmol]
$CH4$	-74.87	16.0425
$O2$	0	31.9988
$N2$	0	28.0134
$CO2$	-393.51	44.0095
$H2O$	-241.83	18.0153

Since the mass flow rate of the fuel (CH4) is 15m^3/h, and the density of the fuel is 0.6443kg/m^3 at 300K and 1bar, the mole flux of the CH4 is calculated as:

$$\dot{n}_{CH4} = 15\frac{m^3}{h}\times\frac{1h}{3600s} \times 0.6443\frac{kg}{m^3}/0.01604\frac{kg}{mol} = 0.1674\frac{mol}{s}$$

the reaction is recalculated for mole flux:

$$(0.2016) \times \quad 0.83CH_4 + 2O_2 + 7.52N_2 \rightarrow 0.83CO_2 + 1.66H_2O + 7.52N_2 + 0.34O_2$$

$$0.1674CH_4 + 0.4033O_2 + 1.516N_2 \rightarrow 0.1674CO_2 + 0.3347H_2O + 1.516N_2 + 0.06854O_2$$

Using Eq. 272:

$$\Delta H_{reaction} = \sum \Delta H_{Products} - \sum \Delta H_{Reactants}$$

$$\Delta\dot{H}_{reaction} = ((0.1674 \times -393.51) + (0.3347 \times -241.83) + (1.516 \times 0) + (0.06454 \times 0))_P - ((0.1674 \times -74.87) + (0.4033 \times 0) + (1.516 \times 0))_R$$

$$\Delta\dot{H}_{reaction} = -134.28[\frac{kj}{s}]$$

Since the mass flow rate is embedded into the equation, the thermal power of the test setup is calculated as 134.28kW.

Heat of combustion of methane is calculated as 50.13MJ/kg from above definitions. This value is close to the values stated as "lower heating value of methane" in literature (50.009MJ/kg in Ref.[63]). On the other hand, the higher heating value is given around 55.5MJ/kgwhich is nearly 10% higher than lower heating value [63]. If the thermal power is calculated by higher heating value:

$$\Delta\dot{H}_{reaction} = -148.66[kW]$$

Which is very close to the value given by references [22-27,43].

CHAPTER 4

NUMERICAL APPROACHES & STUDIED CASES

In the scope of the thesis, three main objectives are obtained. First, the mesh independency for URANS calculations is investigated. After a mesh independent solution is obtained, comparison of available combustion models in ANSYS Fluent 14.0 solver is made. At the end, performance of U-RANS compared to LES is investigated.

All the simulations are performed with 3D geometry which reflects the nature of the flow. It is stated that the length of combustion chamber is 1200mm in Ch.3. Whether the real length can be modeled for simulations, it may be more than needed if there is no effect to primary zone from downstream of the chamber. Nearly 2/3 of combustion chamber height and whole chamber diameter is taken into computational domain. The modeling is started at air swirler inlet ports to calculate any unsteady behavior in swirler exit which is stated in literature (See Chapter 1). The fuel line is also modeled. 41.75mm fuel pipe is taken into computational domain in order to let CFD choose the velocity profile. This part of the fuel line is the whole straight part before entering the combustion zone. 30mm of burnt gas exit is modeled at the top of the computational domain which is same for the experimental data. In order to prevent any miscalculation because of soon wall, zero shear boundary condition is applied to top wall as it is suggested [61].

50mm below the swirl burner exit plane of the combustion chamber is also taken into account to allow any upstream recirculation. Views for CFD model can be seen inFigure 38. A cut view of the swirl burner and the fuel injector can be seen in Figure 39.

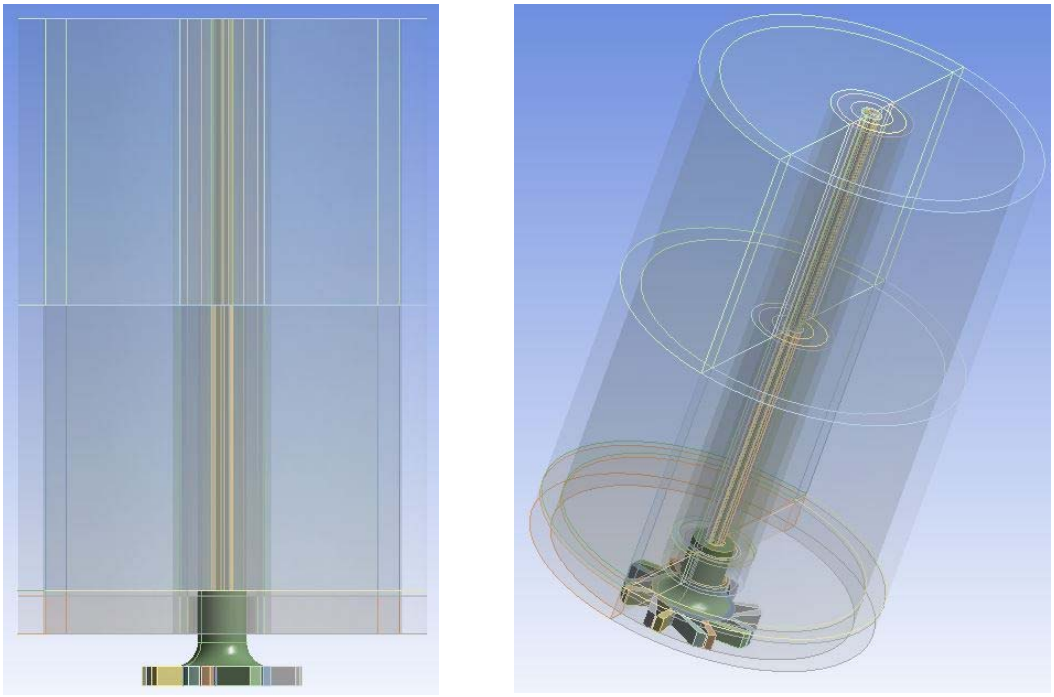

a) Side view b) Isometric view

Figure 38. Side view and isometric view of the CFD model

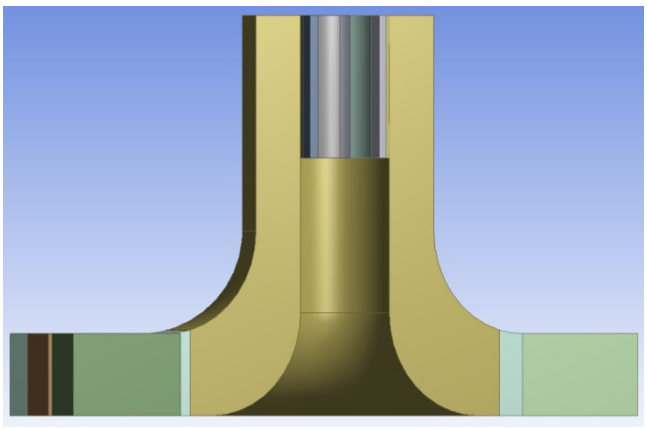

Figure 39. A cut view from swirl burner and fuel injector

4.1 Mesh Studies

In case of mesh sensitivity analysis, five levels of hexahedral meshes are created. The first mesh, which is the most coarse one, has 300 000 hexahedral elements. The ratio of element count between each level of meshes is 3 or higher. The finest mesh therefore has nearly 40 million hexahedral elements. The list of meshes is given in Table 9.

Table 9. The list of meshes

Mesh Number	**Mesh ID**	**Number of CV Elements**	**Ratio of CV elements**	**Grid point**		
				Axial direction	*Radial direction*	*Tangential direction*
1	The most coarse	0.3M	-	64	58	96
2	Coarse	0.9M	3	85	80	128
3	Medium	2.7M	3	114	124	168
4	Fine	11.5M	4.2	167	198	336
5	The Finest	38.5M	3.3	245	290	504

Table 10. Solver options for mesh study

Mesh	0.3M the most coarse (Mesh #1) 0.9M Coarse (Mesh #2) 2.7M Medium (Mesh #3) 11.5M Fine (Mesh #4) 38.5M The Finest (Mesh #5)
Solver	Pressure Based Segregated
Temporal Discretization	First Order Implicit
Spatial Discretization	Second Order Upwind
Pressure – Velocity Coupling	SIMPLE
Turbulence Model	Realizable k-epsilon
Wall Function	Standard
Combustion Model	Eddy Dissipation Model
Reaction Scheme	One Step

Views from mesh number 3 (Medium mesh) can be seen in Figure 40 and Figure 41.

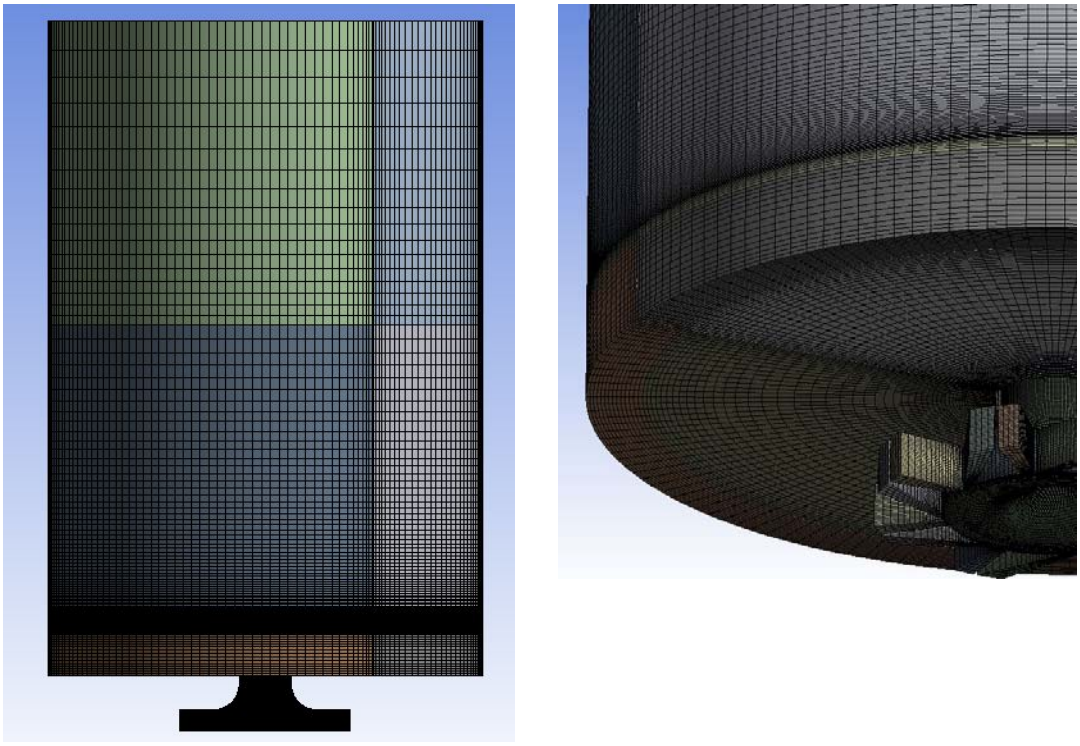

a) Side view b) Close view

Figure 40.Views from 2.7M mesh

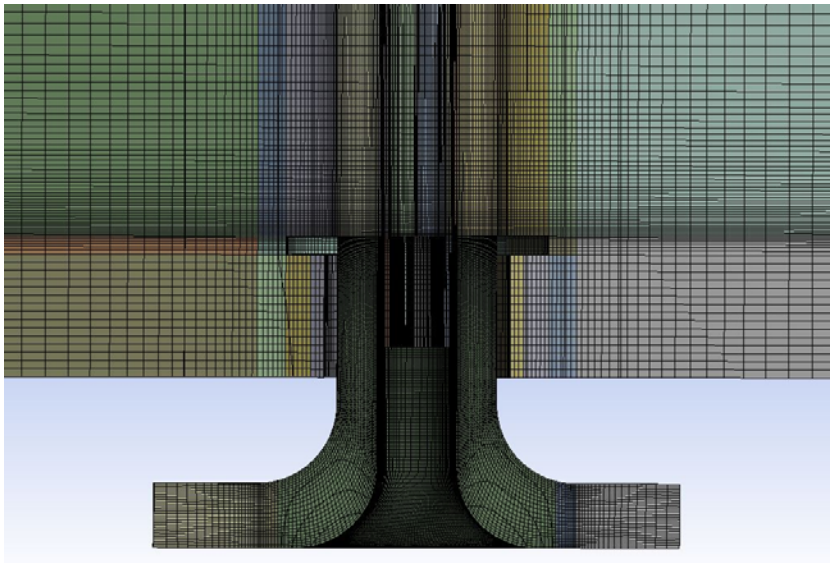

Figure 41.Cut view of 2.7M mesh

Expect time step size, solver options used for this steady kept same for every mesh. Time step size is changed from mesh to mesh for better convergence behavior which is between 1xE-5 to 5xE-5 where CFL number is close to unity. The other solver options for mesh study are given in Table 10.

4.2 Combustion Model Comparisons

After mesh independency is obtained, combustion models are investigated to simulate the flow. Combustion model comparison is made for 4 combustion models (Eddy Dissipation Model, Laminar Rate Model, Finite Rate / Eddy Dissipation Model, Presumed β-PDF Model) and two reaction schemes (One Step and Two Step). These models are available in ANSYS Fluent 14.0 and default parameters for this model can be found in [59].Solver options for combustion model comparison can be seen in Table 11.

Table 11. Solver options for combustion model comparisons

Mesh	2.7M Medium Mesh (Mesh #3)
Solver	Pressure Based Segregated
Temporal Discretization	First Order Implicit
Spatial Discretization	Second Order Upwind
Pressure – Velocity Coupling	SIMPLE
Turbulence Model	Realizable k-epsilon
Wall Function	Standard
Combustion Model	Eddy Dissipation Model Finite Rate / Eddy Dissipation Model (Blend) Laminar Rate Model Presumed β-PDF Model (Equilibrium)
Reaction Scheme	One Step Two Step 14 Specious PDF

4.3 LES Calculations

In order to find out the dependency on turbulence closure, Large Eddy Simulations are performed with the same mesh. Dynamic Smagorinsky-Lilly subgrid model is used by dynamic stress, dynamic energy flux and dynamic scalar flux options. Therefore, the needed parameters in Smagorinsky-Lilly model are computed for each time and each cell which increases the accuracy meanwhile increases CPU need.

LES calculations are performed with 5xE-6 time step size values which decreases CFL number under unity. 0.9M and 2.7M meshes are used for calculations. To focus on flow field capturing, only One Step Eddy Dissipation Combustion Model is used for its simplicity. The other options used in LES calculations are given in Table 12.

Table 12. Solver options for LES calculations

Mesh	0.9M Coarse Mesh (Mesh #2) 2.7M Medium Mesh (Mesh #3)
Solver	Pressure Based Segregated
Temporal Discretization	First Order Implicit
Spatial Discretization	Bounded Central Differencing & Second Order Upwind
Pressure – Velocity Coupling	SIMPLE
Turbulence Model	LES with Dynamic Smagorinsky – Lilly Subgrid Scale Model
Combustion Model	Eddy Dissipation Model
Reaction Scheme	One Step

4.4 Other Comparisons

4.4.1 Including Radiation Effects

Effect of radiation on the temperature field is another investigated phenomenon. In order to obtain a radiation affected simulation, radiative term is included by using Discrete Ordinate Radiation Model [59]. Only one case is simulated by radiation model to observe the radiative effect. Solver options of the simulation with radiation model is listed in Table 13.

Table 13. Solver options for the simulation including radiation model

Mesh	2.7M Medium Mesh (Mesh #3)
Solver	Pressure Based Segregated
Temporal Discretization	First Order Implicit
Spatial Discretization	Second Order Upwind
Pressure – Velocity Coupling	SIMPLE
Turbulence Model	Realizable k-epsilon
Wall Function	Standard
Combustion Model	Finite Rate / Eddy Dissipation Model (Blend)
Reaction Scheme	Two Step

4.4.2 Second Order Upwind vs. QUICK

Another study is made to compare the spatial discretization schemes. Since the swirling flow known for its nonlinear behavior, second order upwind scheme is applied as default spatial discretization scheme. However, quadratic upwind interpolation alters the second order upwind scheme where high nonlinearity is in presence. Therefore, a simulation is performed by QUICK scheme to compare the performance of these two schemes. List of solver options for this simulation is given in Table 14.

Table 14. Solver options for QUICK scheme simulation

Mesh	2.7M Medium Mesh (Mesh #3)
Solver	Pressure Based Segregated
Temporal Discretization	First Order Implicit
Spatial Discretization	QUICK
Pressure – Velocity Coupling	SIMPLE
Turbulence Model	Realizable k-epsilon
Wall Function	Standard
Combustion Model	Finite Rate / Eddy Dissipation Model (Blend)
Reaction Scheme	Two Step

CHAPTER 5

RESULTS

This topic covers the results of simulations performed throughout the thesis. All the investigated data under this section are statistically averaged. Before start averaging, convergence of velocity and static temperature motions are observed. Statistically averaged data are taken at least for 50 times of calculated eddy turnover time ($\tau_{eddy\ time} = 0.0026s$). For some URANS calculations, more time is needed for better averaged results due to calculated slow eddies. Several HPC sources are employed for simulations.

5.1 Results of Mesh Study

Mesh study for TECFLAM s09 has showed that, mesh independent solutions on URANS calculations can be reached by applying 0.9M hexahedral elements or plus. On the other hand, a solution for 38.5M hexahedral elements could not be obtained due to high CPU costs where more than 4 minutes (with 192 compute nodes) is needed for one time step forwarding which means at least one month of iteration time just for mean data gathering. Since the mesh independency is obtained with coarser meshes, no attempt is taken for the finest mesh (Mesh 5).

For comparison of meshes, results of axial velocity are given inFigure 42 - Figure 44. It is found out that results of Mesh 1 which has 300,000 hexahedral elements differ from all higher level of meshes. Meanwhile, results of other meshes are very similar with each other. Therefore, it is claimed that 900,000 or higher elements are enough to have mesh independent solutions for URANS calculations. Since available CPU power is high enough, for the rest of work, 2.7M (Mesh 3) is used to be on the safe side.

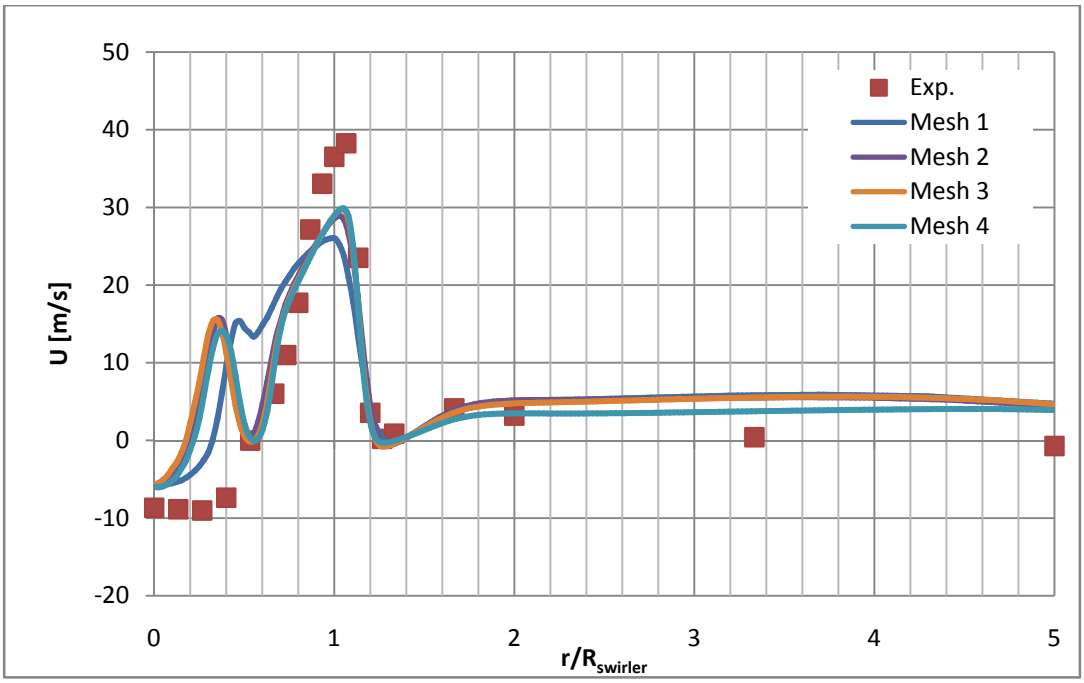

Figure 42. Mean axial velocity distribution at various locations from mesh study; 10mm downstream of swirler exit plane

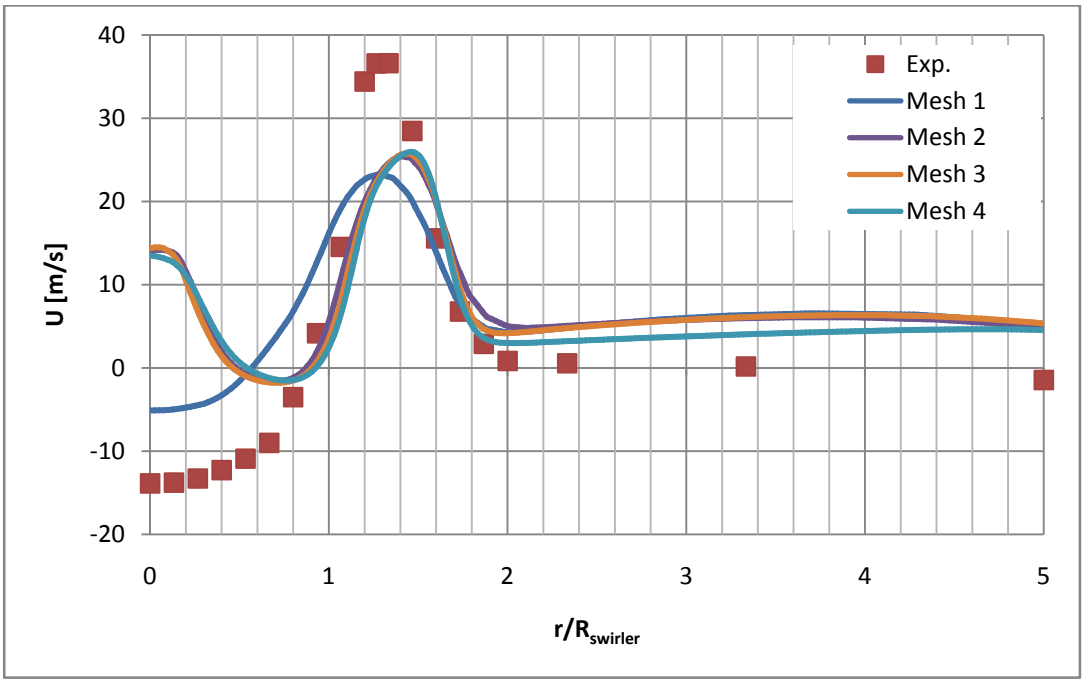

Figure 43. Mean axial velocity distribution at various locations from mesh study; 30mm downstream of swirler exit plane

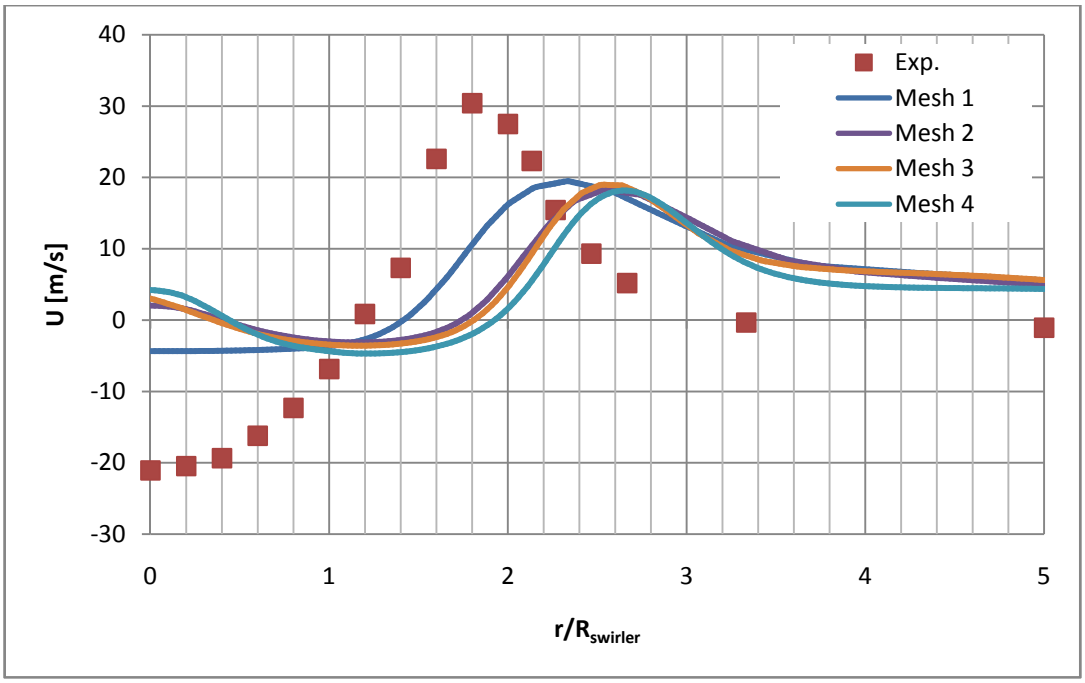

Figure 44. Mean axial velocity distribution at various locations from mesh study; 70mm downstream of swirler exit plane

When Figure 43 and Figure 44 are investigated, Mesh 1 may seem better than the other meshes. However, Mesh 1 has very coarse elements and can only predict the big eddies. Smaller disturbances are damped due to wide elements and causes a mesh depended results. Since this study is made in order to eliminate any mesh depended effects, Mesh 1, whether it gives better results in some locations, shall be eliminated to make a pure comparisons.

The results given in Figure 42 - Figure 44differ from the experimental data very much. To get better solutions, an investigation is made to understand to problem in better way. Mesh study is performed with options given in Table 10. Every parameter given in Table 10 may be questioned for their suitability. In order to have a clear view on results, static temperature field is investigated which is given in Figure 45 - Figure 47. The instantaneous vector plot, mean vector contour and mean temperature contour is given in Figure 48.

InFigure 45, a sudden temperature peak is calculated by simulation which does not exist in experimental data. Meanwhile, temperature rise at center could not be captured with simulations. When axial velocity field at 10mm (Figure 42) is

investigated, it is seen that there is a strong negative velocity at the center which is almost captured by simulations. However, there is also a sudden velocity rise in simulations. The location of this temperature peak and velocity rise corresponds with each other where the location of velocity is just slightly shifted to the central axis. Therefore, it is understood that Eddy Dissipation Model, which is a "mixed is burnt" model, generates a reaction at mixing zone. On the other hand in experimental data, reaction occurs at center of the domain where a strong inner recirculation zone presence which is indicated by the negative axial flow. In another word, in simulations, reaction takes place earlier than it should be. So, a combustion model which covers the reaction delay can solve this problem.

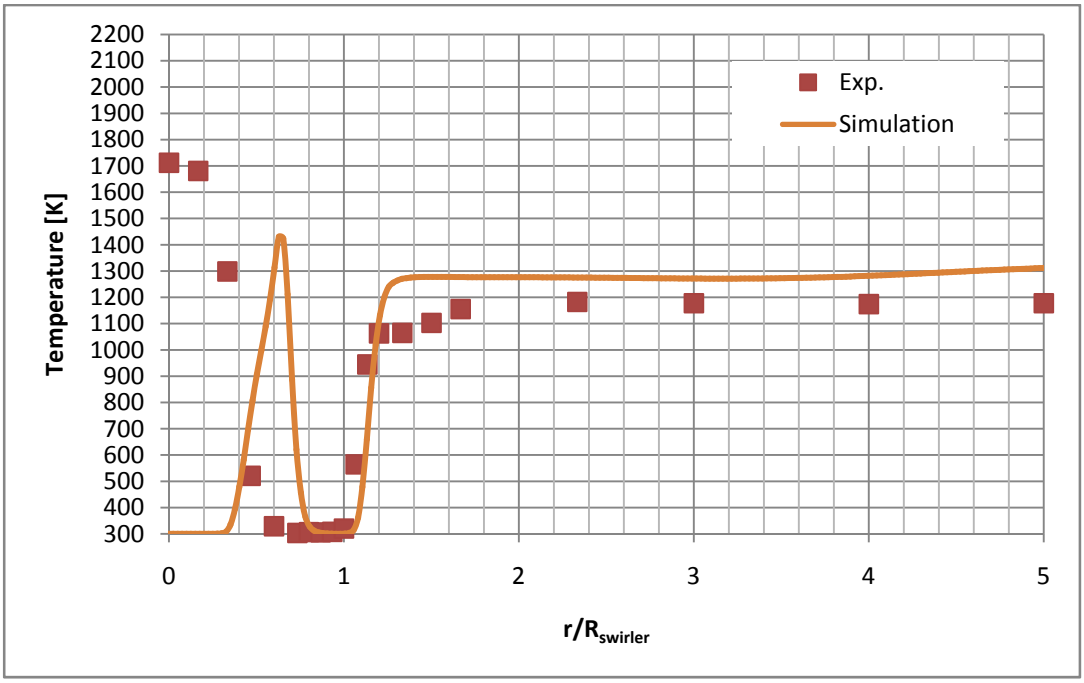

Figure 45. Mean static temperature distribution at various locations from mesh study; 10mm downstream of swirler exit plane

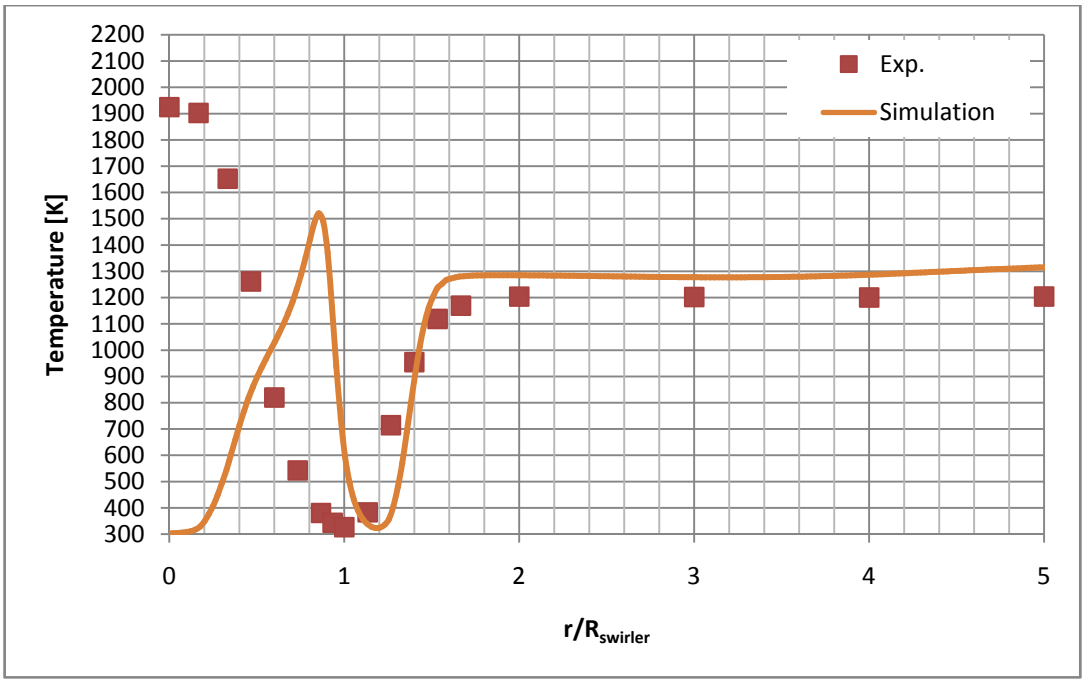

Figure 46. Mean static temperature distribution at various locations from mesh study; 10mm downstream of swirler exit plane

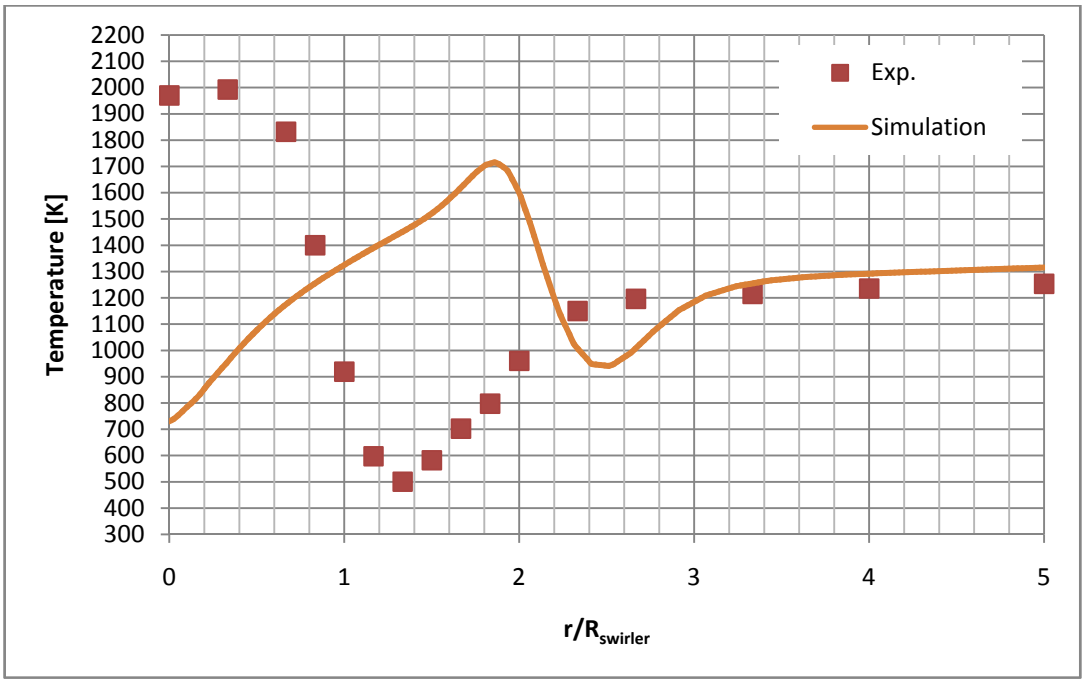

Figure 47. Mean static temperature distribution at various locations from mesh study; 10mm downstream of swirler exit plane

Both for axial velocity and static temperature, simulation data fits quite well with the trend of experimental data on locations after swirler outer diameter when moving on

radial direction. However, negative axial velocity in experimental data shows an outer recirculation effect which could not be observed in simulations. 100K offset of temperature can be a result of miscalculated velocity field or some other causes.

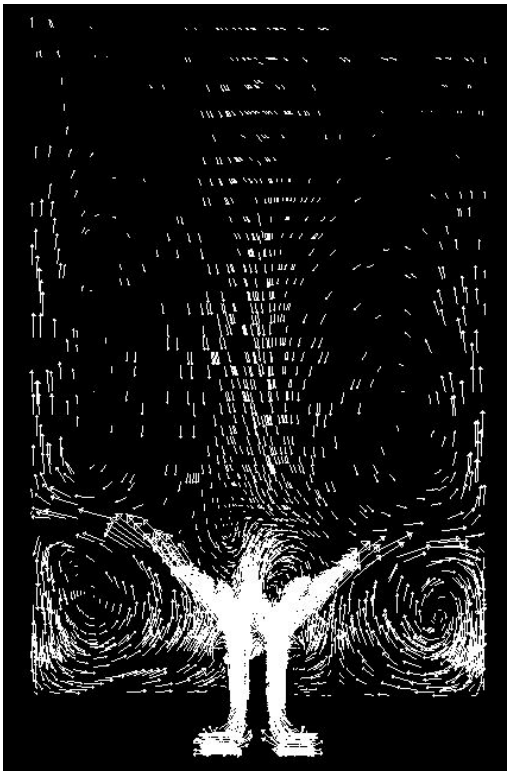

a) Instantaneous vector field

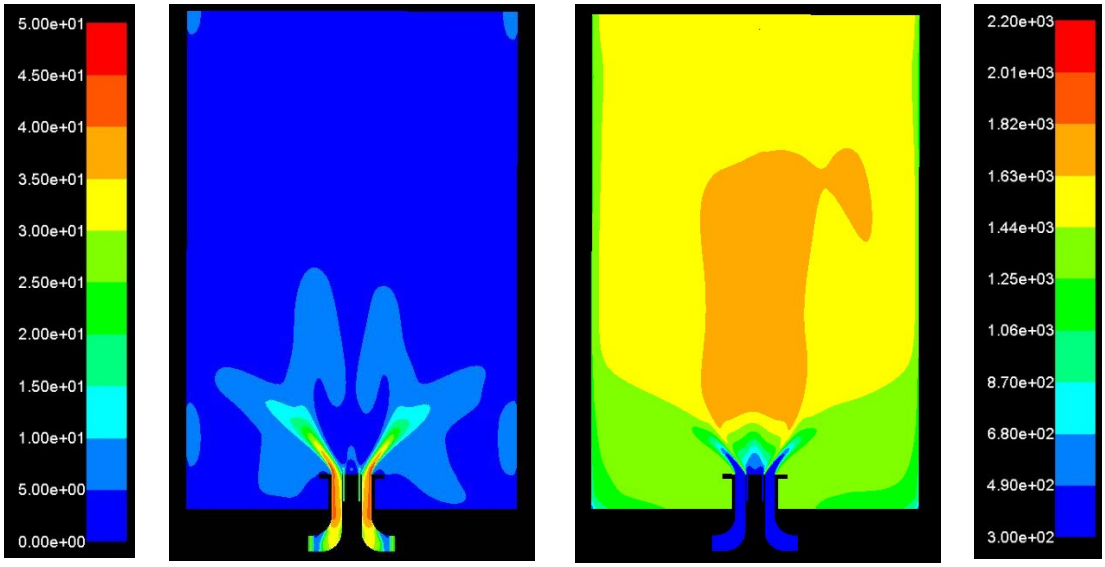

b) Mean velocity contour c) Mean static temperature contour

Figure 48.Instantaneous vector field, mean velocity contour and mean temperature contour of simulation by mesh 3, k-epsilon turbulence model, one step eddy dissipation model

Moving on downstream, a slight shift heading to wall is observed both on temperature and velocity field. This shifting increases at higher downstream locations. The reason of shifted values is bounded on the diameter of inner recirculation zone.

It is concluded from the results of mesh study that, combustion model which is used for mesh study predicts an earlier reaction zone which affects temperature and velocity. A more proper combustion model which includes reaction delays is sought in order to fix this problem.

5.2 Combustion Model Comparison

In the case of combustion model comparison, four combustion models are applied with two different reaction schemes.

5.2.1 One Step vs. Two Step Reaction Schemes

The investigation on combustion model is started with same combustion model with different reaction schemes. One step reaction scheme was used so far. Two step reaction scheme is applied for any refinement in velocity or temperature field. The Results of axial velocity and static temperature are given inFigure 49 - Figure 54. It is understood that one step or two step reaction scheme does not make a great difference in flow field expect in higher downstream regions. InFigure 51, prediction of center velocity is higher for two step reaction scheme. Meanwhile, the peak velocity is closer to the experimental values both in magnitude and radial location. Same trend is also observed in temperature results inFigure 52 - Figure 54. Predicted peak temperature is higher (which is closer to experimental values) and closer to the peak temperature location measured in experiments. Therefore, it is concluded that whether there is no big refinement by applying two step reaction scheme, it is more promising than one step reaction scheme and it is set as default reaction scheme for the rest of the work. The instantaneous vector plot, mean vector contour and mean temperature contour is given in Figure 55.

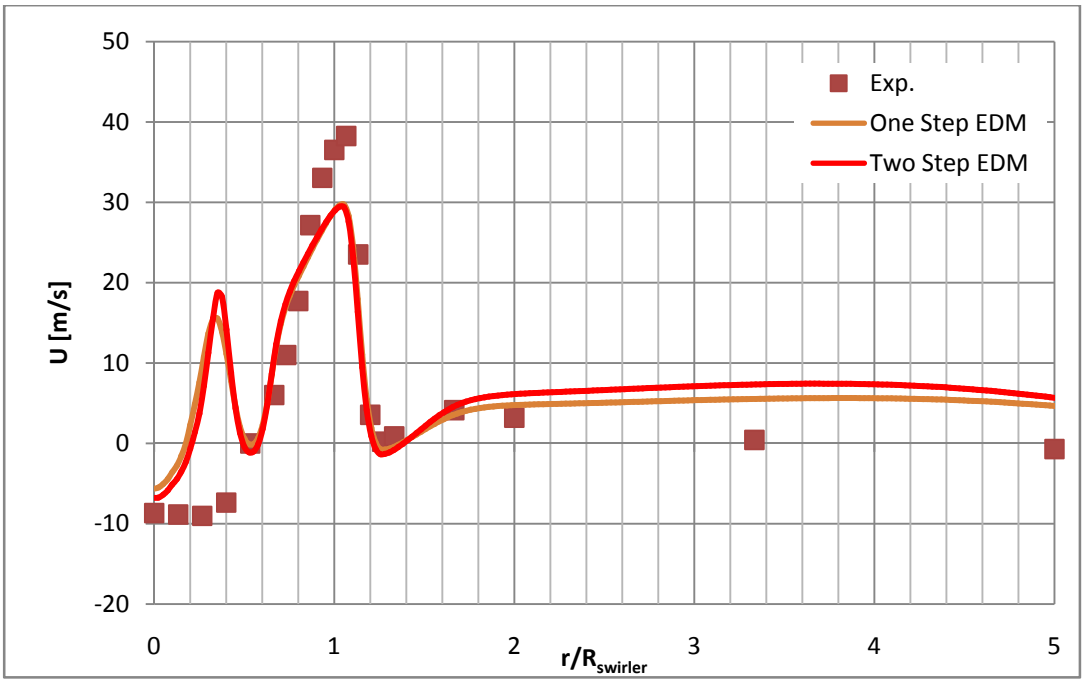

Figure 49. Comparison of mean axial velocity from the results of one step and two step reaction scheme solutions; 10mm downstream of swirler exit plane

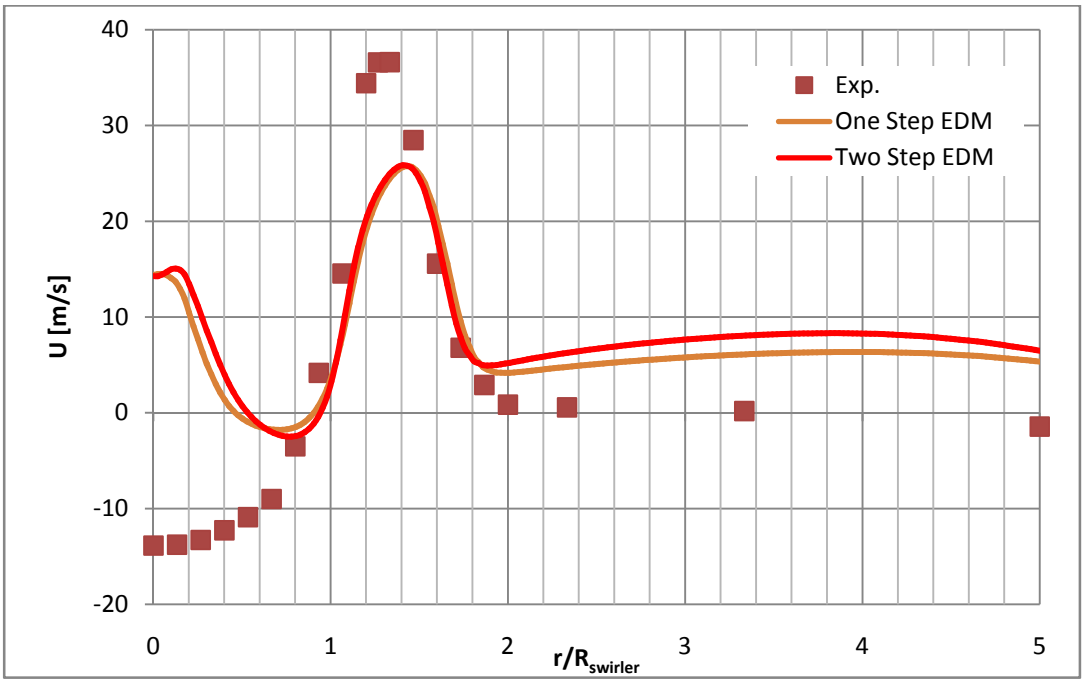

Figure 50. Comparison of mean axial velocity from the results of one step and two step reaction scheme solutions; 30mm downstream of swirler exit plane

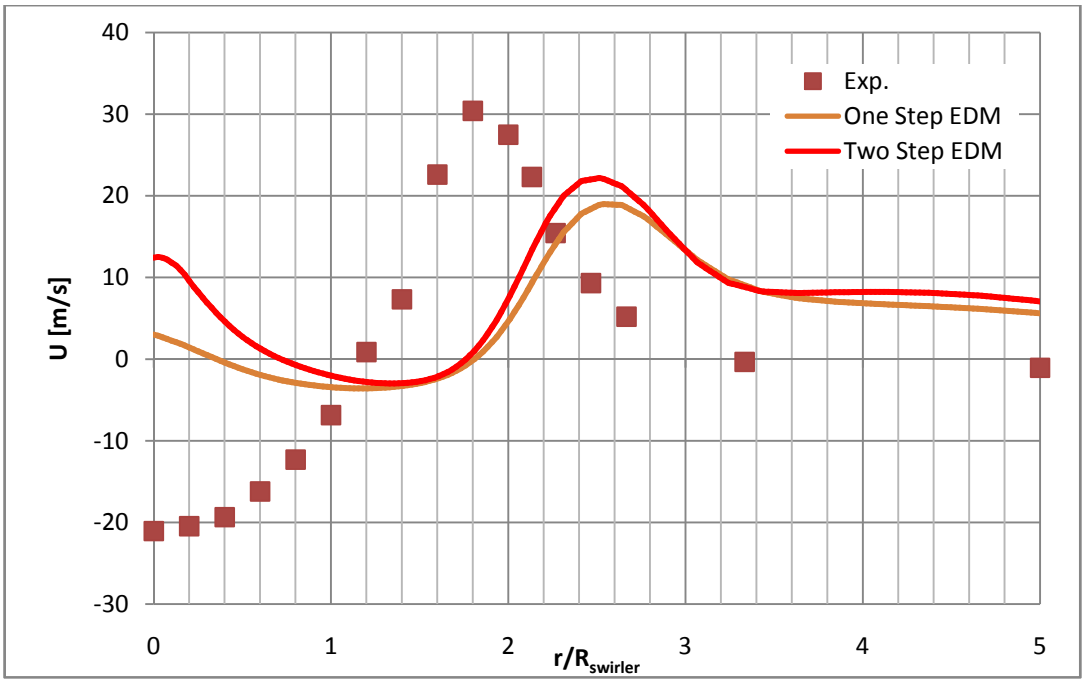

Figure 51. Comparison of mean axial velocity from the results of one step and two step reaction scheme solutions; 70mm downstream of swirler exit plane

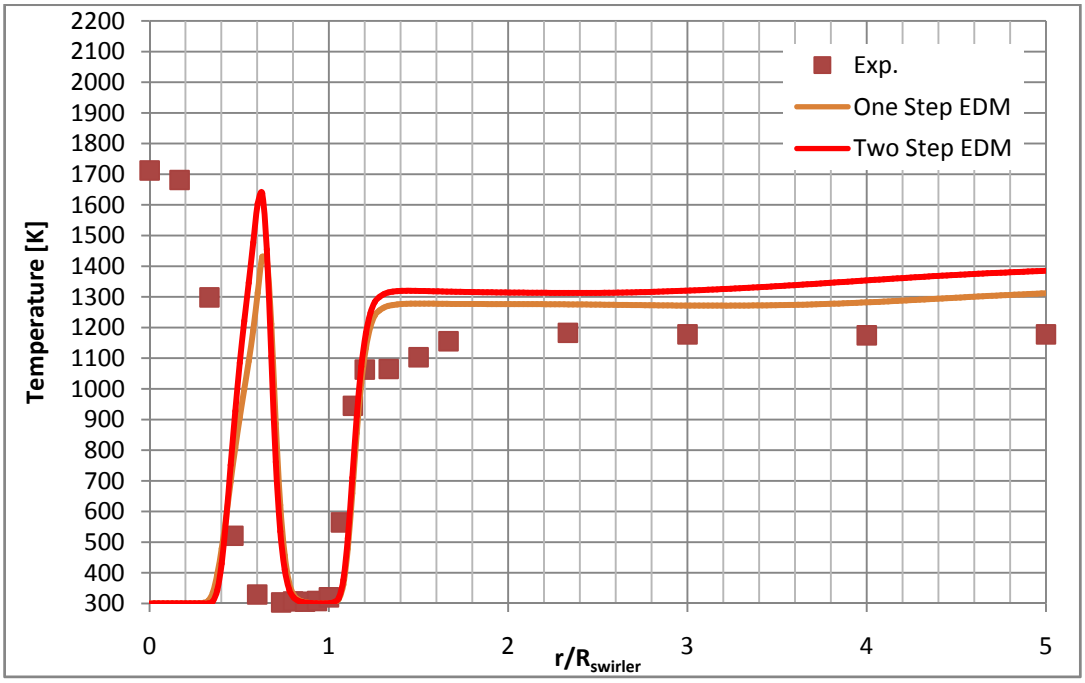

Figure 52. Comparison of mean static temperature from the results of one step and two step reaction scheme solutions; 10mm downstream of swirler exit plane

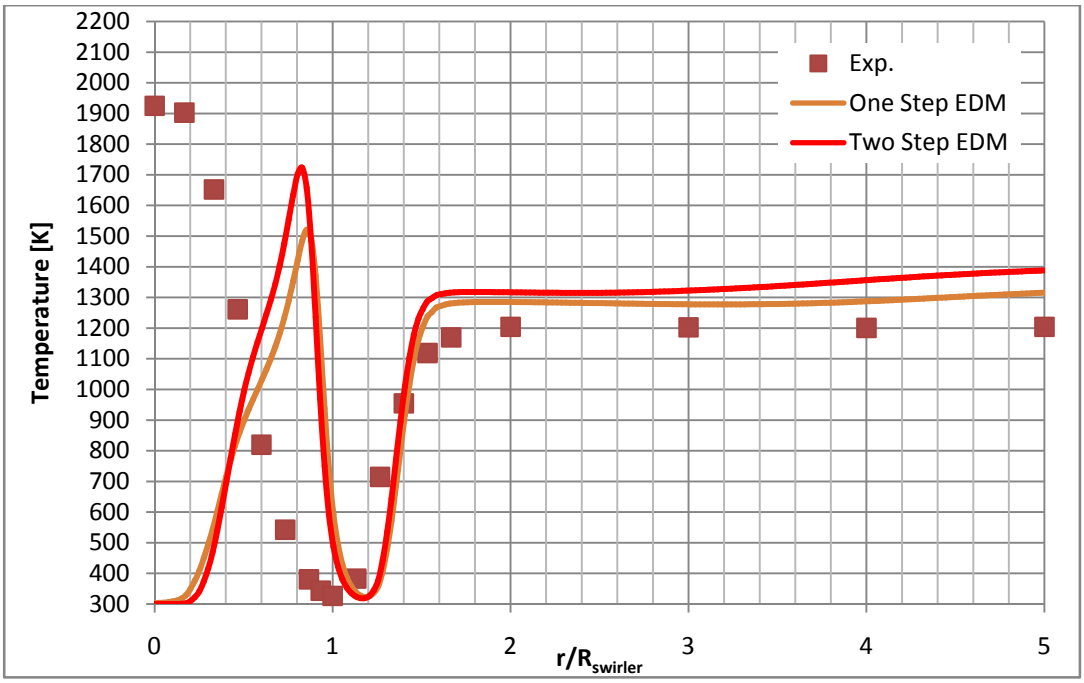

Figure 53. Comparison of mean static temperature from the results of one step and two step reaction scheme solutions; 20mm downstream of swirler exit plane

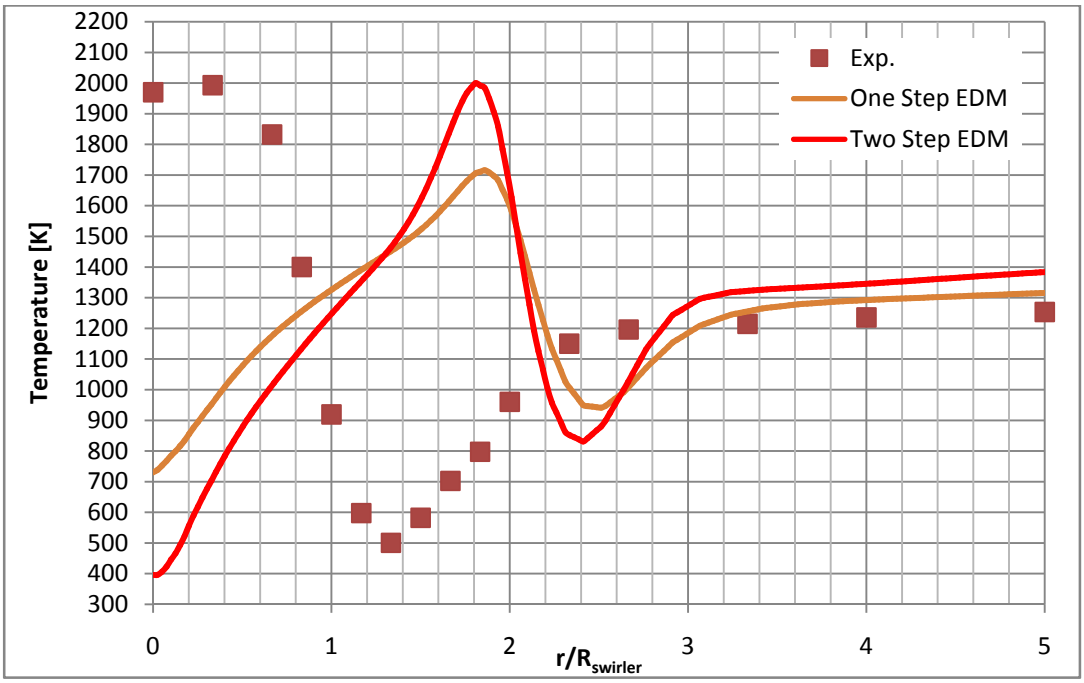

Figure 54. Comparison of mean static temperature from the results of one step and two step reaction scheme solutions; 60mm downstream of swirler exit plane

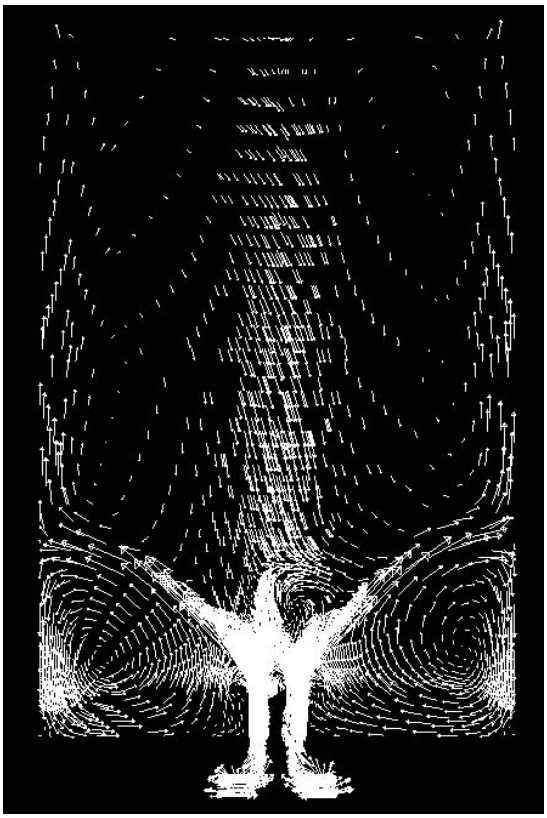

a) Instantaneous vector field

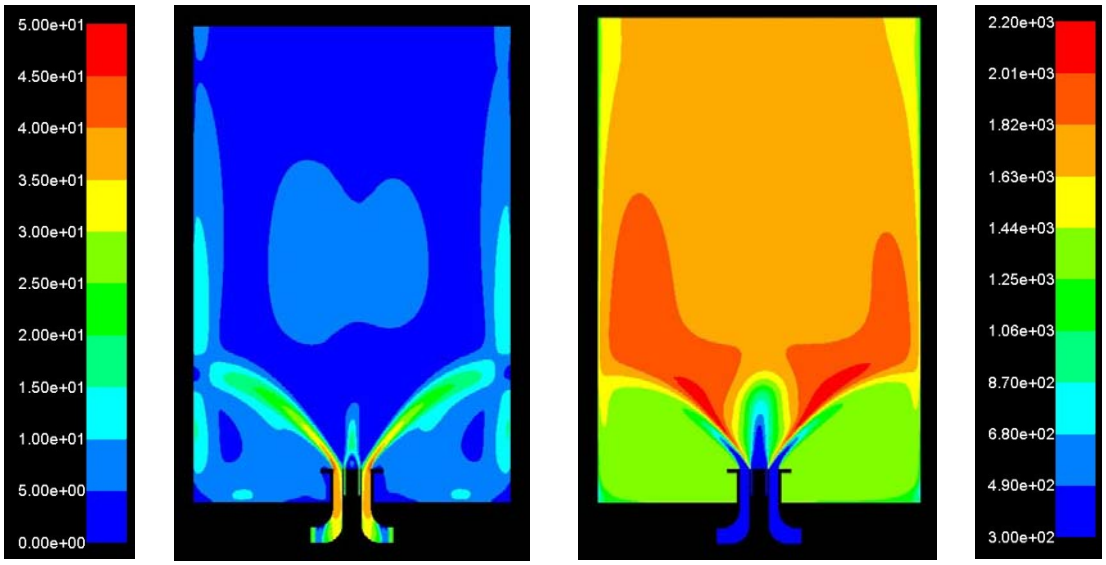

b) Mean velocity contour c) Mean static temperature contour

Figure 55.Instantaneous vector field, mean velocity contour and mean temperature contour of simulation by mesh 3, k-epsilon turbulence model,two step eddy dissipation model

5.2.2 Infinitely Fast Chemistry vs. Laminar Rate Chemistry

Previous results showed that to missing reaction delay in simulations results with an early combustion which is mixing layer of methane and air. To overcome this issue, a new combustion model is taken into account. One of the combustion models which consists reaction delays is Finite Rate (Laminar Rate) Model. This model includes Arrhenius laws of burning. On the other hand, it does not include turbulent effect on reaction. Two step reaction scheme is applied for the reasons stated in previous section. Results are given inFigure 56 - Figure 61. The instantaneous vector plot, mean vector contour and mean temperature contour is given in Figure 62.

Laminar rate combustion model eliminates the sudden temperature and velocity rise in flow domain. WhenFigure 56 is investigated, the central recirculation zone at 10mm downstream of swirler plane is missing in the result of laminar rate simulation while it is predicted by Eddy Dissipation Model. At 10mm downstream of swirler exit plane (Figure 59), temperature is under predicted in central zone, and over predicted in outer zone. In Laminar rate model, there is no coupling between reaction, and turbulence. Heat of reaction affects the flow field, but the turbulence does not play a role in reaction rate. Thus, the location of the flame is not effected after it is stabilized.

In higher downstream regions, velocity and temperature prediction in central zone is closer to experimental data. On the other hand, EDM shows far better performance in outer zone of the domain. Also the velocity distribution is more flattened on laminar rate model simulations since the velocity peak moves away from the center.

In “mixed is burnt” models, fuel burns as soon as it meets with the oxidizer. A huge amount of fuel burns at mixing zone. Since the densities of the products are lower and reaction accelerates the flow, the products leave the reaction zone quickly by wiping out any recirculating flow. Therefore, laminar rate model predicts central recirculation zone while EDM is not able to capture it.

On the other hand, turbulence mixing affects the reaction rate crucially which is not covered by the Laminar Rate model. Reactants burns much slower than it should be which damps the pressure gradient in early and outer combustion zone. Therefore,

higher temperatures are encountered in Laminar Rate Model. And no recirculating flow occurs between upper (70mm) and lower region.

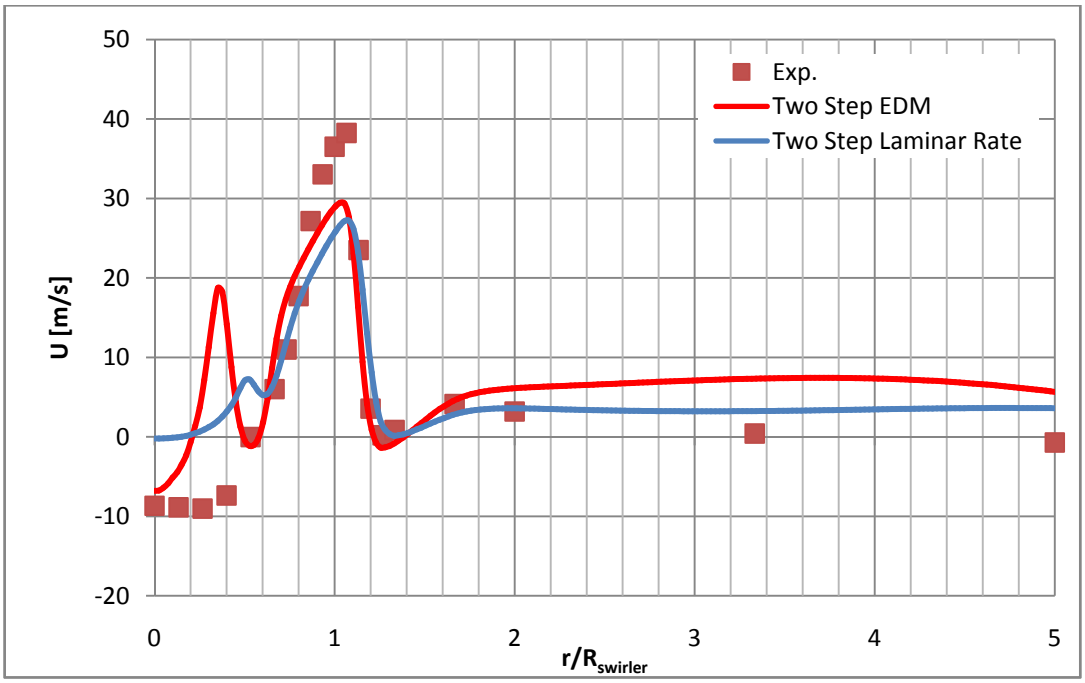

Figure 56. Comparison of mean axial velocity from the results of Eddy Dissipation Model and Laminar Rate Model solutions; 10mm downstream of swirler exit plane

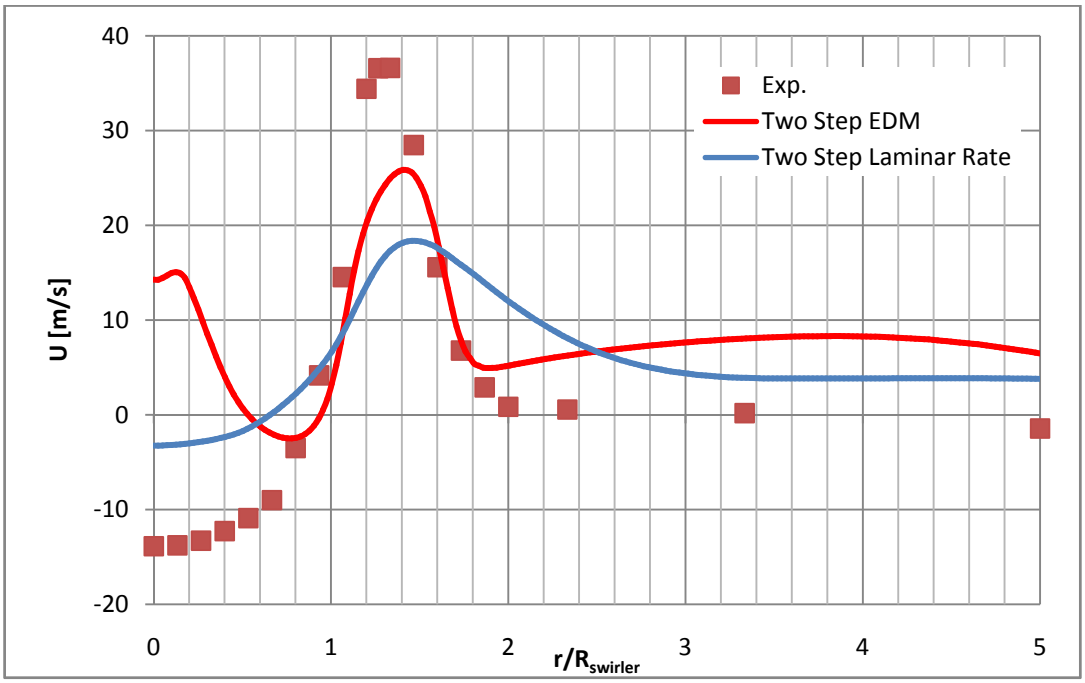

Figure 57. Comparison of mean axial velocity from the results of Eddy Dissipation Model and Laminar Rate Model solutions; 30mm downstream of swirler exit plane

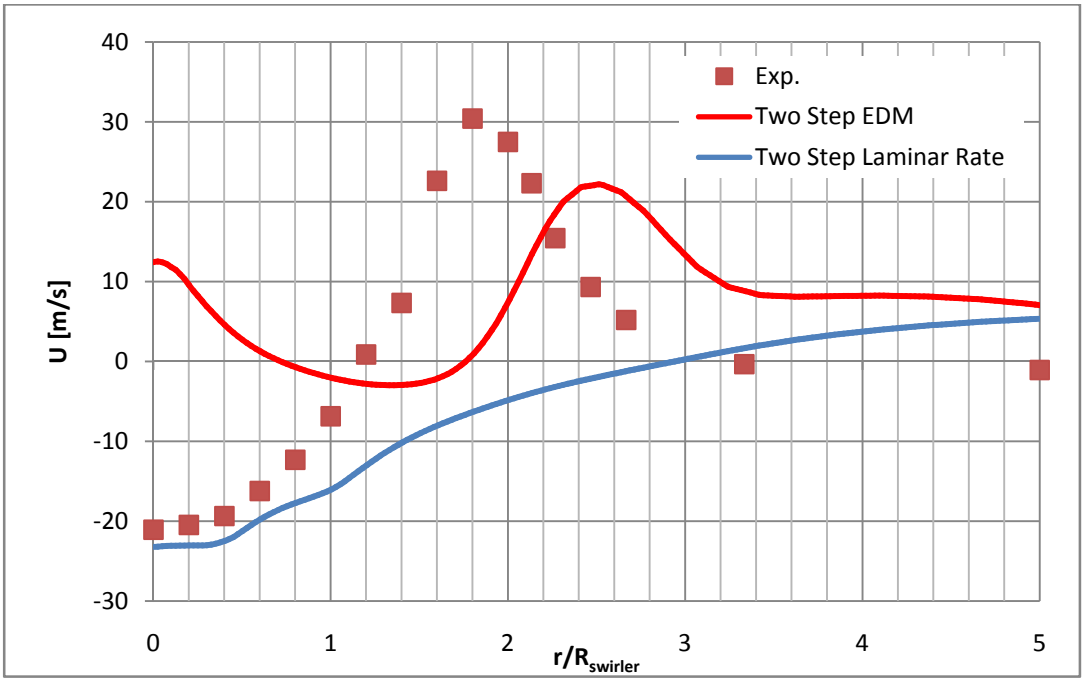

Figure 58. Comparison of mean axial velocity from the results of Eddy Dissipation Model and Laminar Rate Model solutions; 70mm downstream of swirler exit plane

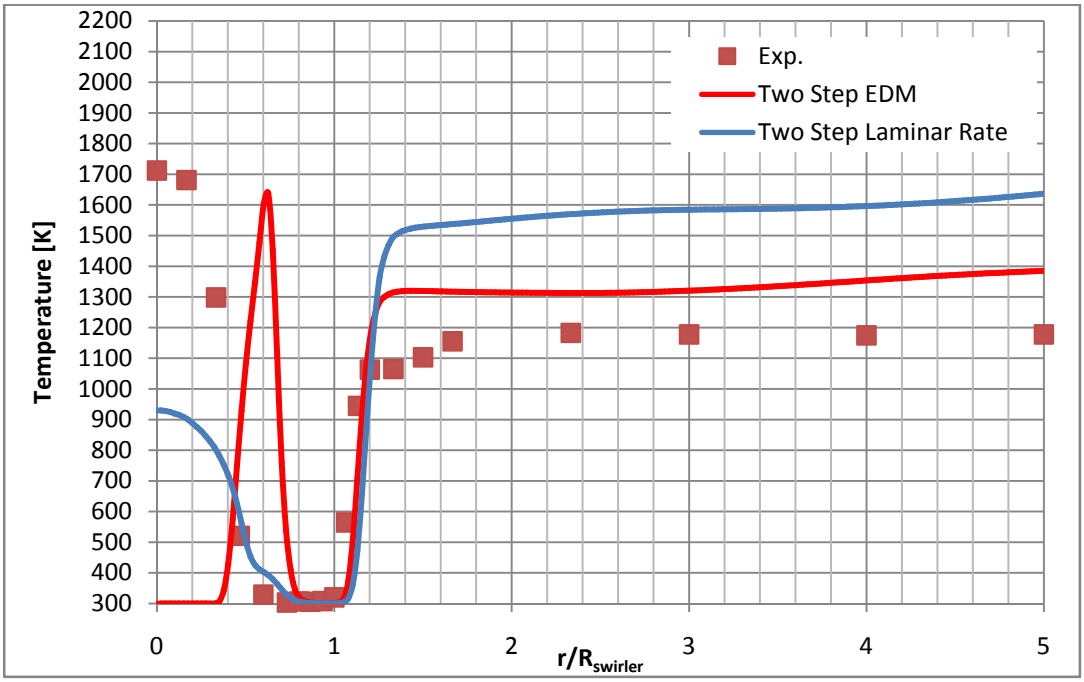

Figure 59. Comparison of mean static temperature from the results of Eddy Dissipation Model and Laminar Rate Model solutions; 10mm downstream of swirler exit plane

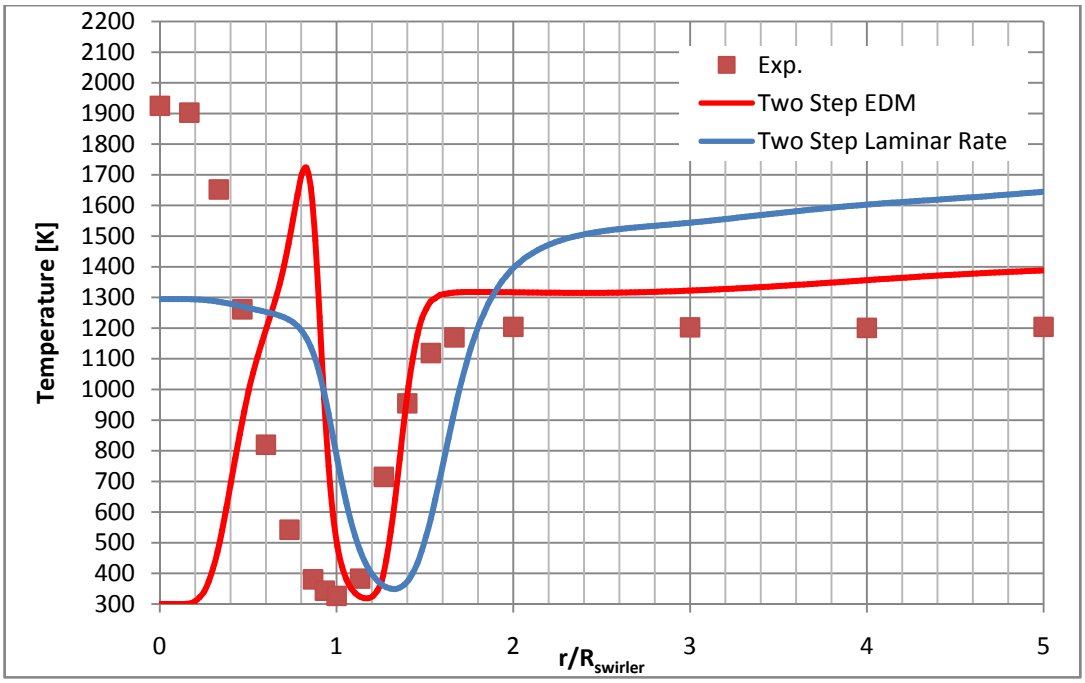

Figure 60. Comparison of mean static temperature from the results of Eddy Dissipation Model and Laminar Rate Model solutions; 20mm downstream of swirler exit plane

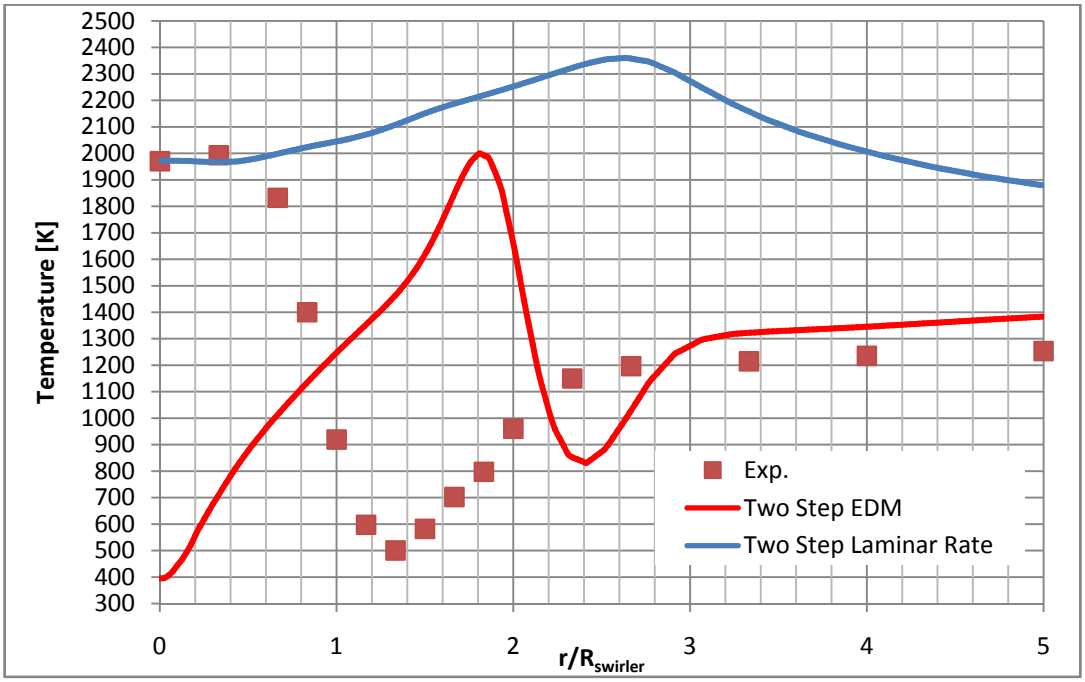

Figure 61. Comparison of mean static temperature from the results of Eddy Dissipation Model and Laminar Rate Model solutions; 60mm downstream of swirler exit plane

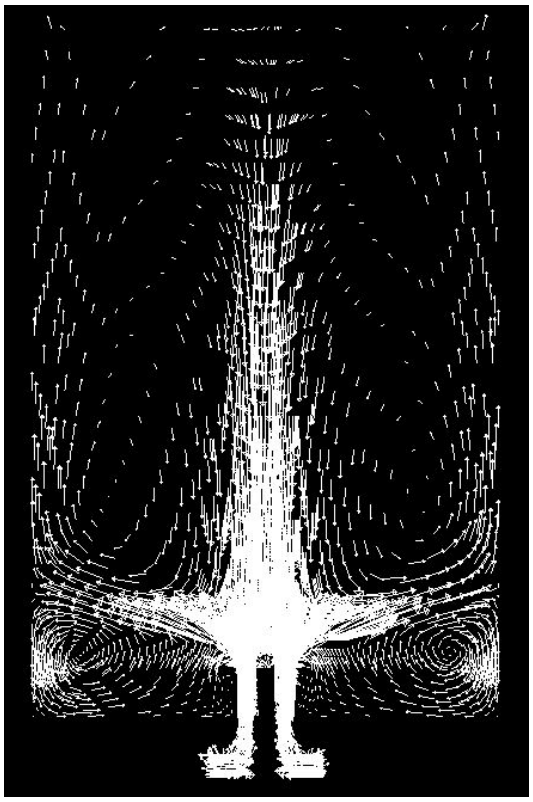

a) Instantaneous vector field

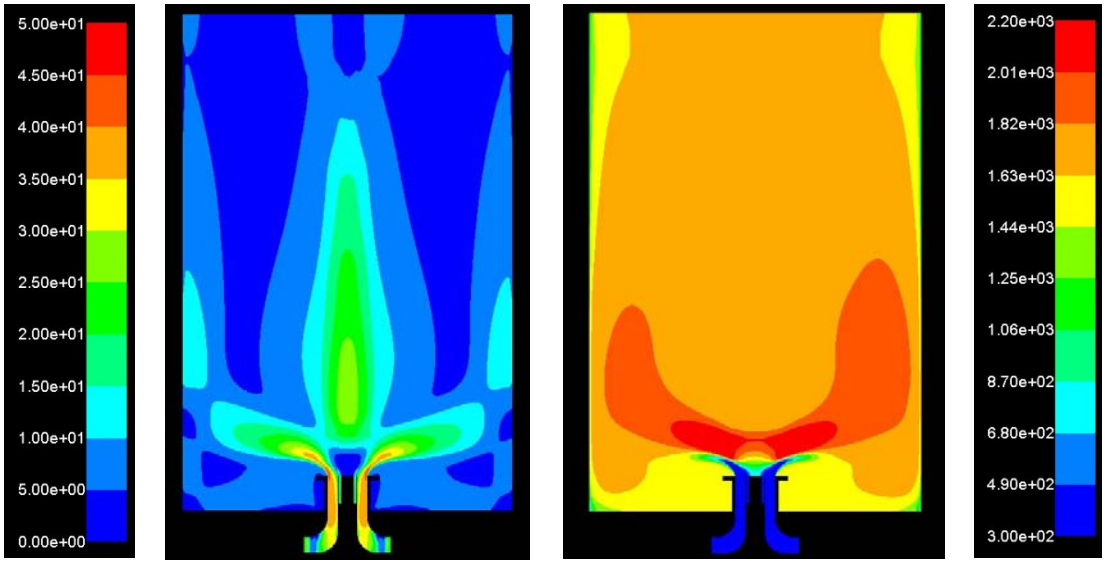

b) Mean velocity contour c) Mean static temperature contour

Figure 62.Instantaneous vector field, mean velocity contour and mean temperature contour of simulation by mesh 3, k-epsilon turbulence model,two step laminar rate model

This part of the study shows that finite rate effect creates a difference in simulations. However, turbulence-chemistry interaction is needed to make connection between these two combustion models.

5.2.3 Finite Rate / Eddy Dissipation Model

The blend of Finite Rate / Eddy Dissipation Model is introduced which uses the minimum reaction rate of infinitely fast EDM and finite rate chemistry. The results are given in Figure 63 - Figure 68. It is observed that Finite Rate / Eddy Dissipation Model shows the best performance among others. The sudden velocity rise at 10mm downstream of swirler exit plane (Figure 63) is dismissed. Temperature distributions at centerline are comparably better (Figure 66 - Figure 68). Trend of temperature is captured well especially at lower positions. On the other hand, outer temperature is again over predicted. Negative axial velocity at central region is under predicted (Figure 63 - Figure 65). And peak points of temperature and velocity are shifted out. Therefore, whether the Finite Rate / Eddy Dissipation Model shows the best performance, improvements are still needed. The instantaneous vector plot, mean vector contour and mean temperature contour is given in Figure 69.

5.2.4 Mixture Fraction Model

Under the topic of combustion model comparison, the other studied model is Presumed β-PDF model with equilibrium state. This is another “mixed is burnt” model. 14 species are used for look-up table calculations. Results are given in Figure 70 - Figure 75. The instantaneous vector plot, mean vector contour and mean temperature contour is given in Figure 76.

Compared to Eddy Dissipation Model, PDF model gives better results both for velocity and temperature. However, the sudden rises at mixing zone exist since infinitely fast chemistry assumption is done.

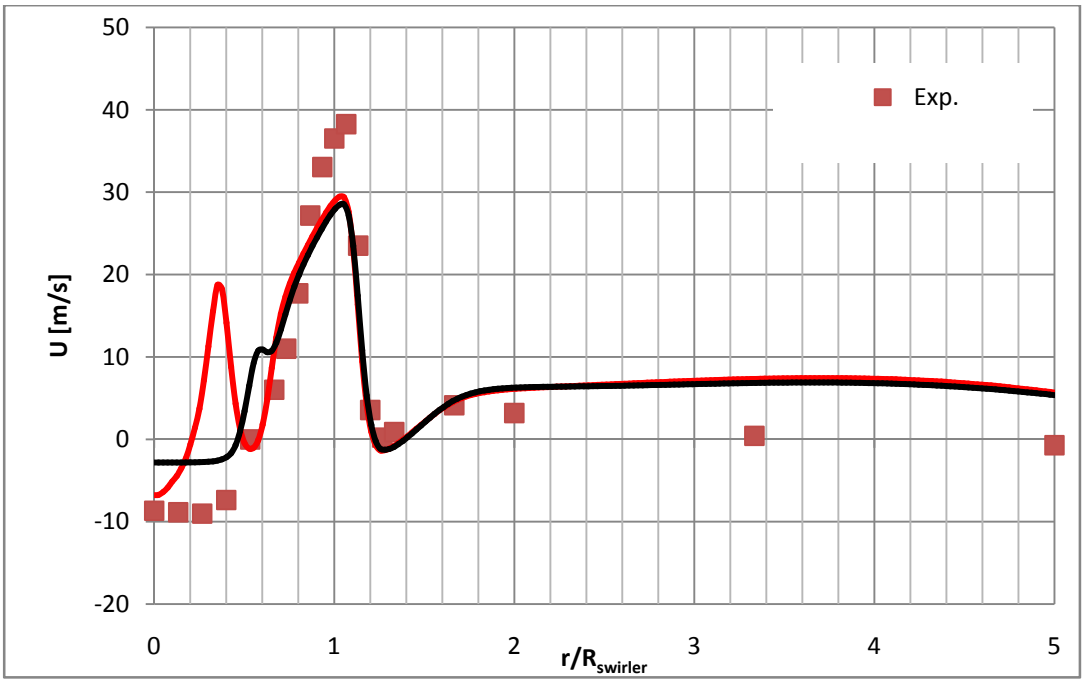

Figure 63. Comparison of mean axial velocity from the results of Eddy Dissipation Model and Finite Rate / Eddy Dissipation Model solutions; 10mm downstream of swirler exit plane

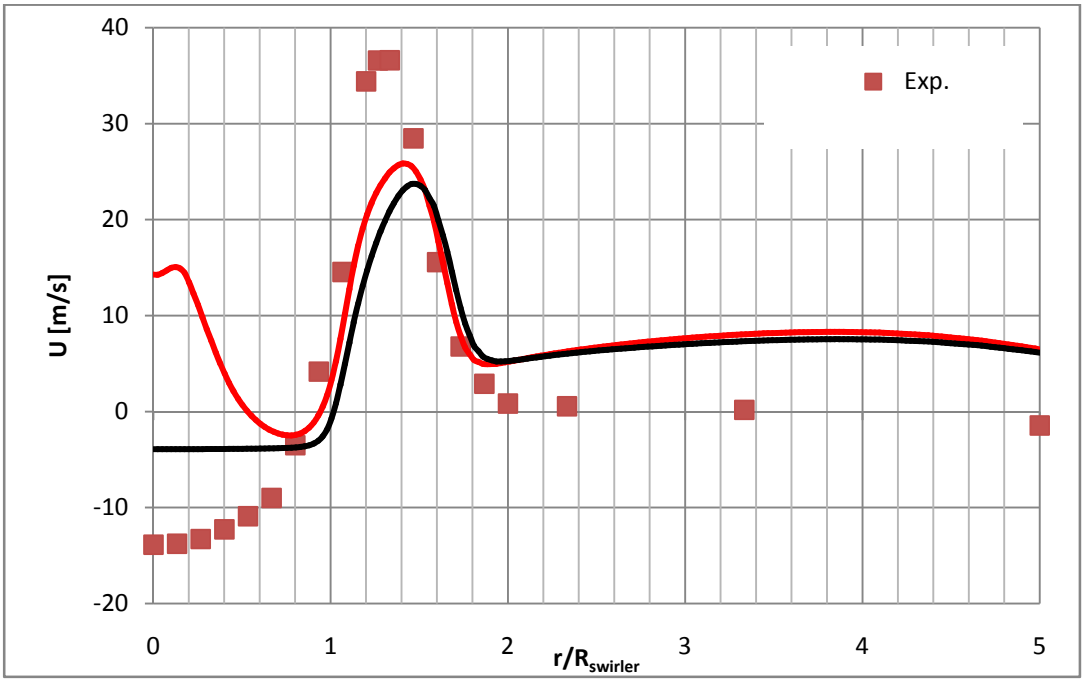

Figure 64. Comparison of mean axial velocity from the results of Eddy Dissipation Model and Finite Rate / Eddy Dissipation Model solutions;30mm downstream of swirler exit plane

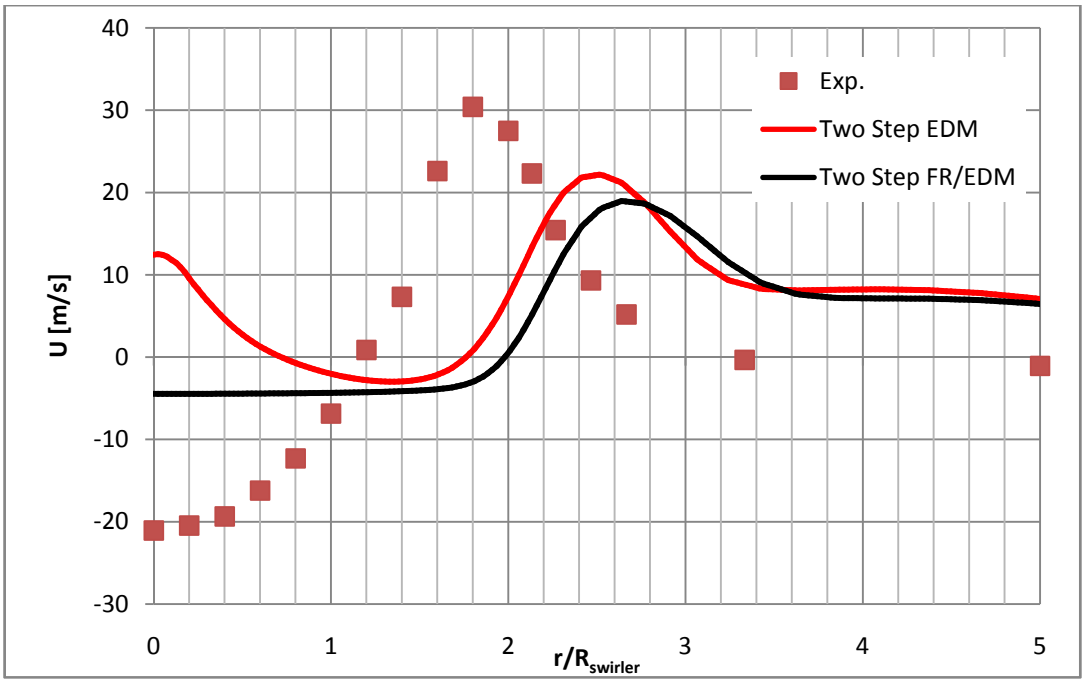

Figure 65. Comparison of mean axial velocity from the results of Eddy Dissipation Model and Finite Rate / Eddy Dissipation Model solutions;70mm downstream of swirler exit plane

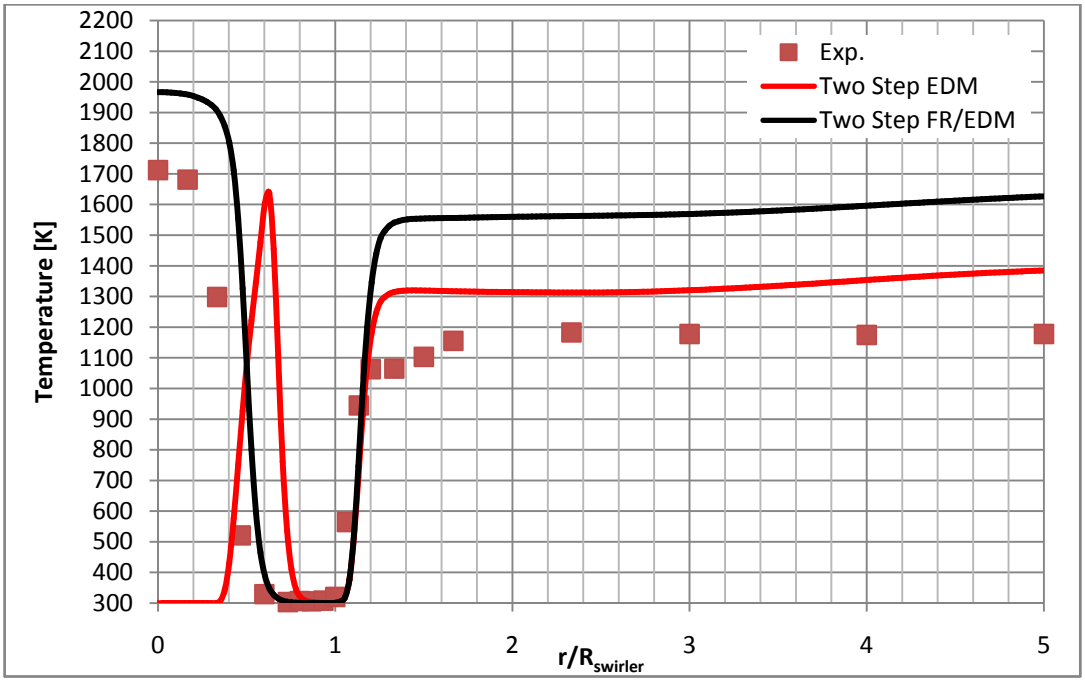

Figure 66. Comparison of mean static temperature from the results of Eddy Dissipation Model and Finite Rate / Eddy Dissipation Model solutions; 10mm downstream of swirler exit plane

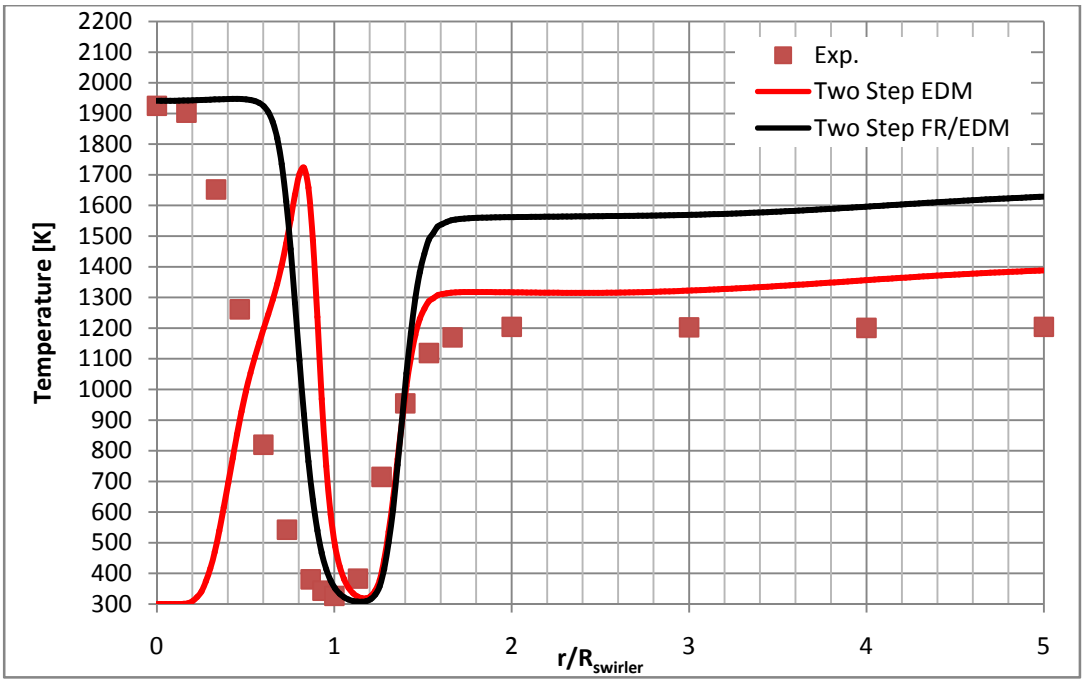

Figure 67. Comparison of mean static temperature from the results of Eddy Dissipation Model and Finite Rate / Eddy Dissipation Model solutions; 20mm downstream of swirler exit plane

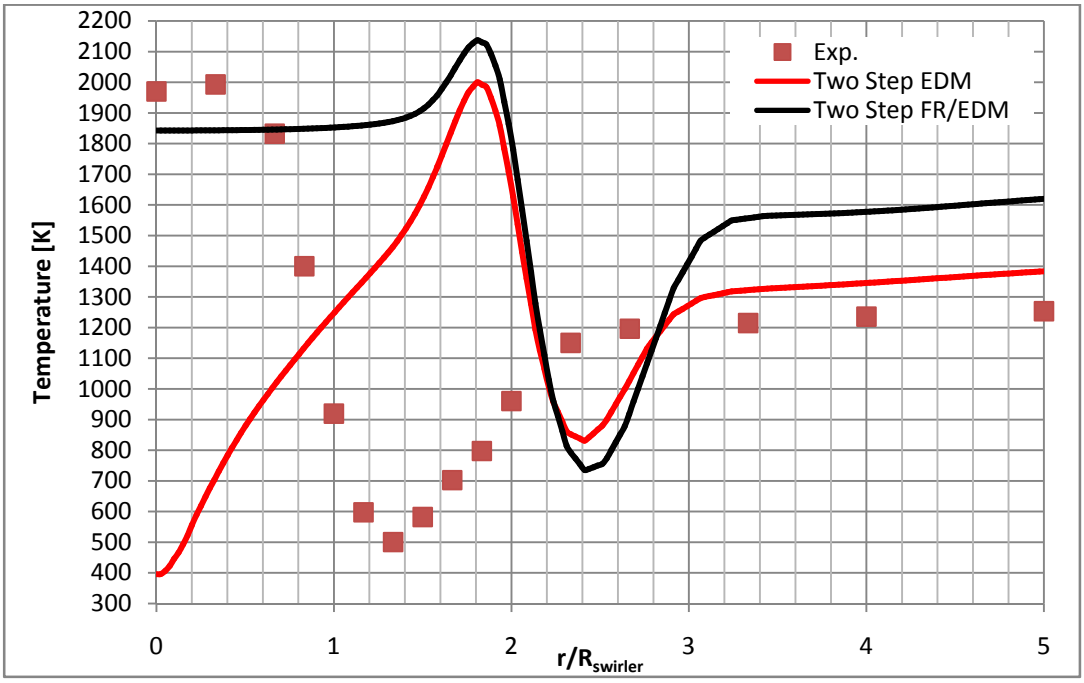

Figure 68. Comparison of mean static temperature from the results of Eddy Dissipation Model and Finite Rate / Eddy Dissipation Model solutions; 60mm downstream of swirler exit plane

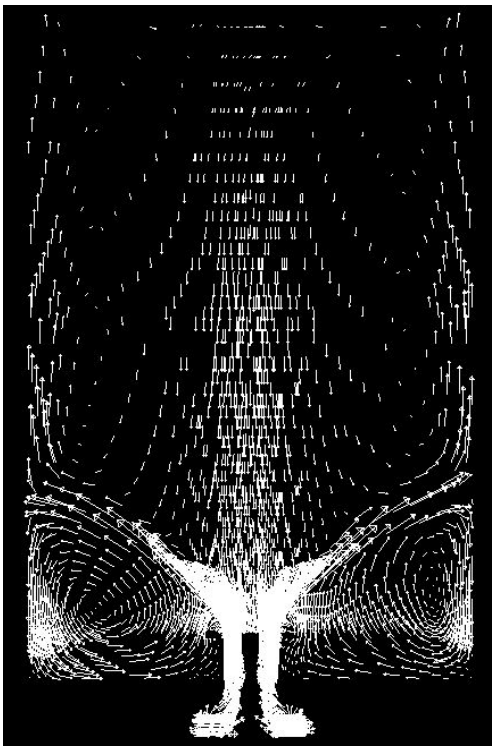

a) Instantaneous vector field

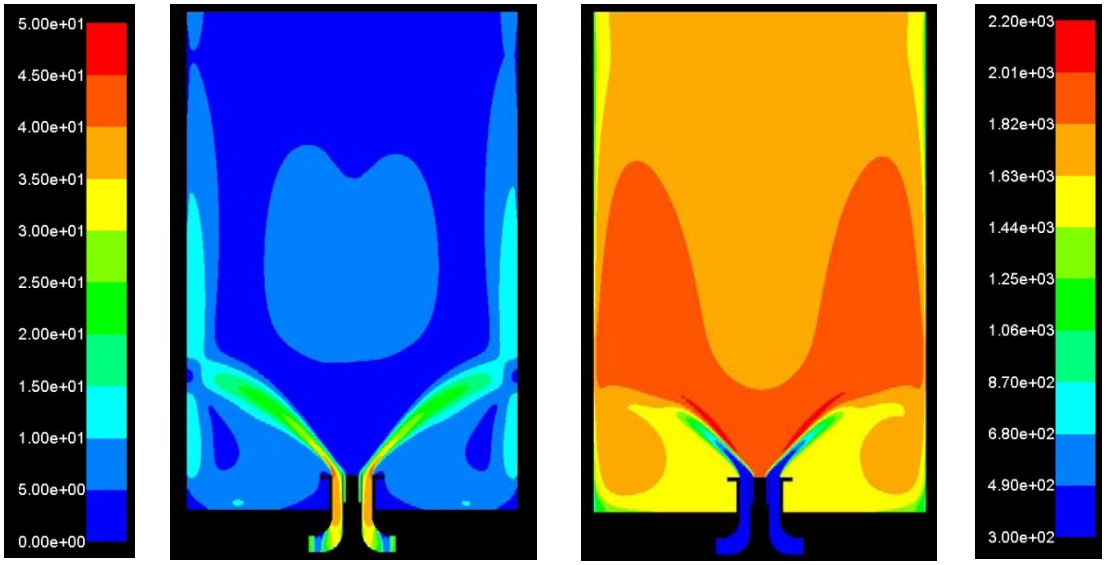

b) Mean velocity contour c) Mean static temperature contour

Figure 69.Instantaneous vector field, mean velocity contour and mean temperature contour of simulation by mesh 3, k-epsilon turbulence model,two step finite rate / eddy dissipation model

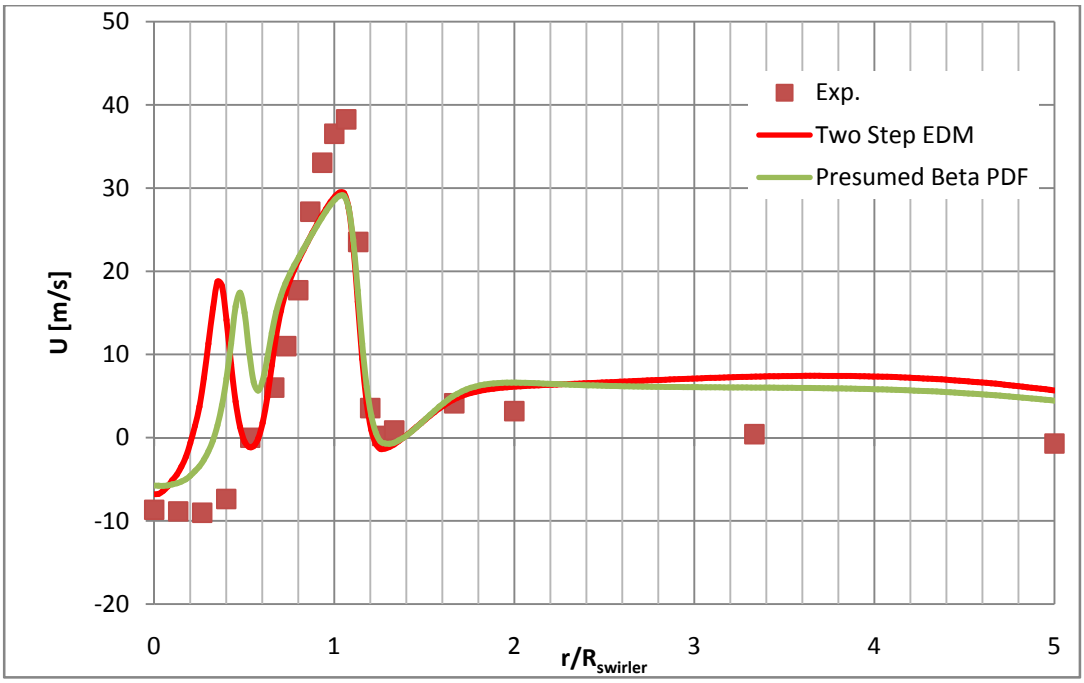

Figure 70. Comparison of mean axial velocity from the results of Eddy Dissipation Model and Presumed β-PDF Model solutions; 10mm downstream of swirler exit plane

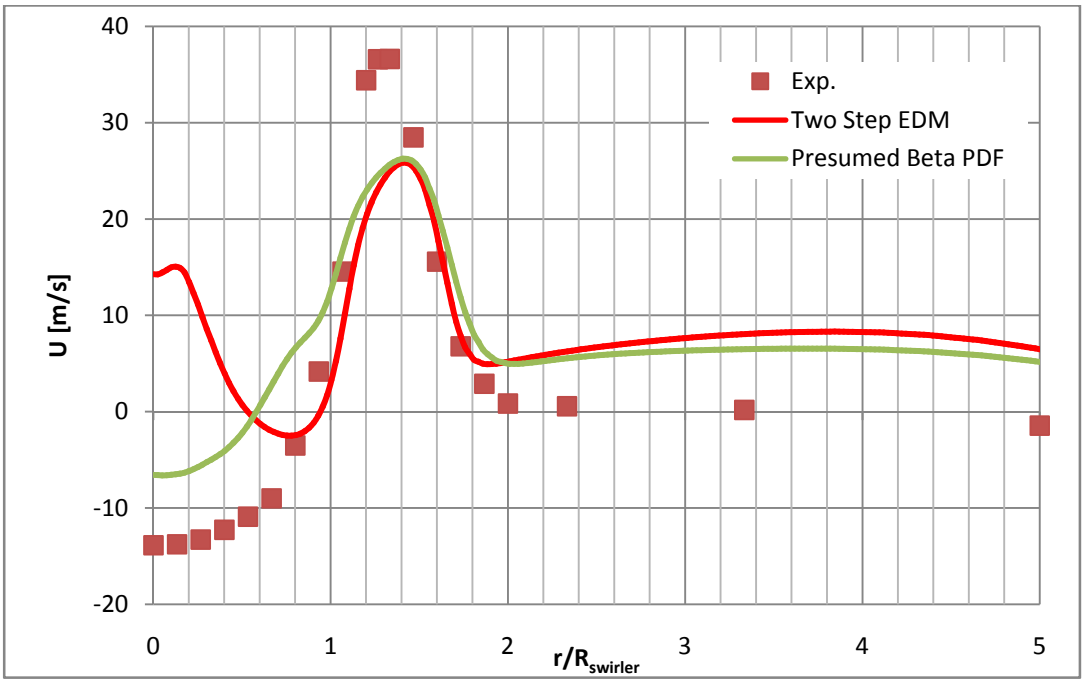

Figure 71. Comparison of mean axial velocity from the results of Eddy Dissipation Model and Presumed β-PDF Model solutions; 30mm downstream of swirler exit plane

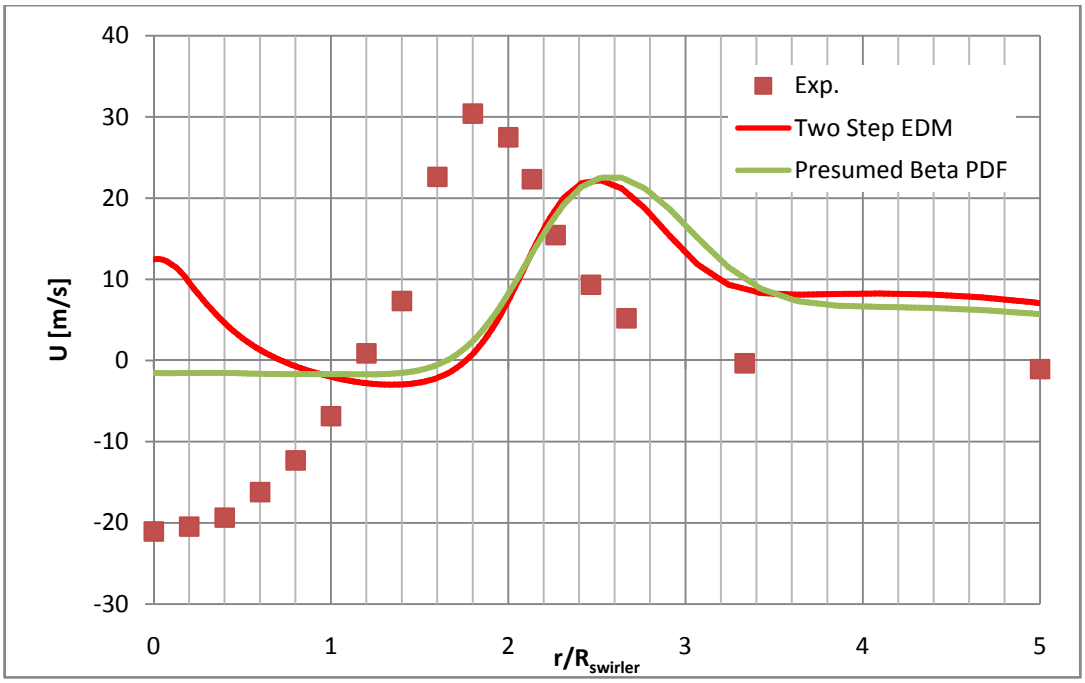

Figure 72. Comparison of mean axial velocity from the results of Eddy Dissipation Model and Presumed β-PDF Model solutions; 70mm downstream of swirler exit plane

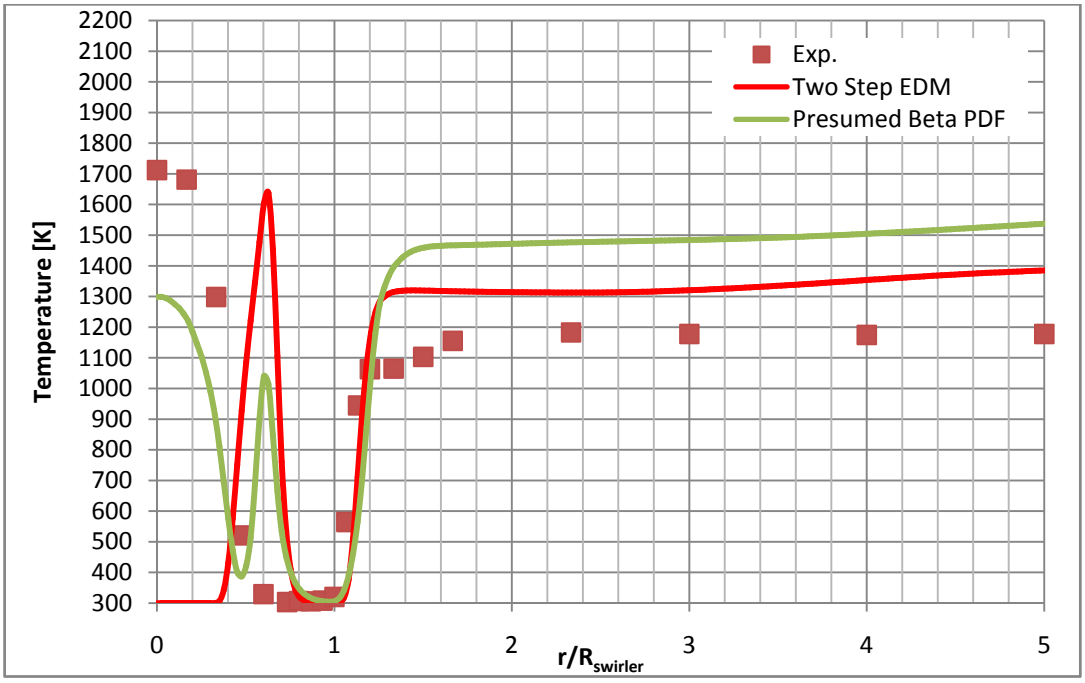

Figure 73. Comparison of mean static temperature from the results of Eddy Dissipation Model and Presumed β-PDF Model solutions; 10mm downstream of swirler exit plane

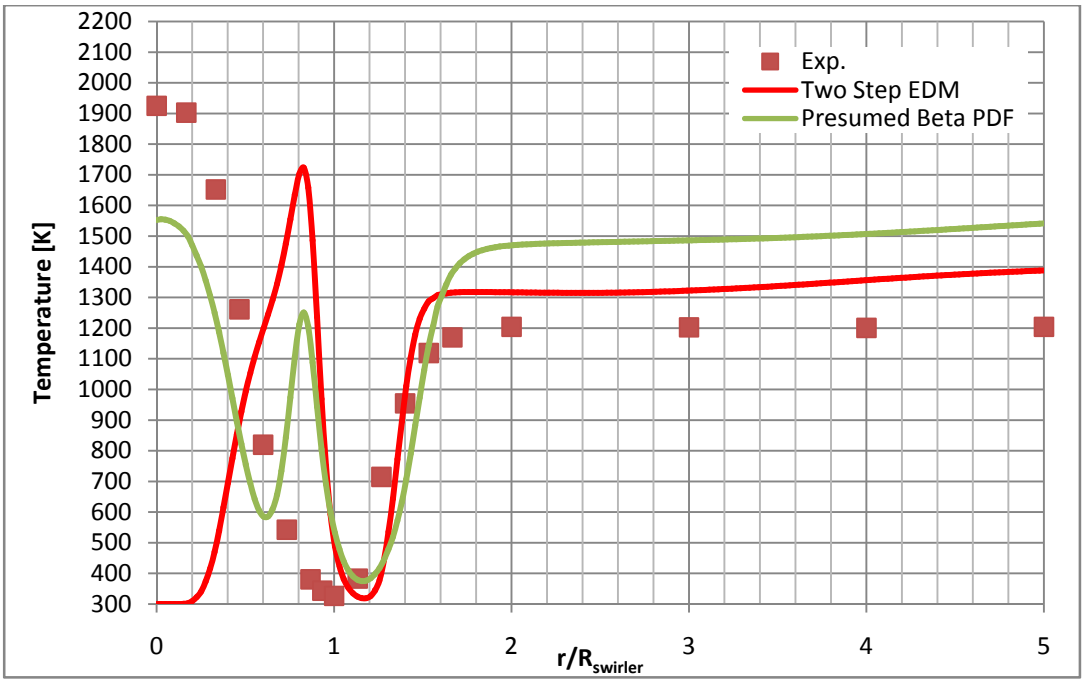

Figure 74. Comparison of mean static temperature from the results of Eddy Dissipation Model and Presumed β-PDF Model solutions; 20mm downstream of swirler exit plane

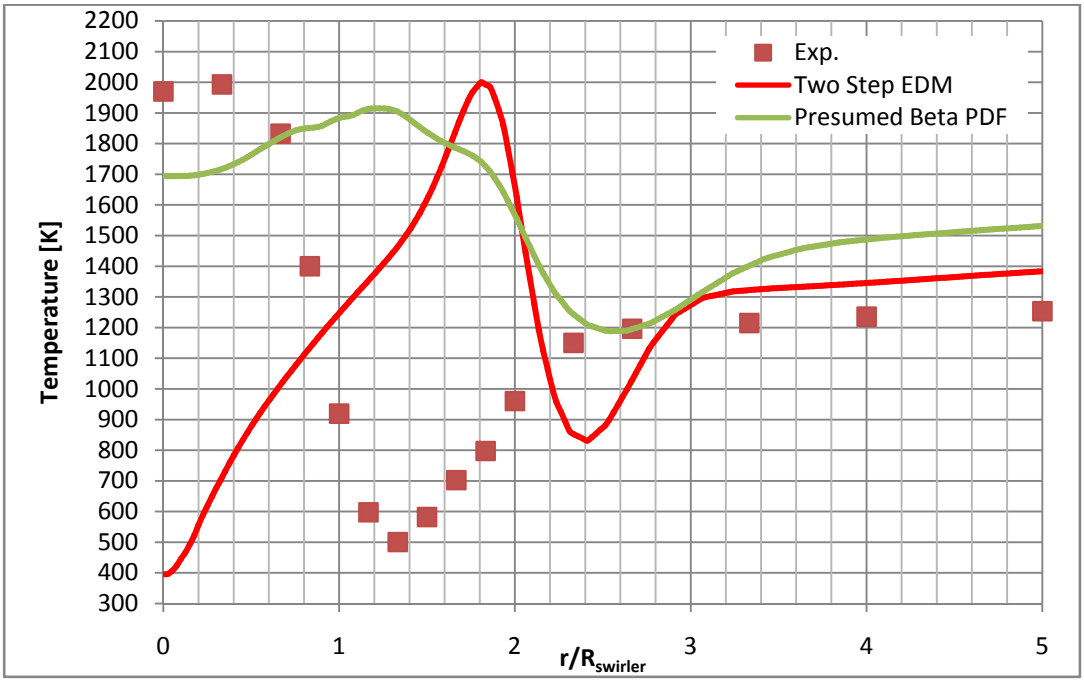

Figure 75. Comparison of mean static temperature from the results of Eddy Dissipation Model and Presumed β-PDF Model solutions; 60mm downstream of swirler exit plane

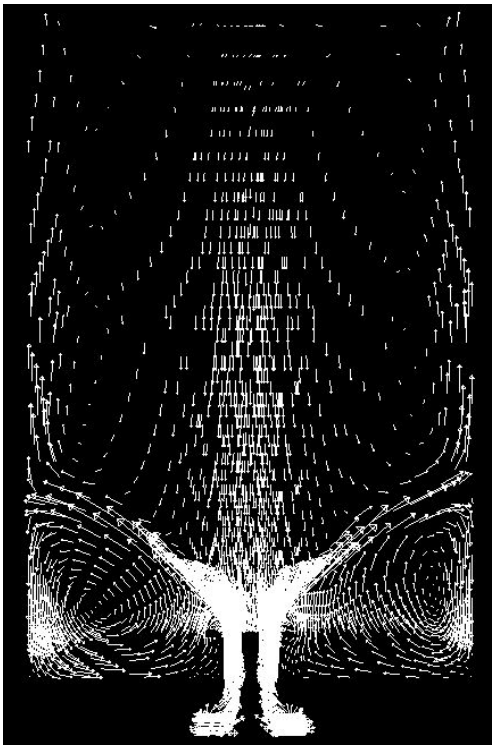

a) Instantaneous vector field

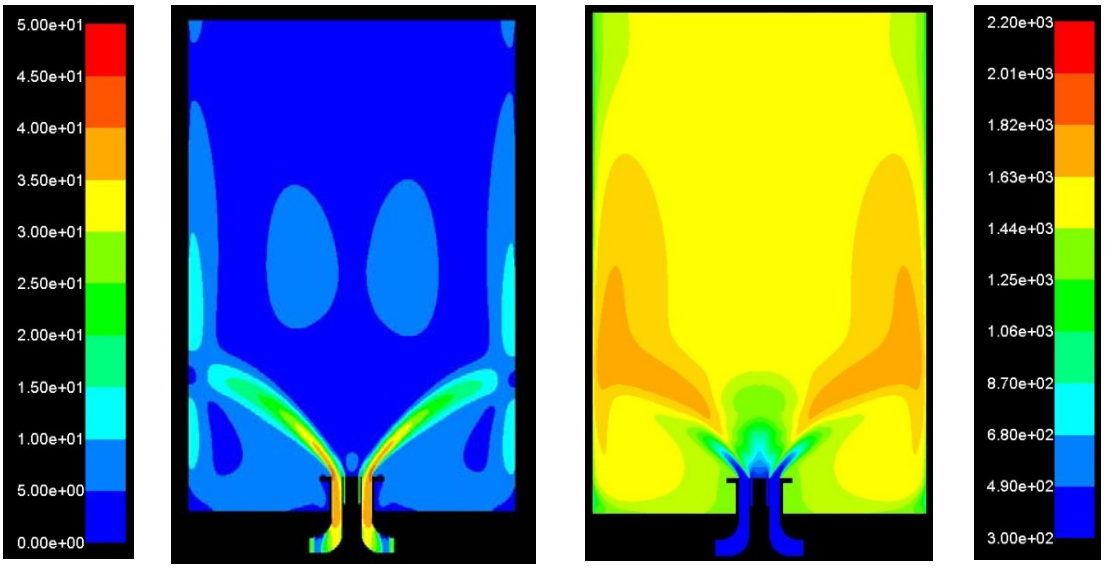

b) Mean velocity contour c) Mean static temperature contour

Figure 76.Instantaneous vector field, mean velocity contour and mean temperature contour of simulation by mesh 3, k-epsilon turbulence model,equilibrium presumed β-shape PDF model

5.2.5 The Best Combustion Model

Four combustion models with two reaction schemes are simulated and results are compared in this section. The mean velocity plots are given in Figure 77. The mean temperature plots are given in Figure 78. Finite Rate / Eddy Dissipation Model, which is a blend of laminar rate model and eddy dissipation model, shows the best performance among others. As for summary, results of all models are plotted together inFigure 79 - Figure 84.

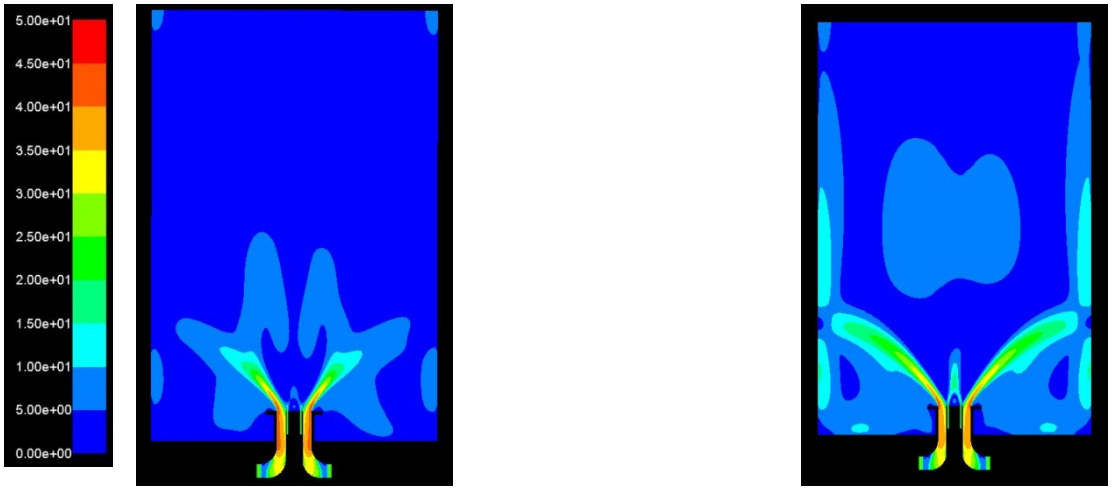

a) One Step EDM

b) Two Step EDM

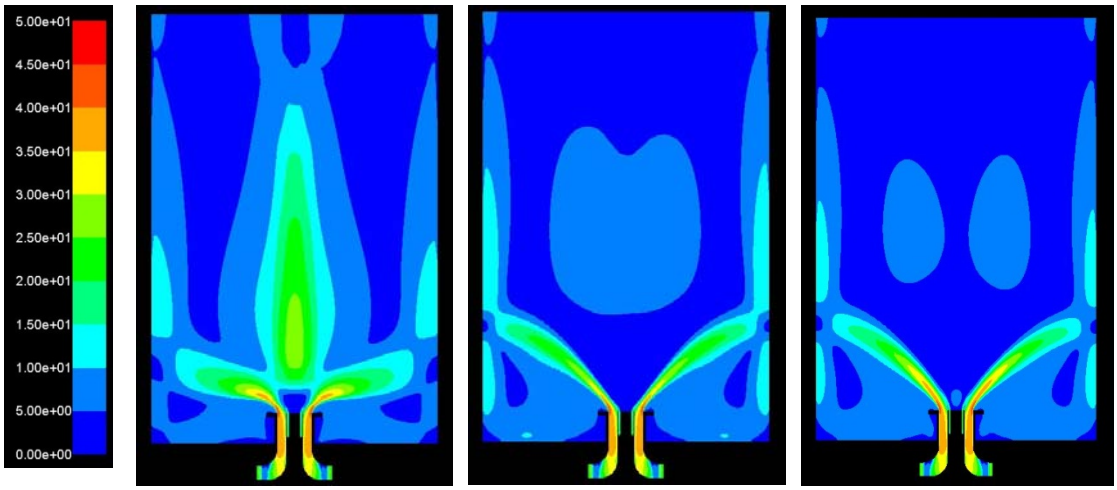

c) Two Step Laminar Rate

d) Two Step Finite Rate /EDM

e) Presumed β-PDF (14 spec.)

Figure 77. Mean velocity contours of combustion model comparison simulations

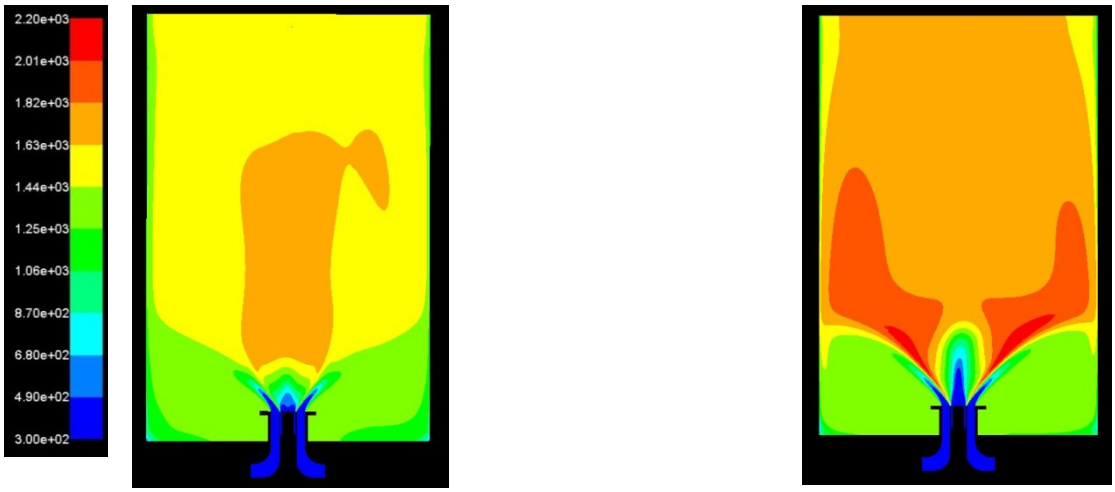

a) One Step EDM

b) Two Step EDM

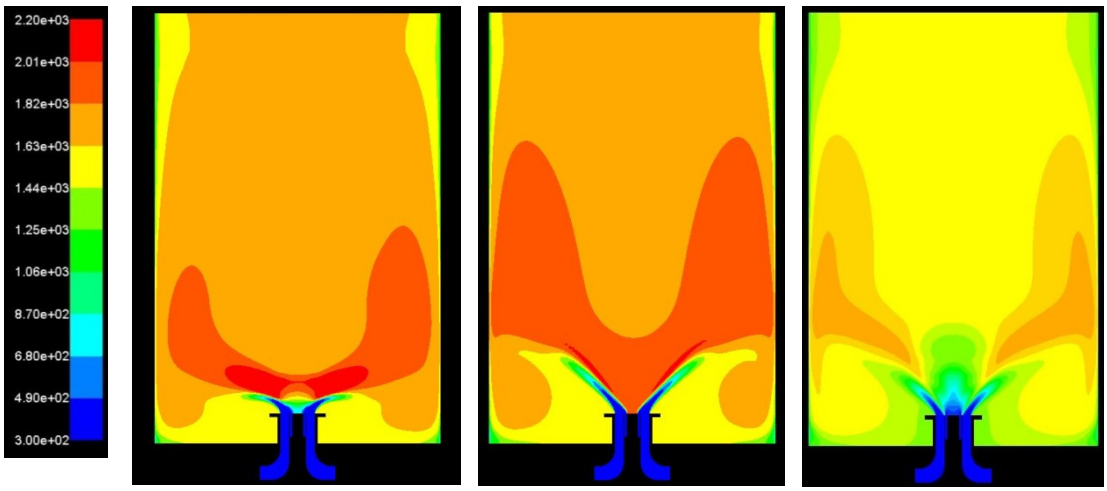

c) Two Step Laminar Rate

d) Two Step Finite Rate /EDM

e) Presumed β-PDF (14 spec.)

Figure 78.Mean static temperature contours of combustion model comparison simulations

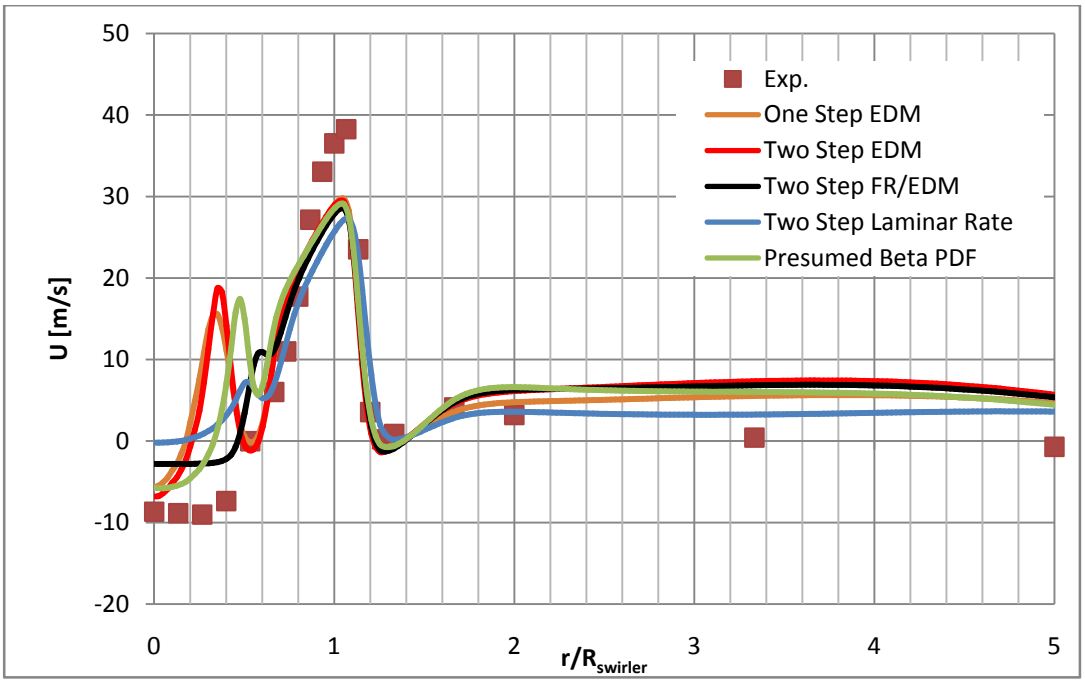

Figure 79. Comparison of mean axial velocity of all combustion models; 10mm downstream of swirler exit plane

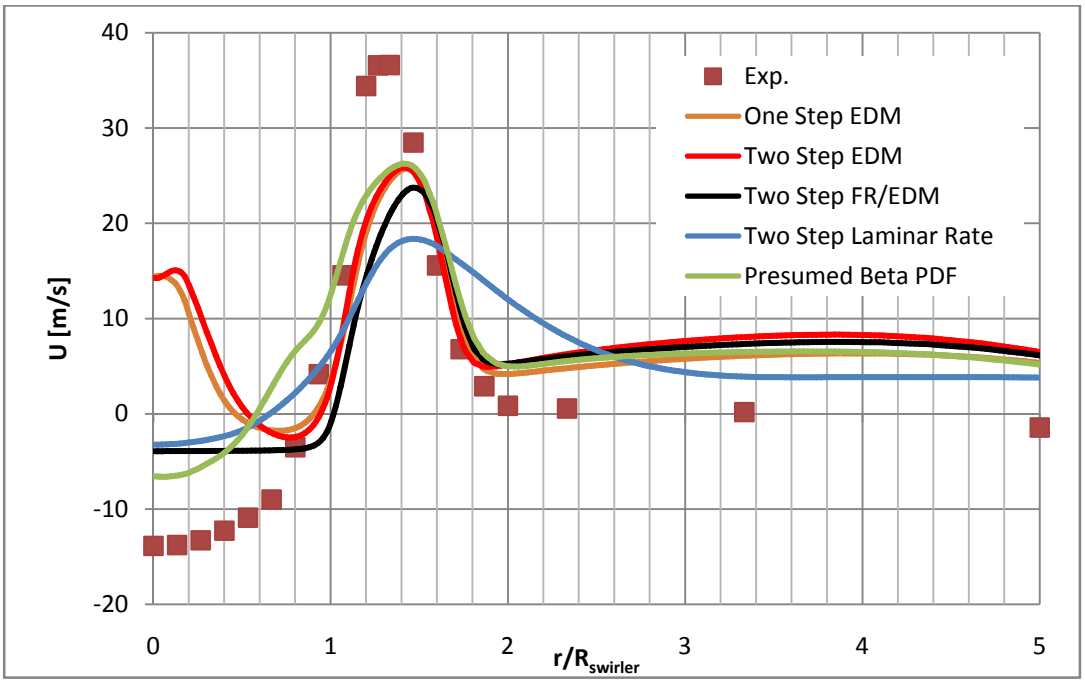

Figure 80. Comparison of mean axial velocity of all combustion models;30mm downstream of swirler exit plane

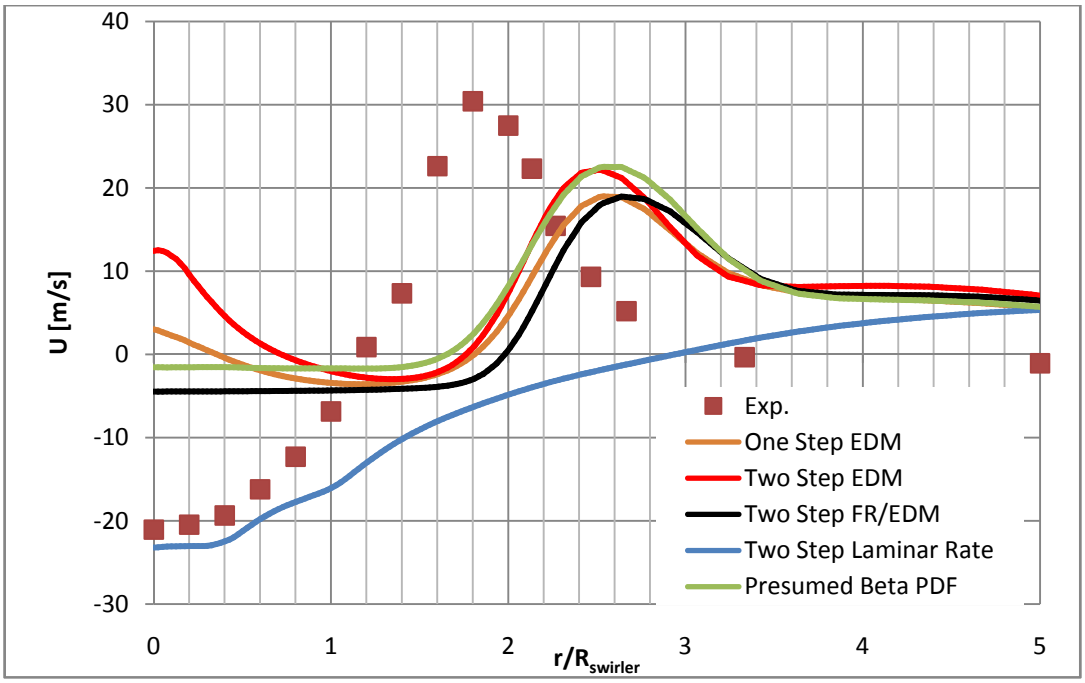

Figure 81. Comparison of mean axial velocity of all combustion models;70mm downstream of swirler exit plane

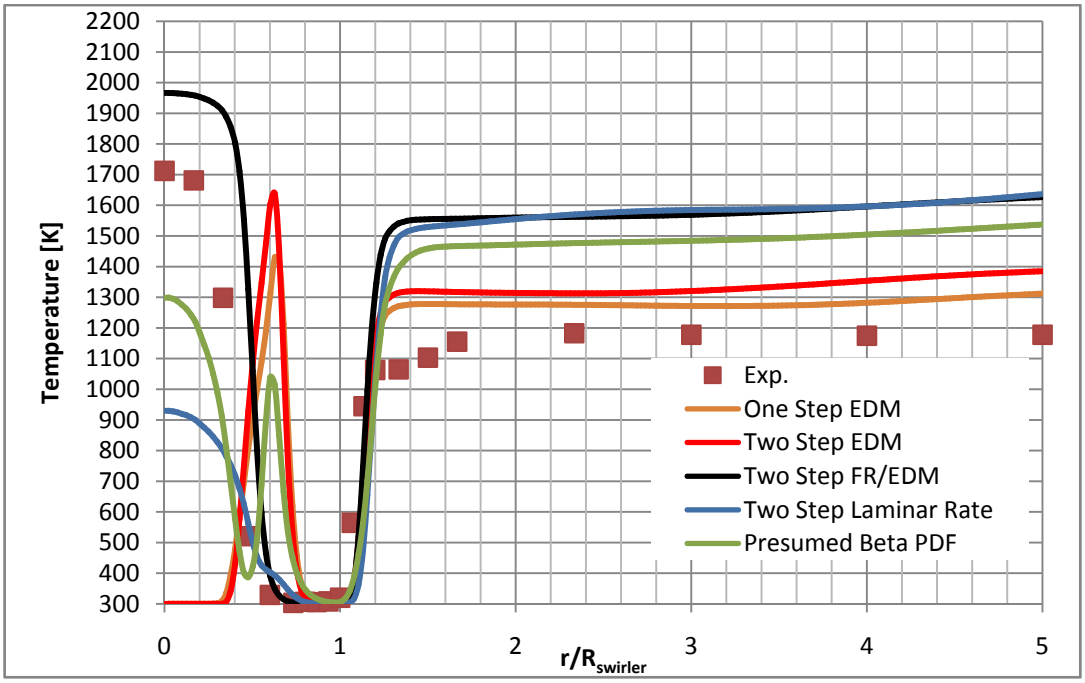

Figure 82. Comparison of static temperatureof all combustion models; 10mm downstream of swirler exit plane

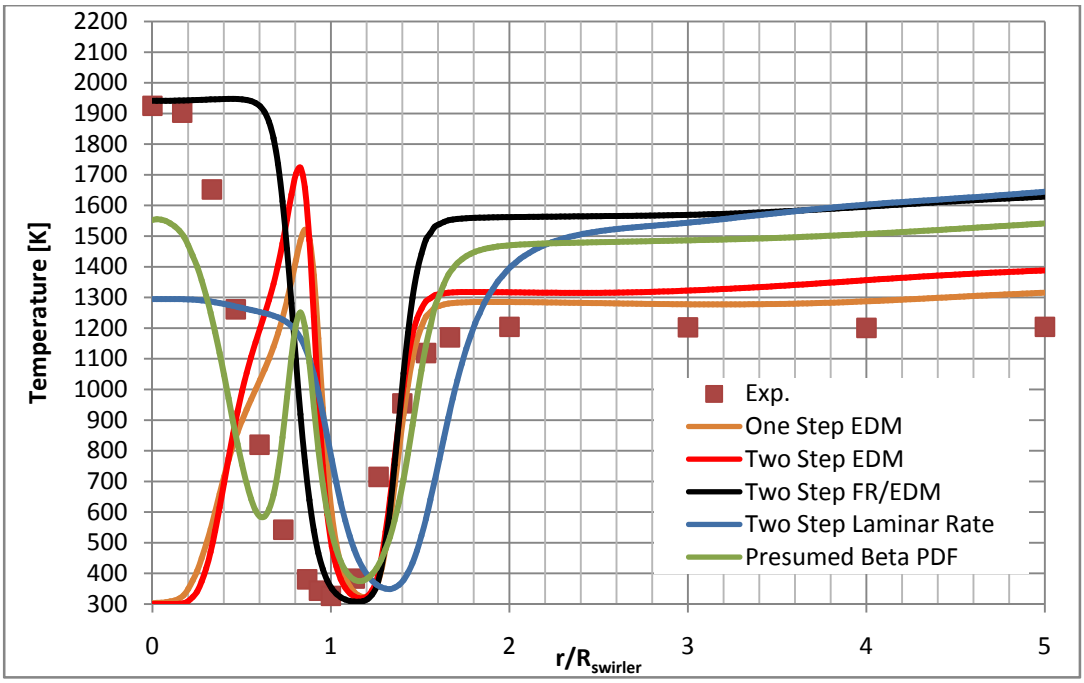

Figure 83. Comparison of static temperatureof all combustion models; 20mm downstream of swirler exit plane

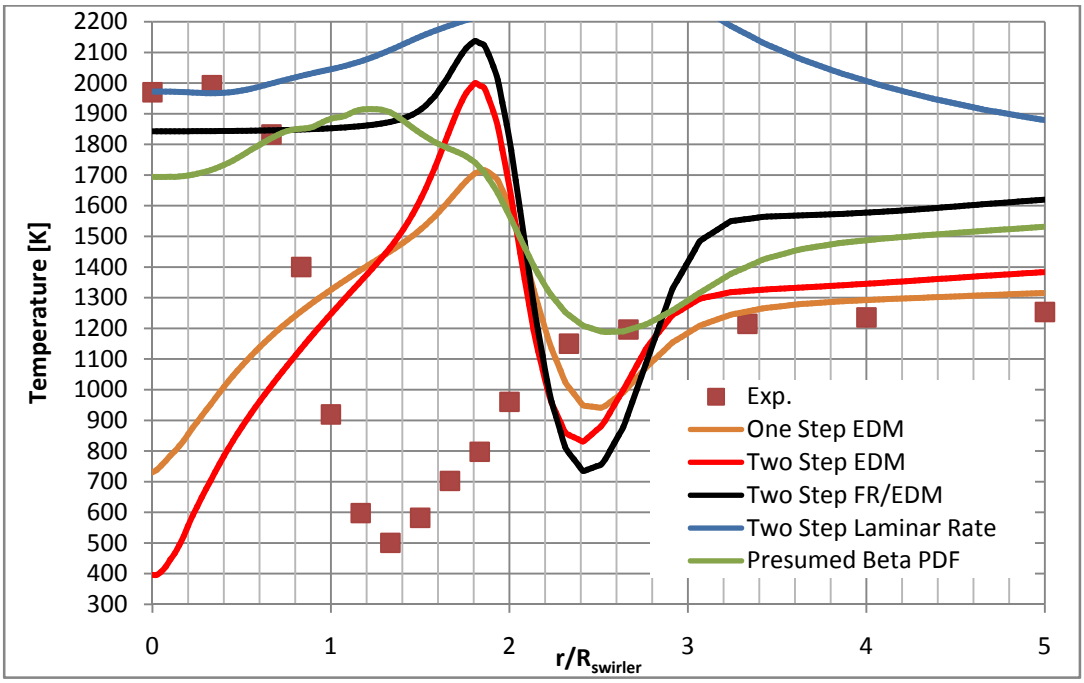

Figure 84. Comparison of static temperatureof all combustion models; 60mm downstream of swirler exit plane

5.3 LES Calculations

The combustion model comparison analyses have showed that there may be improvements by using a proper combustion model. But the main problem still exists. The erroneous results in flow field could not be solved. Any incorrect estimation in flow fieldaffects the temperature field because of reaction occurrence location. Therefore, focusing only on combustion model improvement is not enough to get a satisfactorily accurate result.

Large Eddy Simulation is one of candidates which calculates large scale motions of the flow and models the small scales instead of modeling every scale. This part of the study shows the improvements by using LES. Mesh2 and Mesh3 are used to check mesh dependency and compare with URANS calculations. As combustion model, One Step Eddy Dissipation Model is used for its quick and simple properties. Results, which are given in Figure 85 - Figure 90,show that Large Eddy Simulation is highly mesh dependent even for dynamic model. With a coarse mesh, accuracy of the results may not be increased even may be decreased. On the other hand, with a 2.7M mesh, LES predicts the flow field far better compared to URANS. The axial velocity magnitude at 10mm downstream of swirler exit plane (Figure 85)is in a good agreement with experimental data. In higher positions (Figure 86, Figure 87), direction of axial velocity is predicted but the magnitude is not as high as the measured data. The results at outer section of the domain are captured better with LES. On the other hand, sudden axial velocity (Figure 85) and temperature (Figure 88)rise is observed at 10mm location which is due to combustion model. The accuracy in velocity field prediction increases the accuracy of temperature field prediction which is obviously seen inFigure 88 - Figure 90. The instantaneous vector plot, mean vector contour and mean temperature contour is given in Figure 91.

LES study shows that there may be more accurate results if only the flow field is captured well. Large Eddy Simulation is successful to simulate the highly swirling flow. But it is at least 10 times more expensive than a URANS solution and mesh dependency is very high for a LES computation. Therefore, alternative turbulence models for URANS computations or Detached Eddy Simulation (DES) shall be investigated for a cheaper solution.

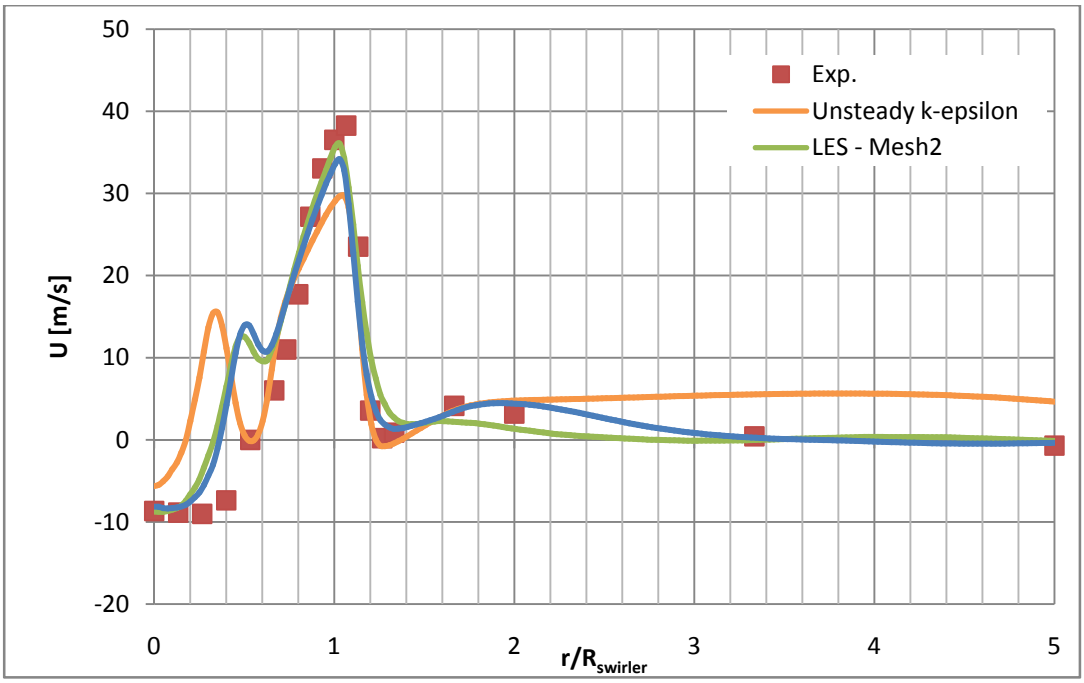

Figure 85. Mean axial velocity from the results of LES and URANS by One Step Eddy Dissipation Combustion Model; 10mm downstream of swirler exit plane

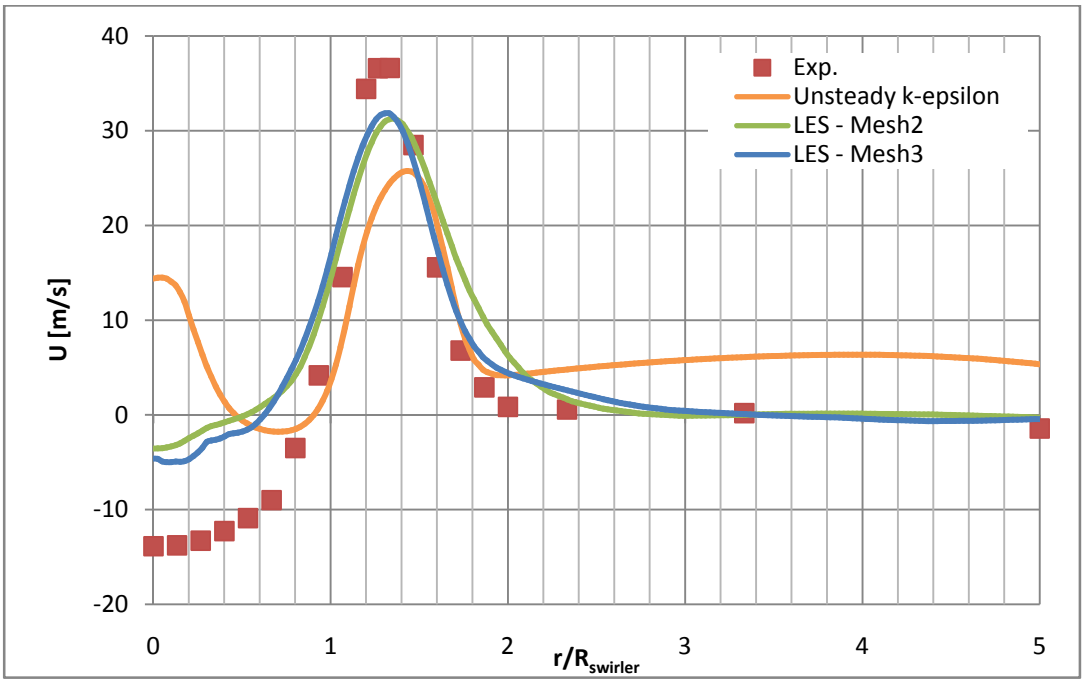

Figure 86. Mean axial velocity from the results of LES and URANS by One Step Eddy Dissipation Combustion Model; 30mm downstream of swirler exit plane

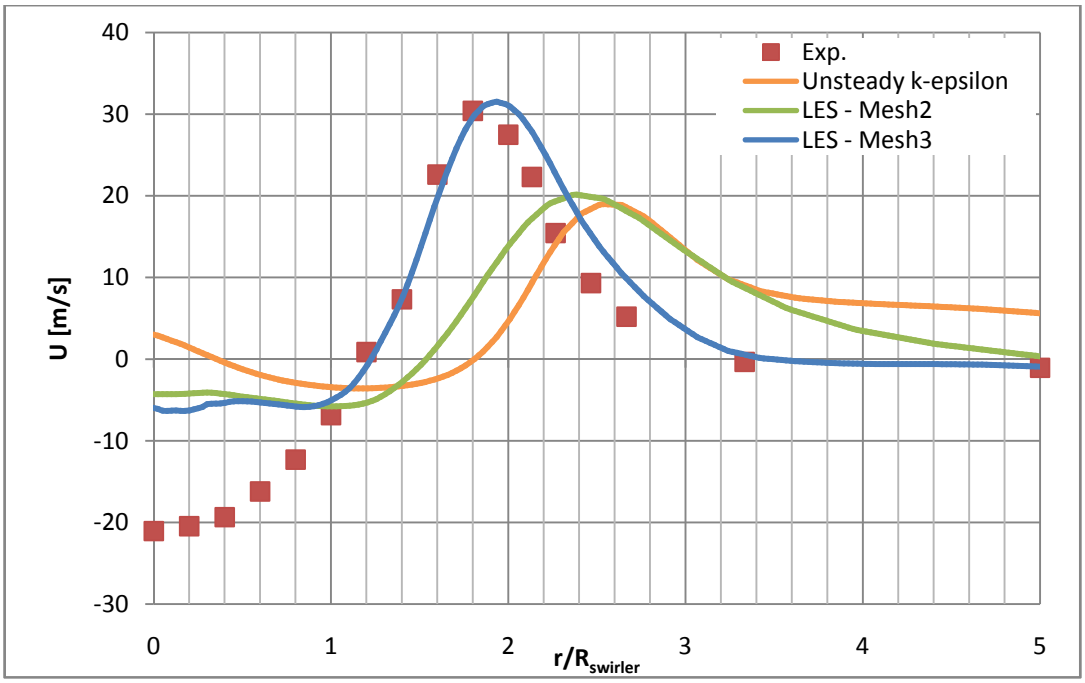

Figure 87. Mean axial velocity from the results of LES and URANS by One Step Eddy Dissipation Combustion Model; 70mm downstream of swirler exit plane

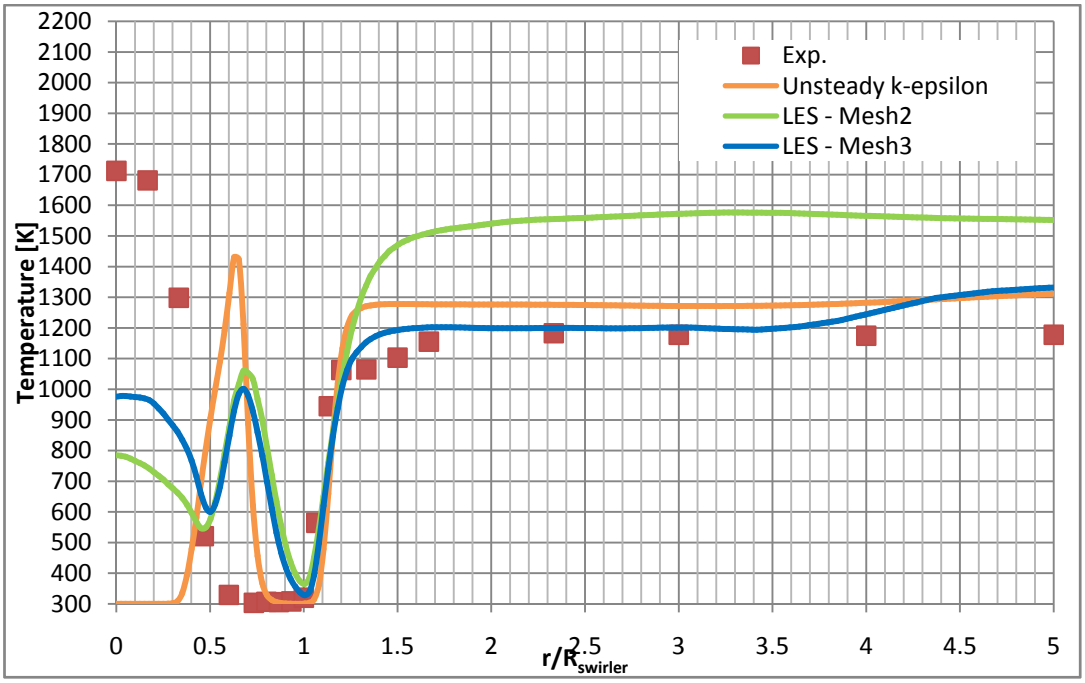

Figure 88. Mean static temperature from the results of LES and URANS by One Step Eddy Dissipation Combustion Model; 10mm downstream of swirler exit plane

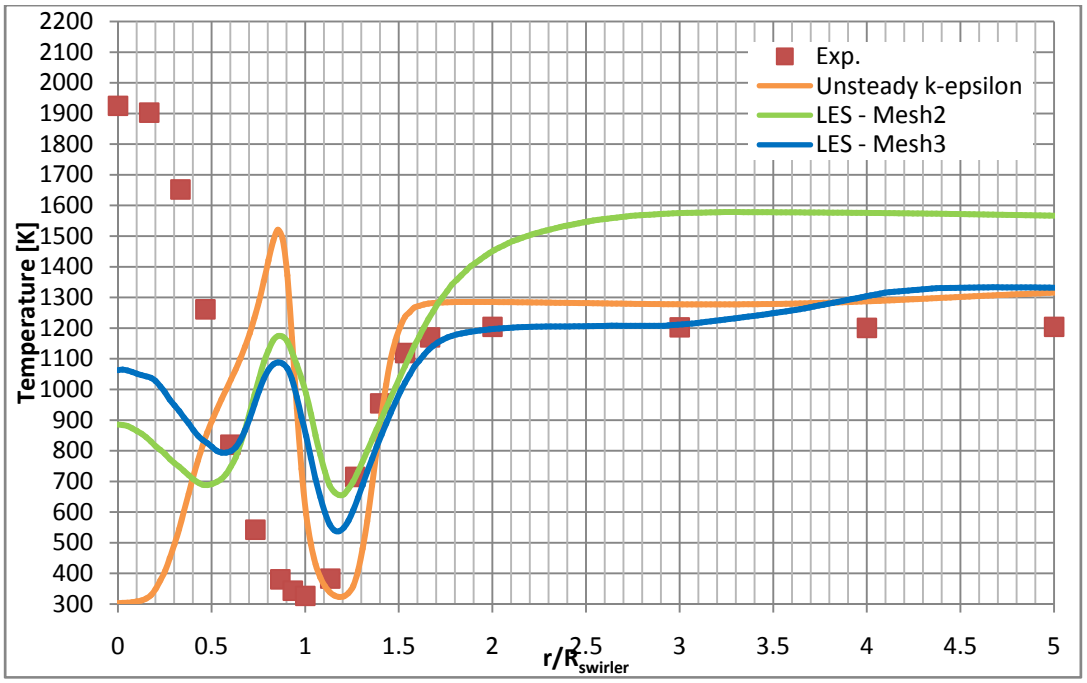

Figure 89. Mean static temperature from the results of LES and URANS by One Step Eddy Dissipation Combustion Model; 20mm downstream of swirler exit plane

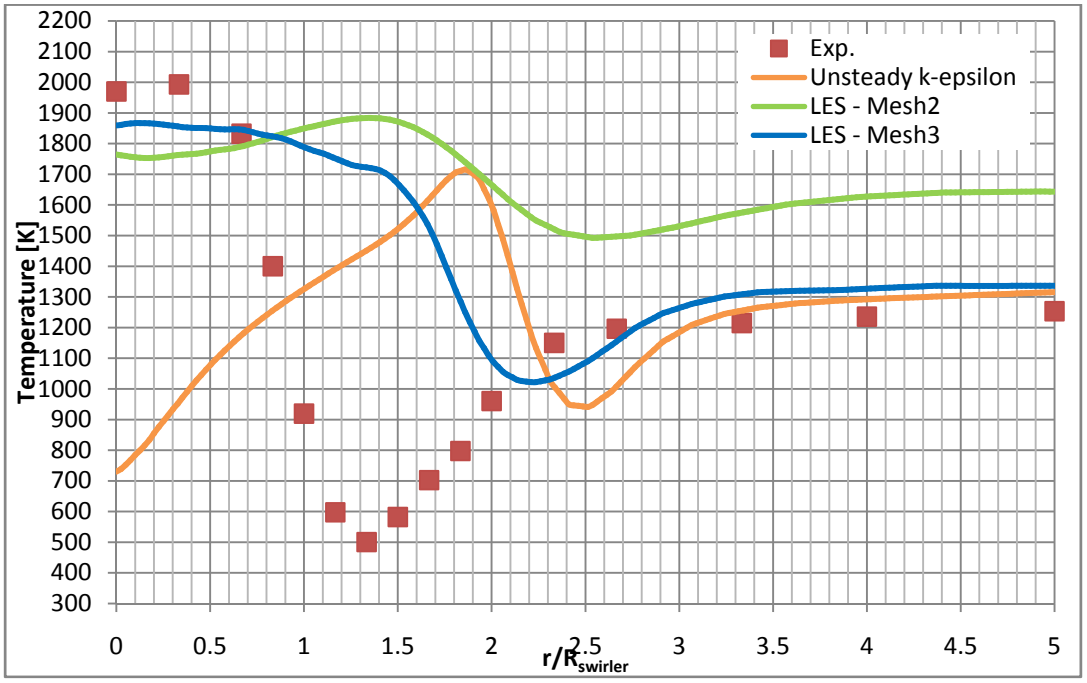

Figure 90. Mean static temperature from the results of LES and URANS by One Step Eddy Dissipation Combustion Model; 60mm downstream of swirler exit plane

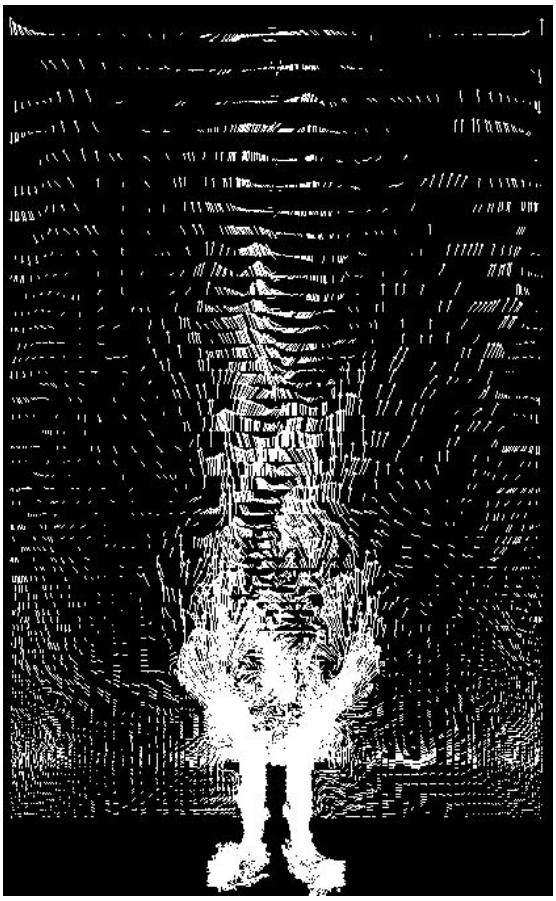

a) Instantaneous vector field

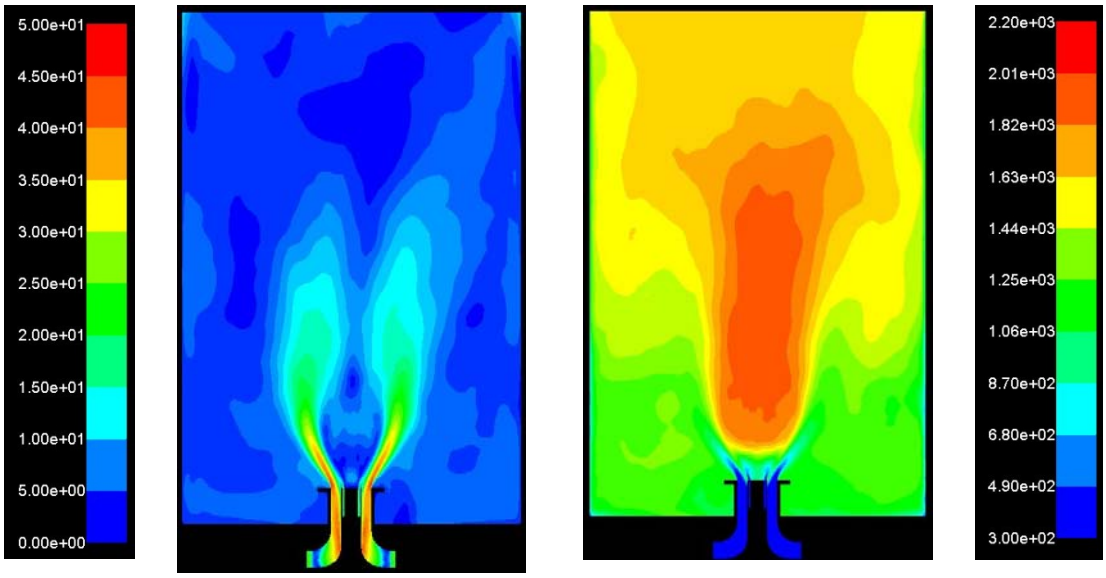

b) Mean velocity contour c) Mean static temperature contour

Figure 91.Instantaneous vector field, mean velocity contour and mean temperature contour of simulation by mesh 3,LES,one step eddy dissipation model

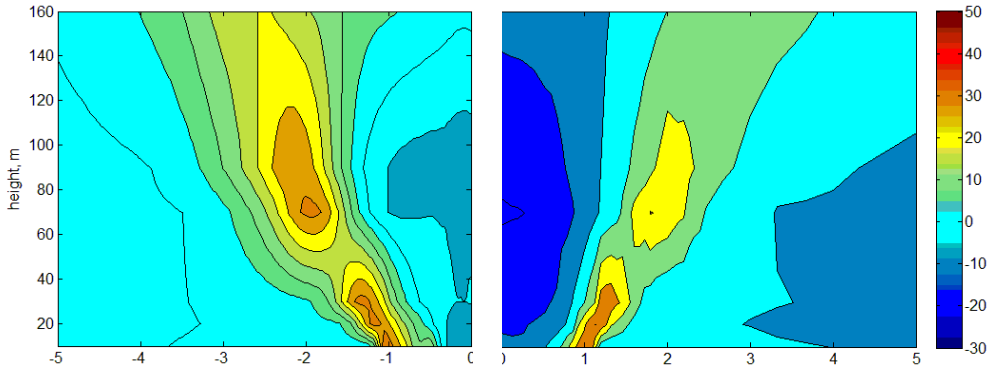

a) LES b) Experiment

Figure 92.Comparison of LES (with One Step EDM) and Experiment. Mean axial velocity field starting from 10mm downstream of swirler exit plane (horizontal axis is $r/R_{swirler}$)

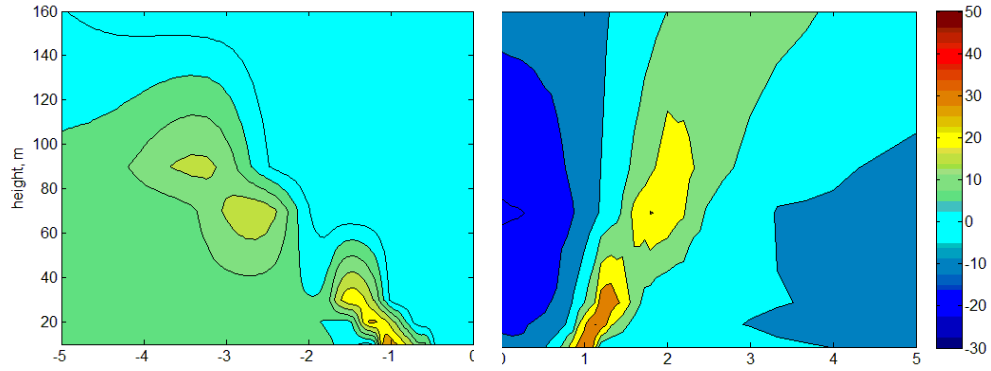

a) Unsteady k-epsilon b) Experiment

Figure 93.Comparison of URANS (with Finite Rate / EDM) and Experiment. Mean axial velocity field starting from 10mm downstream of swirler exit plane (horizontal axis is $r/R_{swirler}$)

5.4 Other Comparisons

5.4.1 Radiation Effects

Discrete Ordinate radiation model is applied in order to see the effect of radiation on temperature field. Results are given inFigure 94 - Figure 96.It is seen that temperature values decreases about 50K – 100K if the radiation model is activated. The heat transfer rate to wall due to radiation is calculated as 16.4kW which is 22% of total heat transfer rate and 11% of total generated power.

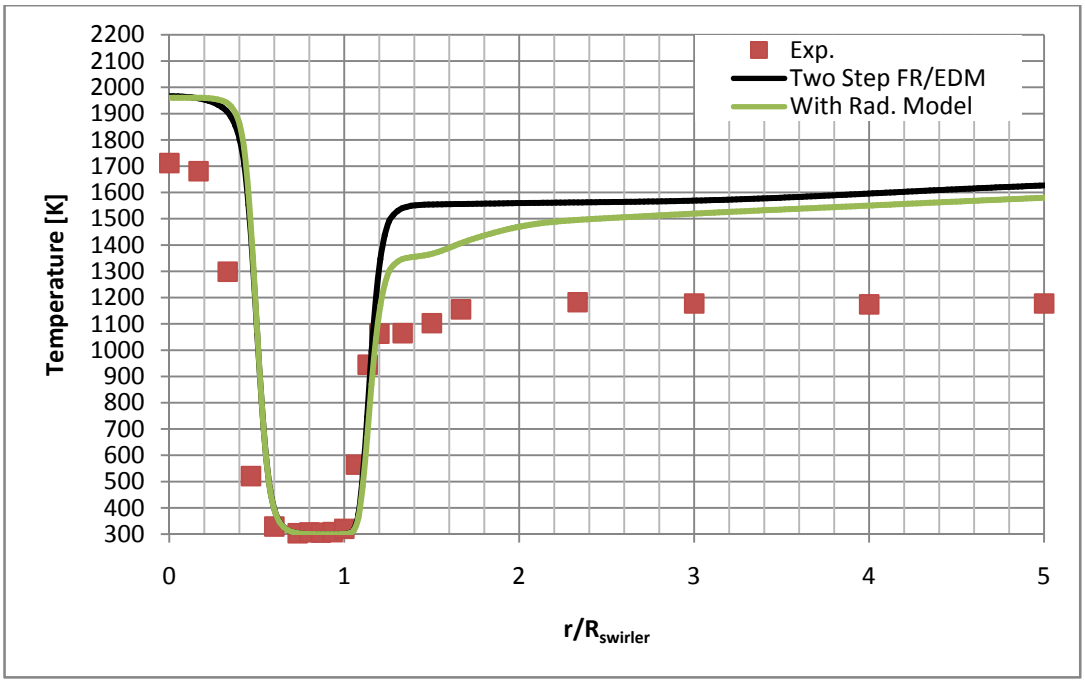

Figure 94. Mean static temperature from the results of Two Step Finite Rate / Eddy Dissipation Combustion Model with Discrete Ordinate Radiation Model; 10mm downstream of swirler exit plane

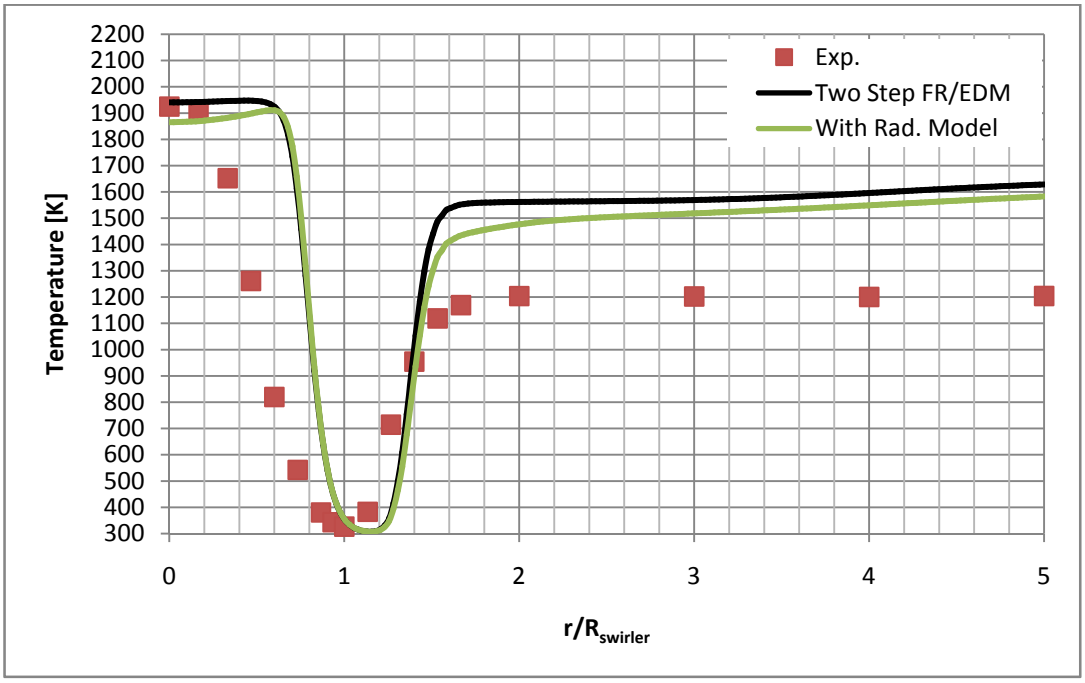

Figure 95. Mean static temperature from the results of Two Step Finite Rate / Eddy Dissipation Combustion Model with Discrete Ordinate Radiation Model; 20mm downstream of swirler exit plane

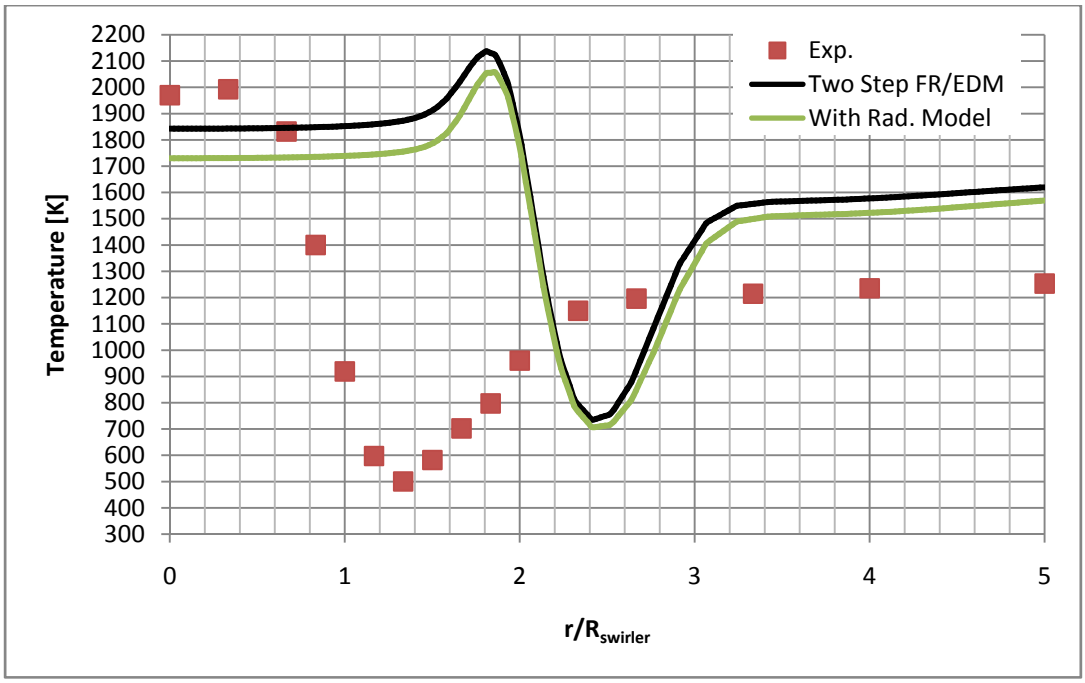

Figure 96. Mean static temperature from the results of Two Step Finite Rate / Eddy Dissipation Combustion Model with Discrete Ordinate Radiation Model; 60mm downstream of swirler exit plane

5.4.2 Effect of Discretization Schemes

Second order upwind scheme, which is the default spatial scheme for every URANS solutions, is known for its capability on calculating non-linear changes along a computational cell. Problems like swirling flows may need a higher order discretization scheme in order to calculate the non-linearity better. Since the grid is hexahedral, third order Quadratic Upwind Interpolation (QUCIK) scheme is available for computations. The effect of discretization scheme is investigated inFigure 97. It is seen that higher order discretization scheme makes no change in velocity field but only small amount of change (around 20K) in temperature field.

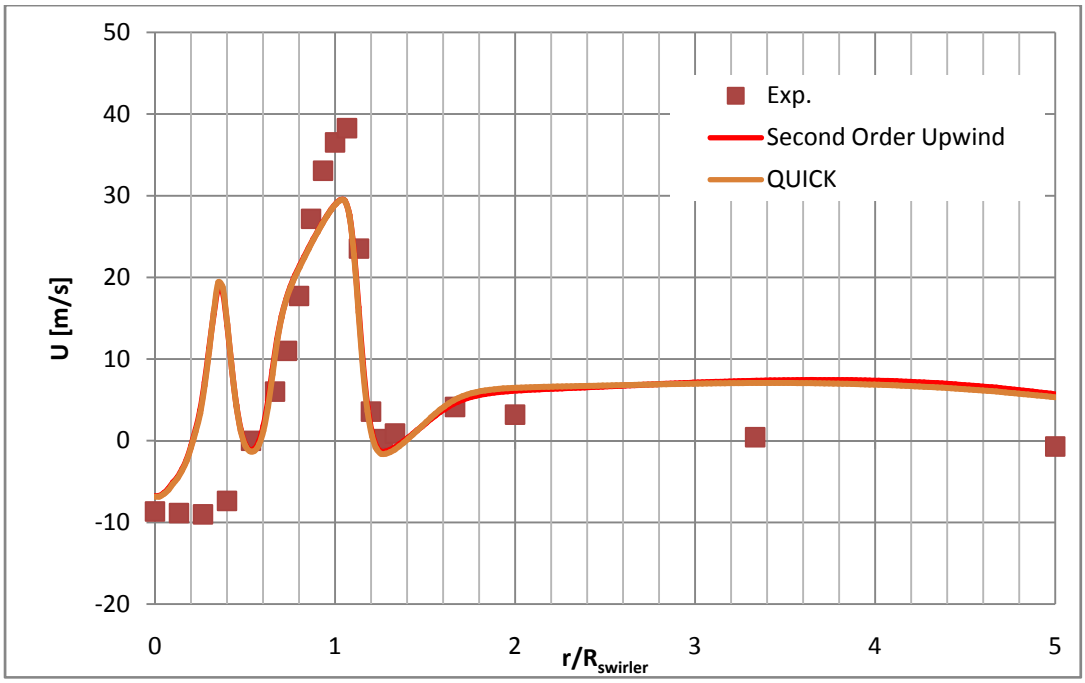

a) Mean static temperature at 10mm downstream of swirler exit plane

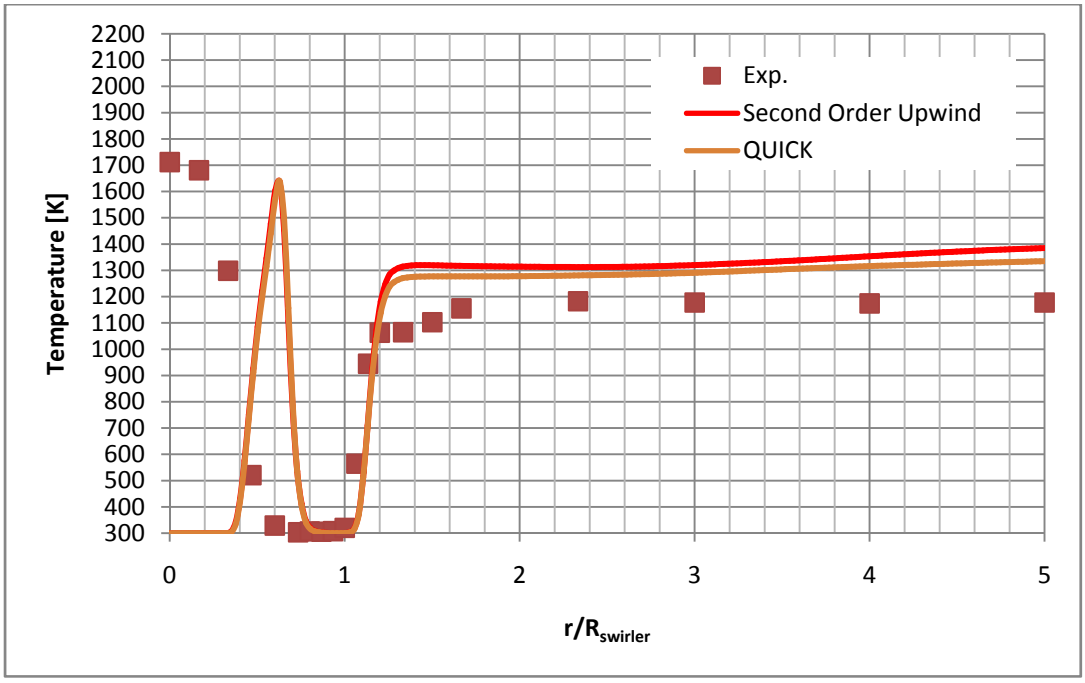

b) Mean static temperature at 10mm downstream of swirler exit plane

Figure 97. Results of mean static temperature and mean axial velocity of two different discretization schemes with Realizable k-epsilon Turbulence Model and Two StepEddy Dissipation Combustion Model

CHAPTER 6

DISCUSSION & CONCLUSION

6.1 Summary and Comments on Results

Non-premixed swirling flames are very common in practical engineering especially in gas turbine combustors. Simulating of a turbulent diffusion flame is still a challenging task.

In this work, a highly swirled confined non-premixed methane-air flame is investigated. TECFLAM s09 flame is chosen due to its similarity between aeronautical gas turbine engine combustors. A commercially available flow solver, ANSYS Fluent 14.0 is used for computations. Performance ofUnsteady – RANS with Realizable k – epsilon turbulence model is tested against the reactive flow. Mesh study is performed. It is observed that mesh independent solutions can be reached by using 0.9M hexahedral grid element which is close to the findings of Schneider [37]. Whether the 0.9M grid element is enough, to be on the safe side, 2.7M grid element is used for the most of the work done in the scope of this thesis.

With available experimental data, comparisons are made to increase the accuracy of URANS simulations. Combustion model comparison is one of the main works of this study. Eddy Dissipation Model, Laminar Rate Model, Finite Rate / Eddy Dissipation Model and Equilibrium Presumed β-shape Function PDF Model are used for comparisons. Also the effect of reaction scheme (one step and two step) is investigated with Eddy Dissipation Model. Cold flow simulations show that, chemistry affects the flow field very much and a simulation which does not include reactions will not provide reactive flow field.

Another finding from combustion model comparison is that, the infinitely fast chemistry algorithms are not proper for this problem. Eddy Dissipation Model and PDF model generates a reaction at mixing zone which is not real. This reaction causes a sudden peak both in temperature and velocity field. The burnt products accelerated and quickly leave from the reaction zone. Since all the mixture burn instantly, a strong mass flow occurs close to the center which affects the central recirculation zone and wipes it out. This phenomenon is especially observed by EDM solutions.The refinement of PDF model is, it covers a mixture fraction for a given temperature. Therefore, a complete reaction does not occur at mixing zone due to the temperature gradient. But it still instantly burns much of the reactants at mixing zone.

When the Laminar Rate Model is employed, the reactions occur very slowly which does not matches with measured data.This is the reason of missing turbulence-chemistry coupling in Laminar Rate Model. Because the effect of turbulence is still high and affects the burning rate. Reactants burns much slower than it should be which damps the pressure gradient in early and outer combustion zone and ends up with no recirculating flow between upper (70mm) and lower region of the chamber. Therefore, it shall be modeled.

Finite Rate / Eddy Dissipation Model, which is blend of Finite Rate and Eddy Dissipation Model shows the best performance among others. The model calculates the reaction rates of finite rate assumption and Eddy Dissipation Model and uses the smaller one. Whether the temperature is over predicted, the trend of the temperature is captured best with this model. On the other hand, the strength of central recirculation zone is under predicted. This is observed with all investigated combustion models. A wider and weaker recirculation core is calculated with URANS simulations which lead to inaccurate solutions. So the problem is not just the combustion modeling, but also the modeling flow itself. Whether the Realizable k-epsilon turbulence model is introduced for its capability on predicting swirling flows, in this case, where a highly swirling flow is employed, it shows insufficient performance.

Other investigated parameters are radiation effect and order of discretization scheme. When the Discrete Ordinate Radiation Model is activated in simulations, the

calculated temperature in simulations is decreased around 50K. The radiated heat to wall is about 22% of total transferred heat rate and 11% of total thermal power. These values does not agree with Meier's findings [24] who calculated radiated heat transfer rate as 33% of total thermal power. Though, Lefebre [1] points that up to 80% of radiation heat can go because of soot. In this study, soot is not modeled and only the gaseous radiation is calculated. Therefore, results may still be reasonable.

Instead of second order upwind scheme, using QUICK as higher order spatial discretization does not increase the accuracy of velocity field. But there is a 20K effect on temperature field. Cost vs. Accuracy comparison can be made for a proper selection between these two schemes when a simulation will be performed.

Although improvements are achieved with different approaches to the problem, the error on URANS simulations is still high. Therefore, Large Eddy Simulations is employed with the same mesh in order to compare the performance of expensive way. At least 10 times longer CPU work is needed for a single simulation. Dynamic stress, dynamic energy flux and dynamic scalar flux are activated to decrease the mesh dependency. Results show that solutions are very mesh sensitive. However, the improvement on accuracy is very high compared to URANS solutions. The inner recirculation flow prediction is stronger and tighter which is in close vicinity with experimental data. Since the flow field capturing is better, temperature prediction is also refined. Tough, improvements can still be made where the recirculation power is stronger in experiments and central temperature distribution prediction includes erroneous results. Besides, mesh independency is not checked since the results of two meshes are obviously mesh dependent.

All in all, the URANS methodology is still not valid for highly swirling reactive flow. LES is more promising since it gives reasonably good results with same mesh level while it is more expensive. Chemistry closures also affect the simulations. Turbulence effect on burning rate should be modeled.

6.2 Future Work

This study presents answers about simulating of highly swirling reactive flow with URANS methodology. The accuracy level of results is not high enough compared to LES results. In order to increase the accuracy of URANS, several approaches are made and more can be made. One of the first attempts can be done by turbulence model investigation. Realizable k-epsilon model is used in this study since it is introduced for rotating flows. k-ω SST or Reynolds Stress Models can be employed for more accurate solutions. Further, Detached Eddy Simulation (DES) can be used to decrease the cost of LES calculations.

Another attempt to carry out this work can be made on combustion model study. Finite rate chemistry which includes real time turbulence effect can increase the accuracy of the results. But the CPU expenses should always be checked in order to realize the costs of gathered accuracy level.

One other subject which should be clarified is the calculated radiated heat. The difference in this study should be questioned. The methodology of radiation modeling can be revised or another experiment with radiation heat data measurements can be investigated.

In this work, simulations are started from swirler inlet ports since there is a value for validation. For a fresh design, only the mass flow rate will be known and a methodology is needed to obtain mass flow rate ratios. Therefore, full combustion chamber simulations can be performed to be sure about the accuracy level of the calculated swirler mass flow ratio by simulations.

REFERENCES

1. Lefebre A.H., "Gas Turbine Combustion", Taylor&Francis, 2nd Edition, 1999
2. KOCH R., "Spray Combustion", VKI Lecture Series Turbulent Combustion, 2013
3. Ayache S., "Simulations of Turbulent Swirl Combustors", Department of Engineering University of Cambridge SelywnColloge, PhD Thesis, 2011
4. Kuo K.K., “Principles of Combustion”, John Wiley & Sons Inc., 2005
5. Yoon J., Kim M., Hwang J., Lee J., Yoon Y., "Effect of Fuel Air Mixture Velocity on Combustion Instability of a Model Gas Turbine Combustor", Applied Thermal Engineering Vol.54 Issue 1, 2013
6. Stöhr M, Boxx I., Carter C., Meier W., "Dynamics of Lean Blowout of a Swirl Stabilized Flame in a Gas Turbine Model Combustor", Proceedings of the Combustion Institute, Vol. 33 Issue 2, 2011
7. Meier W., Duan X.R., Weigand P., "Investigations of Swirl Flames in a Gas Turbine Combustor: II. Turbulence-Chemistry Interactions", Combustion and Flame, Vol. 144 Issue 1-2, 2006
8. Poinsot T., Veynante D., “Theoretical and Numerical Combustion”, R.T. Edwards Inc., 2001
9. Beer J. M., Chigier N. A., "Combustion Aerodynamics", John Willey & Sons Inc., 1972
10. Kuo K.K., Acharya R., “Fundamentals of Turbulent and Multiphase Combustion”, John Wiley & Sons Inc., 2012
11. Veynante D., Vervisch L., “Turbulent Combustion Modeling”, VKI Turbulent Combustion Lecture Series, 2013
12. Syreed N., Beer J. M., “Combustion in Swirling Flows: A Review”, Combustion and Flame, 1974
13. Chigier N.A., Beer J. M., Trans ASME 86D, J. Basic Eng., 4, 788, 1964
14. Katsnelson B.D., Bogdanov B.A., Thermal Eng, 17 (4), 82 (1970)
15. Claypole and Syreed [82] (Chapter 9 Swirl Stabilized Flame Study :Experimental Procedure)

16. Gupta A.K., "Swirl Flows", Technomic Publishing Co., 1984
17. Syreed N., “A Review of Oscillation Mechanisms and role of the precessing vortex core (PVC) in swirl combustion systems”, Progress in Energy and Combustion Science, 2006
18. Lucca-Negro O., O’Doherty T., “Vortex Breakdown: A Review”, Progress in Combustion and Energy Science, 2001
19. Umeh C.O.U., Rusak Z., Gutmark E., Villalva R. and Cha D.J., “Experimental and Computational Study of Non-Reacting Vortex Breakdown in aSwirl Stabilized Combustor”, 47 th AIAA Aerospace Sciences Meeting Including the New Horizons Forum and Aerospace Exposition, 2009
20. Froud D., O’Doherty T., Syreed N., “Phase Averaging of the Precessing Vortex Core in a Swirl Burner Under Piloted and Premixed Combustion Conditions”, Combustion and Flame, 1995
21. Hillemanns R., Lenze B., Leuckel W., “Flame Stabilization and Turbulent Exchange in Strongly Swirling Natural Gas Flames”, 21st Symposium (International) on Combustion/ The Combustion Institute, 1986
22. Lartigue et al., 30th Symp Comb, 2004, J. Comp. Physics.,
23. Bergmann V., Meier W., Wolff D., Stricker W., “”, Applied Physics, 1998
24. Meier W., Keck O., Noll B., Kunz O., Stricker W., “Investigations in the TECFLAM Swirling Diffusion Flame: Laser Raman Measurements and CFD Calculations”, Applied Physics, 2000
25. Böckle S., Kazenwade J., Kunzelmann T., Shin D.-I., Schulz C., “Sigle-Shot Laser-Induced Fluorescence Imaging of Formaldehyde with XeF Excimer Excitation”, Applied Physics, 2000
26. Böckle S., Kazenwadel J., Kunzelmann T., Shin D.-I., Schulz C., Wolfrum J., “Simultaneous Single-Shot Laser-Based Imaging of Formaldehyde, OH and Temperature in Turbulent Flames”, Proc. Combust. Inst. 28,
27. Böckle S., Kazenwadel J., Schulz C., “Laser Diagnostic Multi-Species Imaging in Strongly Swirling Natural Gas Flames”, Applied Physics, 2000
28. Landenfeld T., Kremer A., Hassel E.P., Janicka J., Schäfer T., Kazenwadel J., Schulz C., Wolfrum J., “Laserdiagnostic and Numerical Studies of Strongly Swirling Natural-Gas Flames”, 27th Symposium (International) on Combustion/The Combustion Institute, 1998

29. Dreizler A., “Experiments in Turbulent Combustion”, VKI Turbulent Combustion Lecture Series, 2013
30. Freitag M., Klein M., “An Improved Method to Assess the Quality of Large Eddy Simulations in the Context of Implicit Filtering”, Journal of Turbulence, 2012
31. Wegner B., Maltsev A., Schneider C., Sadiki A., Dreizler A., Janicka J., “Assessment of Unsteady RANS in Predicting Swirl Flow Instability”, Heat and Fluid Flow, 2004
32. Frassoldati A., Frigerio S., Colombo E., Inzoli F., Faravelli T., “Determination of NOx Emissions From Strong Swirling Confined Flames with an Integrated CFD-Based Procedure”, Chemical Engineering Science, 2005
33. Kuenne G., Ketelheun A., Janicka J., “LES modeling of Premixed Combustion Using a Thickened Flame Approach Coupled with FGM Tabulated Chemistry”, Combustion and Flame, Vol. 158, 2011
34. Khelil A., Naji H., Loukarfi L., Mompean G., “Prediction of a High Swirled Natural Gas Diffusion Flame Using a PDF Model”, Fuel Vol.88, 2009
35. Repp S., Sadiki A., Schneider C., Hinz A., Landenfeld T., Janicka J., “Prediction of Swirling Confined Diffusion Flame with a Monte-Carlo and a Presumed-PDF-Model”, International Journal of Heat and Mass Transfer, Vol. 45, 2002
36. Yang W., Zhang J., “Simulation of Methane Turbulent Swirling Flame in the TECFLAM Combustor”, Applied Mathematical Modeling, vol. 33, 2009
37. Schneider E., Maltsev A., Sadiki A., Janicka J., “Study on the Potential of BML-Approach and G-Equation Concept-Based Models for Predicting Swirling Partially Premixed Combustion Systems: URANS Computations”, Combustion and Flame Vol.152, 2008
38. Sadiki A., Maltsev A., Wegner B., Flemming F., Kempf A., Janicka J., “ Unsteady Methods (URANS and LES) for Simulation of Combustion Systems”, International Journal of Thermal Science, Vol.45, 2006
39. Meier W., Noll B., Bockhorn H., Leuckel W., Schulz C., Wolfrum J., Schneider C., Repp S., Sadiki A., Dreizler A., Janicka J., “Confined

TECFLAM Swirl Burner: Experimental Investigations and Numerical Simulations", TNF 5 Proceedings, 2000

40. Barlow R. (Ed.), "Proceedings of the TNF Workshops", Sandia National Laboratories, Livermore, CA, http://www.ca.sandia.gov/TNF
41. Kempf A., Schneider C., Sadiki A., Janicka J., "LES of a Highly Turbulent Methane Flame: Application to the DLR Standard Flame", TSFP2,2001
42. Meier W., Barlow R., Chen J.-Y., "Rama/ Rayleigh/ LIF Measurements in a Turbulent CH4/H2/N2 Jet Flame: Experimental Techniques and Turbulence Chemistry Interaction", Combustion Flame Vol.123, 2000
43. Landenfeld T., Kremer A., Hassel E.P., Janicka J., "Ansätze zur Modellierung eingeschlossener Drallflammen" In TECFLAM-Seminar, Drallflammen und Industriecodeentwicklung, Vol.13, 1997
44. S. Böckle, J. Kazenwadel, C. Schulz, J. Wolfrum, "Laserspektroskopische Bestimmung von NO Konzentrations- und Temperaturfeldern in turbulenten, nicht-vorgemischten Drallflammen", in TECFLAM Seminar, Drallflammen und Industriecodeentwicklung, Arbeitsgemeinschaft TECFLAM, ISBN 3-926751-21-5, S. 99-109 (1999).
45. Triantafyllidis A. and Mastorakos E., "Implementation issues of the Conditional Moment Closure Model in Large Eddy Simulations", Flow Turbulence and Combustion,2010
46. Triantafyllidis A., Mastorakos E., and Eggels R.L.G.M., "Large Eddy Simulations of Forced Ignition of a Non-Premixed Bluff-Body Methane Flame with Conditional Moment Closure", Combustion and Flame, Vol. 159, 2009.
47. Smith G.P., Golden D.M., Frenklach M., Moriarty N. W., Eiteneer B., Goldenberg M., Bowman C. T., Hanson R.K., Song S., Gardiner W. C., Lissianski V. V., Qin Z., Gri-mech 3.0 web-site,.90, 129
48. Munson B.R., Young D.F, Okiishi T.H., "Fundamentals of Fluid Mechanics", John Wiley & Sons Inc., 5th Edition, 2006
49. Ferziger J.H., Peric M., "Computational Methods for Fluid Dynamics", Springer-Verlag, 3rd Rev. Edition, 2002
50. Tennekes H., Lumley J.L., "A First Course in Turbulence", The MIT Press, 1972

51. Kolmogorov A. N., “The local structure of turbulence in incompressible viscous fluid for very large Reynolds numbers”, C.R. Acad. Sci. USSR 30. 301
52. Pope S.B., “Ten Question Concerning the Large Eddy Simulation of Turbulent Flows”, New Journal of Physics 6 35, 2004
53. Veynante D., “Introduction to Turbulent Combustion”, VKI Turbulent Combustion Lecture Series, 2013
54. Ferziger J.H., Perić M., “Computational Methods for Fluid Dynamics”, Springer, 3rd Edition.
55. Jones W. P., Launder B. E., “ The prediction of laminarization with a 2-equation model of turbulence”, International Journal of Heat and Mass Transfer 15, 1972
56. Vervisch L., “Turbulent Combustion Modeling for Non-Premixed Flames” , VKI Turbulent Combustion Lecture Series, 2013
57. Spalding D.B., “Mixing and Chemical Reaction Steady Confined Turbulent Flames”, 13th Symposium on Combustion, the Combustion Institute, 1971
58. Magnussen B. F., Hjertager B.H., “On Mathematical Modeling of Turbulent Combustion”, 16th Symposium on Combustion, the Combustion Institute, 1976
59. ANSYS Fluent Theory Guide, Release v.14
60. Libby P.A., and Williams F.A., “Turbulent Combustion: Fundamental Aspects and A Review”, Academic Press London, 1994
61. Dreizler A., Personal conversation, May 2013
62. Adiabatic Flame Temperature Calculator, eLearning@Cerfacs Online Courses, Combustion Tools,http://elearning.cerfacs.fr/, last accessed on September 2014
63. NIST Chemistry WebBook, Data From NIST Standard Reference Database69, http://webbook.nist.gov/chemistry/, last accessed on September 2014